THE
PHYSICAL REVIEW
A Journal of Experimental and Theoretical Physics Established by E. L. Nichols in 1893
VOL. 54, NO. 10 NOVEMBER 15, 1938 SECOND SERIES

Radioactive Isotopes of Iodine

J. J. LIVINGOOD
Radiation Laboratory, Physics Department, University of California
AND
G. T. SEABORG
Chemistry Department, University of California, Berkeley, California
(Received September 7, 1938)

Five radioactive iodine isotopes are described, three of which are new. These were produced, by use of 8 Mev deuterons, 16 Mev helium ions and neutrons. Evidence is presented for the following isotopic assignments and properties:

REACTION	HALF-LIFE	PARTICLE RANGE GRAMS/CM² AL	GAMMA—HALF-THICKNESS GRAMS/CM² PB
$I^{127}(n, \gamma)I^{128}$ $Te^{128}(d, 2n)I^{128}$	25±1 min. (−)	1.05	3.5
$I^{127}(n, 2n)I^{126}$ $Sb^{123}(\alpha, n)I^{126}$ $Te^{125}(d, n)I^{126}$	13.0±0.3 days (−)	0.44	4.5
$Sb^{121}(\alpha, n)I^{124}$	4.0±0.3 days (+)	—	—
$Te^{128 \text{ or } 130}(d, n)$ $I^{129 \text{ or } 131}$	8.0±0.2 days (−)	0.50	3.3
$Te^{130}(d, 2n)I^{130}$	12.6±1.0 hr. (−)	0.40	6.0

It is shown that the 8-day activity is also produced by the radioactive decay of $Te^{129 \text{ or } 131}$. Chemical identification has been made in every case. A table of approximate yields is given.

INTRODUCTION

THE radioactive isotopes of iodine studied in this paper were produced by the bombardment of iodine, tellurium, or antimony by neutrons, deuterons, or helium ions. Fig. 1 shows the percent abundance of the stable antimony, tellurium, iodine and relevant xenon isotopes, as compiled by Livingston and Bethe.[1]

The bombardments were made with the Berkeley cyclotron. The deuteron currents were about 50 microamperes at 8 Mev, the helium ion currents 0.6 microampere at 16 Mev. In the final experiments, tellurium metal was melted onto a copper plate and bombarded in an atmosphere of helium at reduced pressure. The projectiles entered the chamber through a thin aluminum window. In the preliminary work, to

[1] Livingston and Bethe, Rev. Mod. Phys. **9**, 380 (1937).

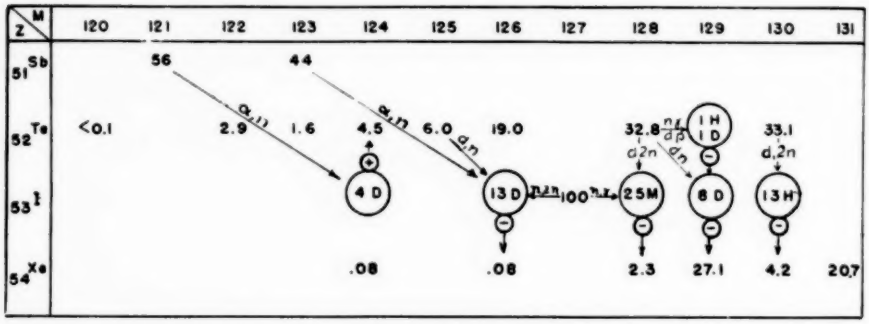

FIG. 1. Percent abundance of stable isotopes in the region of iodine. The half-lives of radioactive isotopes are encircled, and the transmutations are indicated by arrows.

avoid possible contamination of copper, sticks of metallic tellurium were supported outside the aluminum window and were bombarded in air. Antimony was activated in vacuum. Slabs of the metal were soldered to water-cooling pipes and the activated side was then filed off.

The signs of the disintegration products were determined by magnetic deflection in air. Activities were observed on a Lauritsen-type quartz-fiber electroscope. The background activity, about 0.001 division per second, was subtracted from all data.

All of the measurements were made upon chemically analyzed samples. In many cases, the activated tellurium was dissolved in nitric acid after the addition of a small quantity of sodium iodide to act as a carrier. The iodine which was liberated during the solution process was distilled into a reducing solution of sodium sulfite. The iodide was then precipitated as silver iodide upon the addition of silver nitrate solution. The same procedure was followed after alpha-particle bombardment of antimony and fast neutron activation of sodium iodide. On several occasions, a liter of ethyl iodide was exposed to neutrons and then shaken with an aqueous solution of sodium sulfite and sodium bicarbonate. The iodine was separated from the aqueous phase as silver iodide. For the study of the growth of radioactive iodine from tellurium, the iodine was separated by successive distillations during two experiments, while in a third more quantitative investigation, the procedure was followed of successive precipitations as silver iodide directly from the tellurium solution.

RADIOACTIVE ISOTOPE I^{128}: FROM $I+n$ AND $Te+D$; HALF-LIFE 25 ± 1 MINUTES $(-)$

This well-known activity, produced strongly by slow neutrons on iodine, was first observed by Fermi and his associates.[2] The work of Aston, and more recently, that of Nier,[3] shows only one stable iodine isotope, I^{127}, so that this activity has been assigned definitely to I^{128} through $I^{127}(n, \gamma)I^{128}$.

We have produced this same active isotope by bombarding tellurium with 8 Mev deuterons. It cannot have been formed by the usual (d, n) reaction, since Te^{127} is not stable. Consequently the transmutation must be either $Te^{126}(d, \gamma)I^{128}$ or $Te^{128}(d, 2n)I^{128}$. At present, the choice between these alternatives must be made from theoretical

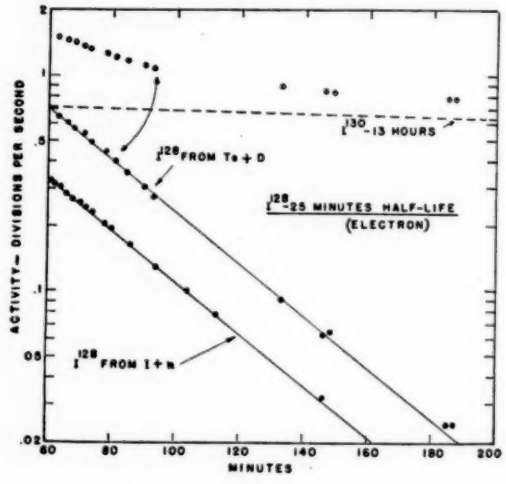

FIG. 2. Decay curves of I^{128}.

[2] Amaldi, d'Agostino, Fermi, Pontecorvo, Rasetti, Segrè, Proc. Roy. Soc. **A149**, 522 (1935).
[3] Nier, Phys. Rev. **52**, 933 (1937).

considerations, and the second alternative appears more likely.

The reactions leading to I^{128} are therefore,

$$_{53}I^{127}+{}_{0}n^{1}\rightarrow{}_{53}I^{128}+\gamma$$

and either

$$_{52}Te^{126}+{}_{1}D^{2}\rightarrow{}_{53}I^{128}+\gamma$$

or

$$_{52}Te^{128}+{}_{1}D^{2}\rightarrow{}_{53}I^{128}+2{}_{0}n^{1}.$$

The decay is

$$_{53}I^{128}\rightarrow{}_{54}Xe^{128}+{}_{-1}e^{0}\ (25\ \text{minutes}).$$

Figure 2 shows the 25-minute half-life of a neutron-activated sample of iodine and the initial portion of the iodine from a deuteron bombardment of tellurium (with correction for the longer-lived iodines also produced).

The absorption curves in aluminum and lead for the 25-minute I^{128} are given in Fig. 3, after correction for decay. The negative electrons have a maximum range of 1.05 ± 0.05 gram per cm² Al, corresponding to an energy of 2.2 Mev, according to the relation of Widdowson and Champion:[4] Energy (Mev) = [Range (gram/cm²) + 0.165]/0.536. The downward curvature of the plot suggests the presence of another component, possibly a monokinetic line from an internally converted gamma-ray. Cloud-chamber observations by others agree remarkably well with these measurements: Alichanian, Alichanow and Dzelepow[5] and Bacon, Grisewood and van der Merwe[6] find the maximum energy at 2.1 Mev, while the latter workers have further evidence for another group at 1.2 Mev.

The gamma-ray is absorbed to half-value by 3.5 grams per cm² Pb, which indicates an energy of 0.4 Mev, according to Gentner's correlation.[7] This is not in agreement with the difference of the maximum energies of the two electron groups quoted above.

Radioactive Isotope I^{126}: From I+Fast n, Te+D and Sb+He; Half-Life 13.0 ± 0.3 Days (−)

The existence of an activity with 13 days' half-life after irradiating iodine with fast neutrons from the (Li+D) reaction was discovered by Tape and Cork.[8] We have shown[9] the isotope to be chemically identifiable with iodine. The majority of the particles are electrons, but the method of sign determination does not rule out the existence of additional positron decay to stable Te^{126}. There can be no doubt that it is I^{126} formed by $I^{127}(n, 2n)I^{126}$.

We have found that the bombardment of antimony with 16 Mev helium ions gives rise to two radioactive iodine isotopes, with half-lives 4 days and 13 days. The appearance of the latter affords a good check on the assignment of the 13-day activity to I^{126}, since here it is formed by $Sb^{123}(\alpha, n)I^{126}$. (The interpretation given to the 4-day period will be discussed later.)

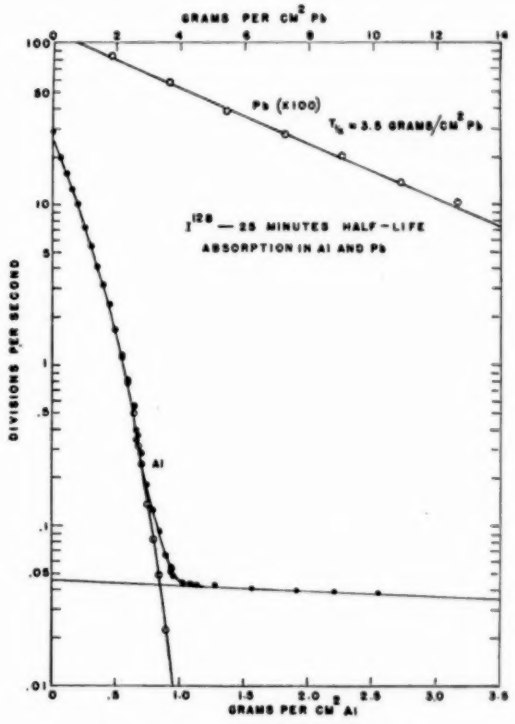

FIG. 3. Absorption curves of I^{128}.

Figure 4 shows decay curves of the 13-day activity obtained in these two reactions.

It is to be expected that the transmutations $Te^{125}(d, n)I^{126}$ or $Te^{126}(d, 2n)I^{126}$ should occur, but direct evidence for this is masked by another activity.

[4] Widdowson and Champion, Proc. Phys. Soc. **50**, 192 (1938).
[5] Alichanian, Alichanow and Dzelepow, Physik. Zeits. Sowjetunion **10**, 78 (1936).
[6] Bacon, Grisewood and van der Merwe, Phys. Rev. **54**, 315 (1938).
[7] Gentner, J. de phys. et rad. **6**, 274 (1935).
[8] Tape and Cork, Phys. Rev. **53**, 676 (1938).
[9] Livingood and Seaborg, Phys. Rev. **53**, 1015 (1938).

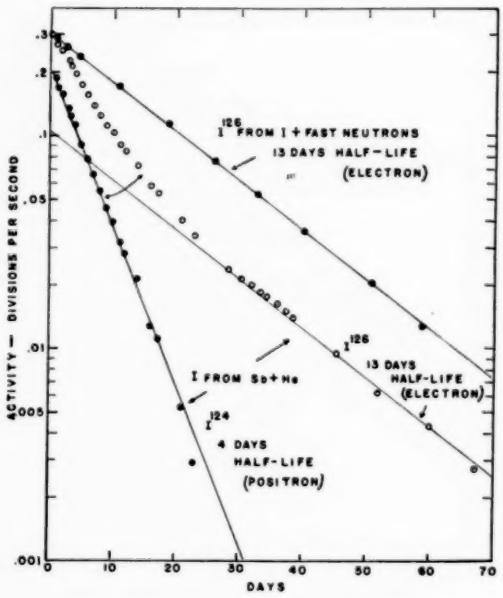

FIG. 4. Decay curves of I^{124} and I^{126}.

In Fig. 5 may be seen the decay of a first separation of iodine from a deuteron bombardment of tellurium; the observed half-lives are 25 minutes, 13 hours, and about 8.5 days. We will show later on that one can interpret the observed 8.5-day figure as the combination of an 8.0-day period found with independent evidence and a comparatively weak activity with the expected 13-day half-life. The intensity of this latter component, as indicated in Fig. 5, is what should be expected on the basis of the abundance of the tellurium isotopes, the half-lives and ionizing powers of the 8- and 13-day radiations.

We may therefore write as the transmutations leading to I^{126}:

$$_{53}I^{127}+{}_0n^1\rightarrow{}_{53}I^{126}+2{}_0n^1,$$

$$_{51}Sb^{123}+{}_2He^4\rightarrow{}_{53}I^{126}+{}_0n^1,$$

$$_{52}Te^{125}+{}_1D^2\rightarrow{}_{53}I^{126}+{}_0n^1,$$

followed by

$$_{53}I^{126}\rightarrow{}_{54}Xe^{126}+{}_{-1}e^0 \text{ (13 days)}.$$

Figure 6 shows absorption curves of the 13-day period, obtained from a sample of iodine activated with fast neutrons from a Li+D source. The negative electrons have a range of 0.44 ± 0.02 gram per cm² Al, corresponding[4] to an energy of 1.13 Mev. The gamma-ray is reduced to half-value by 4.5 grams per cm² Pb, which indicates[7] an energy of 0.5 Mev.

RADIOACTIVE ISOTOPE I^{124}: FROM Sb+He; HALF-LIFE 4.0 ± 0.3 DAYS (+)

As mentioned above, the bombardment of antimony with 16 Mev helium ions causes the formation of two active iodine isotopes, one emitting electrons with a half-life of 13 days and the other positrons with a 4-day half-life. There are but two stable antimony isotopes, Sb^{121} and Sb^{123}, which by the (α, n) reaction would lead to radioactive I^{124} and I^{126}. Since prolonged exposure of iodine to fast neutrons yields only the 13-day period [through $I^{127}(n, 2n)I^{126}$] but not the 4-day activity, it is certain that this latter must be due to I^{124}, the disintegration being:

$$_{51}Sb^{121}+{}_2He^4\rightarrow{}_{53}I^{124}+{}_0n^1,$$

followed by

$$_{53}I^{124}\rightarrow{}_{52}Te^{124}+{}_{+1}e^0 \text{ (4 days)}.$$

The decay of the 4-day activity is shown in Fig. 4.

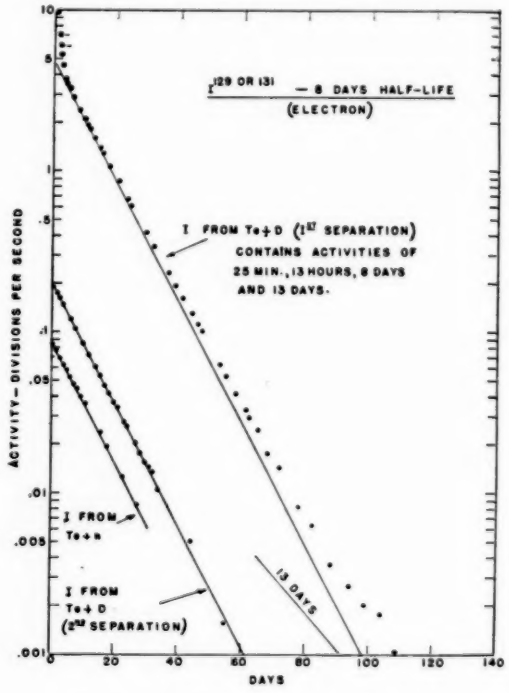

FIG. 5. Decay curves of I^{129} or I^{131}.

Radioactive Isotope I^{129} or I^{131}: From Te+D and $Te^{129, 131} \rightarrow I^{129, 131}$; Half-Life 8.0±0.2 Days (−)

We have briefly reported[9] the existence of an iodine isotope with 8 days' half-life, emitting negative electrons, that can be produced directly by bombarding tellurium with deuterons and which grows in activated tellurium. The evidence for this is now reported in detail. The 8-day period has been observed by Tape and Cork,[8] but was erroneously ascribed by them to a tellurium isotope.

In the iodine separated from a Te+D bombardment there is found a strong activity with 8 days' half-life, in addition to the other periods reported in this paper. If further extractions of iodine are made from the tellurium solution, the 8-day activity is again obtained in each, but not the other periods. This indicates a double decay from tellurium to iodine to stable xenon, and study of the isotopes shows that the chain must be either $Te^{129} \rightarrow I^{129} \rightarrow Xe^{129}$ or $Te^{131} \rightarrow I^{131} \rightarrow Xe^{131}$. The much greater intensity of the 8-day period in the first extraction suggests that a direct transmutation from tellurium to the active iodine also occurs, and it is seen that the expected reactions $Te^{128}(d, n)I^{129}$ or $Te^{130}(d, n)I^{131}$ lead to the same iodine isotope involved in the double decay.

To clinch the argument for a double decay, tellurium was irradiated with slow neutrons, which by no known reaction possibly could cause a direct transmutation to iodine. Nevertheless, the 8-day period was found in the chemically separated iodine fraction, thus proving conclusively that it grows from active tellurium.

Figure 5 gives examples of the decay curves obtained. A first extraction of iodine from deuteron-activated tellurium gives a multiplicity of periods, including that of 8 days' half-life, while a second extraction shows the 8-day period only. This also is the only activity found in iodine removed from neutron activated tellurium.

It has not been possible to determine the period of the parent tellurium by observations on the tellurium activity before and after iodine extractions, because of the overwhelming intensity of other tellurium activities. Recourse

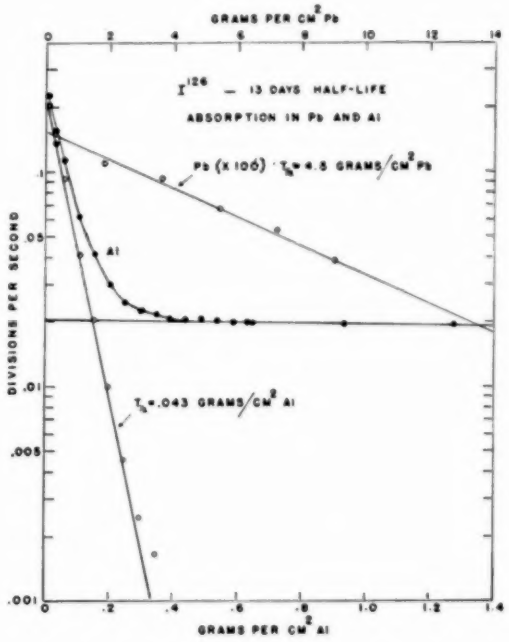

FIG. 6. Absorption curves of I^{126}.

therefore has been made to the procedure of observing the growth of the 8-day iodine and noting the time when this activity reaches its maximum value. This was done by making successive extractions of iodine from the same solution of deuteron-activated tellurium and by following each sample for a number of days in order to establish with precision the intensity of its 8-day period. The growth curve was then obtained by adding to the intensity of each sample (extrapolated back to the time of its separation) the intensities of all previously removed specimens, each also as of that moment. The resulting curve shows the total amount of 8-day iodine present as a function of time, zero being taken at a preliminary separation which removed all iodine directly produced by the $Te(d, n)I$ reaction.

Figure 7 shows such a curve, obtained from a run in which every precaution was taken to make the separations quantitative. It is seen that the 8-day activity reaches a maximum value in about 4 days' time.

The general equation describing the growth of a daughter substance from its parent is:

$$N_2 = N_1^0 \frac{\lambda_1}{\lambda_2 - \lambda_1}(e^{-\lambda_1 t} - e^{-\lambda_2 t})$$

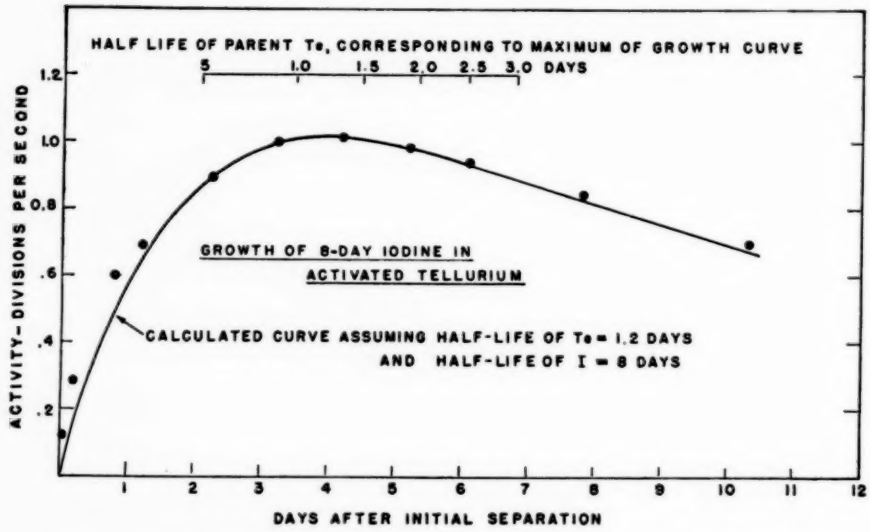
HALF LIFE OF PARENT Te, CORRESPONDING TO MAXIMUM OF GROWTH CURVE
.5 1.0 1.5 2.0 2.5 3.0 DAYS
ACTIVITY-DIVISIONS PER SECOND
1.2
1.0
0.8
.6
.4
.2
GROWTH OF 8-DAY IODINE IN ACTIVATED TELLURIUM
CALCULATED CURVE ASSUMING HALF-LIFE OF Te = 1.2 DAYS AND HALF-LIFE OF I = 8 DAYS
1 2 3 4 5 6 7 8 9 10 11 12
DAYS AFTER INITIAL SEPARATION

FIG. 7. The growth of 8-day iodine in tellurium. The ordinate of the calculated curve has been adjusted to fit at the maximum. See text for the possible significance of the abrupt initial rise of the experimental points.

where $\lambda = 0.693/T$ and T is the half-life. From this it follows by differentiation that the time required for the daughter to grow to a maximum amount is:

$$t_{(\max N_2)} = \frac{1}{\lambda_2 - \lambda_1} \ln \frac{\lambda_2}{\lambda_1} = 3.32 \frac{T_1 T_2}{T_1 - T_2} \log_{10} \frac{T_1}{T_2}.$$

With T_2 taken as 8 days and $t_{(\max N_2)}$ as 4 days, the half-life T_1 of the parent tellurium is found to be 1.2 days. This is admittedly rough, since the result is very sensitive to the chosen value for $t_{(\max N_2)}$.

The smooth curve in Fig. 7 was drawn from the general equation above, by using $T_1 = 1.2$ days and $T_2 = 8$ days, and adjusting the vertical scale to fit the experimental points at the maximum. It is seen that the observed rise at the beginning is somewhat faster than the calculated curve, which suggests that possibly the 8-day iodine is also growing from the well-known[2, 8, 10, 11] one-hour period of tellurium. This abrupt initial rise has been observed by us on other growth curves, and is more pronounced when the separations are made very soon after the bombardment ceases. This rapid growth at the beginning cannot be spurious because of incompletely separated iodine made directly through Te(d, n)I, since the other directly formed iodine activities (25 minutes and 13 hours) do not appear in the growth fractions.

If it is true that the 8-day iodine grows from the one-hour as well as the 1.2-day period, then these two activities must be isomers and may be assigned definitely to Te^{129}, since the one-hour activity has been produced by 17 Mev gamma-rays on tellurium, through $Te^{130}(\gamma, n)Te^{129}$. (Our unpublished work on radioactive tellurium has shown that the one-hour period must be assigned to Te^{129} rather than to Te^{127} or Te^{121}.)

Our decay curves of active tellurium, after neutron or deuteron bombardments, suggest confirmation of a tellurium activity with the predicted half-life of a little over a day, but the analysis is complicated and somewhat uncertain, because of the presence of the first growing and then decaying 8-day iodine period intermixed with many strong true tellurium activities.

To capitulate this discussion of the 8-day iodine: it is produced by direct transmutation of tellurium,

$$_{52}Te^{128 \text{ or } 130} + {}_1D^2 \rightarrow {}_{53}I^{129 \text{ or } 131} + {}_0n^1,$$

followed by

$$_{53}I^{129 \text{ or } 131} \rightarrow {}_{54}Xe^{129 \text{ or } 131} + {}_{-1}e^0 \text{ (8.0 days)}.$$

It can also be obtained as a double decay after

[10] Bothe and Gentner, Naturwiss. **25**, 191 (1937).
[11] Heyn, Nature **139**, 842 (1937).

either of two primary processes:

$$_{52}Te^{128 \text{ or } 130} + {}_{1}D^{2} \rightarrow {}_{52}Te^{129 \text{ or } 131} + {}_{1}H^{1}$$

or $$_{52}Te^{128 \text{ or } 130} + {}_{0}n^{1} \rightarrow {}_{52}Te^{129 \text{ or } 131} + \gamma,$$

followed by

$$_{52}Te^{129 \text{ or } 131} \rightarrow {}_{53}I^{129 \text{ or } 131} + {}_{-1}e^{0}$$

($\sim$1.2 days and perhaps one hour)

and

$$_{53}I^{129 \text{ or } 131} \rightarrow {}_{54}Xe^{129 \text{ or } 131} + {}_{-1}e^{0}$$ (8.0 days).

If it is true that the iodine grows from the one-hour tellurium as well as from the 1.2-day tellurium, then the chain of decay can be definitely assigned to $Te^{129} \rightarrow I^{129} \rightarrow Xe^{129}$. An unambiguous check on this would lie in a deuteron bombardment of xenon, since the (d, α) reaction could lead to I^{129} but not to I^{131}, because stable Xe^{131} exists while stable Xe^{133} is unknown. We have little hope of accomplishing this with the 8 Mev deuterons available, since it is our experience that the (d, α) reaction becomes rapidly less efficient as one progresses up the periodic table, and we are not definitely sure of its occurrence even as far up as tin, four elements below xenon.

The characteristics of the radiations of the 8-day iodine are shown in Fig. 8. The electrons have a range of 0.50 ± 0.04 gram per cm^2 Al, or an energy[4] of 1.24 Mev. The gamma-ray is absorbed to half-value by 3.3 grams per cm^2 Pb, which indicates[7] an energy of 0.4 Mev.

Radioactive Isotope I^{130}: From Te+D; Half-Life 12.6 ± 1.0 Hours (−)

The bombardment of tellurium with 8 Mev deuterons gives rise to a chemically identified iodine isotope with half-life about 13 hours, as we have briefly reported.[9] The emitted particles are negative electrons with a normal type of absorption curve. Since this period is not obtained by very intense bombardment with fast or slow neutrons, it cannot be due to I^{126} or I^{128}, and since it is not produced by activating antimony with alpha-particles (see above) it cannot be assigned to I^{124} or I^{126}. The remaining iodine isotopes that could be electron emitters are I^{129}, I^{130} and I^{131}. If it is due to either the first or third of these, the 13-hour activity should be found growing from radioactive Te^{129} or Te^{131} and hence also should be produced by irradiating tellurium with neutrons. (We have found strong activities corresponding to both Te^{129} and Te^{131} in the tellurium fractions of our deuteron and neutron bombardments of tellurium.) We have not been able to find any trace of this 13-hour period growing in deuteron-activated tellurium, nor do we find it after neutron bombardments of tellurium. We therefore feel confident that it must be assigned to I^{130}, formed in either of these two ways:

$$_{52}Te^{130} + {}_{1}D^{2} \rightarrow {}_{53}I^{130} + 2{}_{0}n^{1}$$

or $$_{52}Te^{128} + {}_{1}D^{2} \rightarrow {}_{53}I^{130} + \gamma,$$

followed by

$$_{53}I^{130} \rightarrow {}_{54}Xe^{130} + {}_{-1}e^{0}$$ (13 hours).

It will be recalled that it also was necessary to postulate the existence of either the $(d, 2n)$ or (d, γ) reaction to explain the production of the 25-minute I^{128} by deuteron bombardment of tellurium (see above).

Figure 10 gives the absorption curves of this 13-hour activity. These data were obtained by taking the difference between corresponding

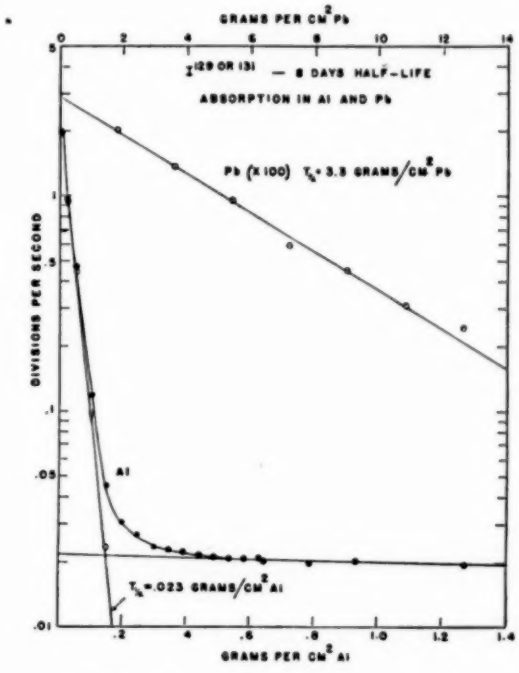
GRAMS PER CM² Pb
I¹²⁹ OR ¹³¹ — 8 DAYS HALF-LIFE
ABSORPTION IN Al AND Pb
Pb (X 100) τ½ = 3.3 GRAMS/CM² Pb
DIVISIONS PER SECOND
Al
τ½ = .023 GRAMS/CM² Al
GRAMS PER CM² Al

FIG. 8. Absorption curves of I^{129} or I^{131}.

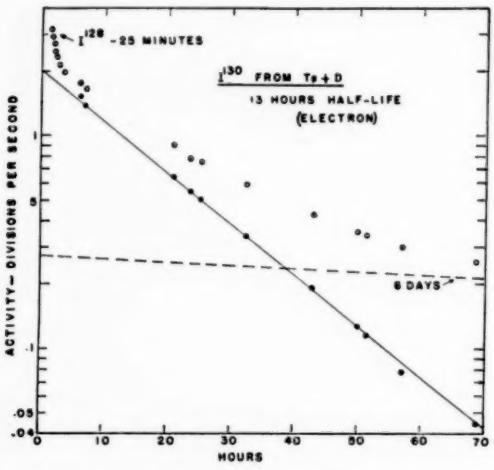

FIG. 9. Decay curve of I^{130}.

readings made (*a*) when the activity was composed of both the 13-hour and 8-day periods and (*b*) when only the 8-day period was existent; these latter figures were corrected for decay back to their appropriate values at the earlier date. The electrons show a maximum range of 0.40 ±0.02 gram per cm² Al, or an energy[4] of 1.05 Mev, while the gamma-ray, showing a half-thickness of 6.0 grams per cm² Pb, has an energy[7] of 0.6 Mev.

TABLE I. *Transmutations and thick target yields.*

HALF-LIFE	REACTION	PROJECTILE ENERGY	PROJECTILES PER ACTIVE NUCLEUS
8 days	$Te^{128, 130}(d, n)I^{129, 131}$	8 Mev	5×10^6
25 min.	$Te^{128}(d, 2n)I^{128}$	8 Mev	2×10^7
13 hours	$Te^{130}(d, 2n)I^{130}$	8 Mev	1×10^7
4 days	$Sb^{121}(\alpha, n)I^{124}$	16 Mev	2×10^7
13 days	$Sb^{123}(\alpha, n)I^{126}$	16 Mev	1×10^7

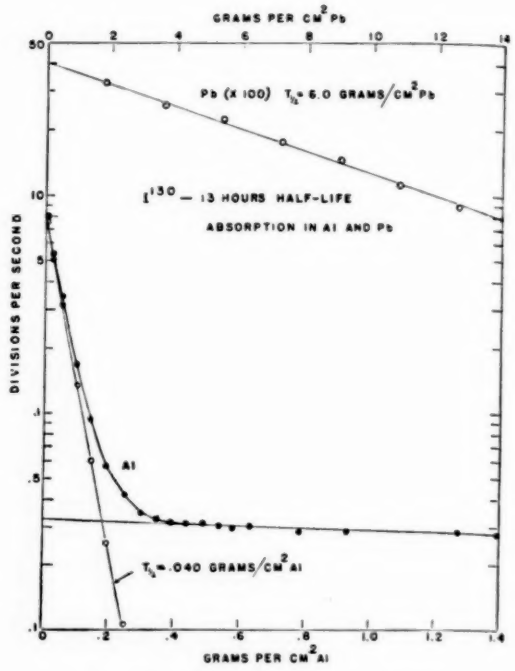
GRAMS PER CM² Pb
Pb (X 100) $T_{1/2}$ = 6.0 GRAMS/CM² Pb
I^{130} — 13 HOURS HALF-LIFE
ABSORPTION IN Al AND Pb
DIVISIONS PER SECOND
Al
$T_{1/2}$ = .040 GRAMS/CM² Al
GRAMS PER CM² Al

FIG. 10. Absorption curves of I^{130}.

YIELDS

In Table I are given the approximate yields for thick targets, corrected for the abundance in nature of the primary isotope involved. These figures have been derived from the duration and intensity of the bombardment, and the initial activity and an approximate calibration of the electroscope, and because of uncertainties in these factors, are necessarily rough.

We are happy to acknowledge the generous support of the Research Corporation and the Chemical Foundation which made this work possible. The work was facilitated by W.P.A. assistance.

Grain-Spacing of Alpha-Ray, Proton and Deuteron Tracks in Photographic Emulsions

T. R. Wilkins and H. J. St. Helens
University of Rochester, Rochester, New York

A statistical study has been made of the grain-spacing of alpha-ray, deuteron and proton tracks in an Ilford *R* 2 emulsion with standardized processing and viewing technique. The alpha-rays were from ThC and ThC′ and the deuterons and protons from cyclotrons. A theoretical explanation of the difference in grain spacing is given and some applications of the technique in the study of cosmic rays and nuclear research.

FOR nearly thirty years it has been known that alpha-particles in passing through photographic emulsions make tracks consisting of rows of silver grains.[1] These tracks can be seen if the emulsion is developed and viewed through a microscope with magnification and illumination adequate to reveal the individual grains. A fine-grained emulsion of the process (or lantern slide) type with average grain size of somewhat less than 10^{-4} cm radius gives well-defined tracks of rather uniformly spaced grains as shown in Fig. 1. A statistical study of the spacing of the grains in these alpha-ray tracks was made by W. Michl[2] as early as 1912. He concluded (a) that the number of silver grains in a track was directly proportional to the length of the track and (b) that both the number of silver grains in the tracks and the lengths of the tracks were directly proportional to the residual air range which the particles had on entering the emulsion.

More recently tracks due to protons (obtained by bombarding beryllium by alpha-particles) were studied.[3] It was noticed by all workers (a) that the grain-spacing was distinctly larger for proton tracks than for alpha-rays, (b) that the spacing was not uniform but was greater the higher the speed of the particle and (c) that the actual spacing depended on the photographic emulsion used.

Obviously if the photographic emulsion was found to distinguish thus simply between these fundamental atomic particles of nuclear physics, it became highly important to obtain data on grain-spacing for some standard emulsion, processing, and viewing technique, and secondly to attempt to formulate some theoretical explanation for this variation in spacing which was so unexpected by those who thought that either type of projectile must affect the same number of grains in a given length, *viz.* the number which were encountered by the particle—a supposedly fixed number for a given emulsion.

In addition to a study of the spacing in alpha-particle and proton tracks the present work includes data on deuteron tracks not previously reported. The emulsion chosen as a standard was the Ilford R2 which was found to have the right grain size to give tracks for all three types of particles.

Exposure of the Plates

Alpha-rays

Two plates of usual microscope slide size (1×3 inches) were stood on edge, emulsion to

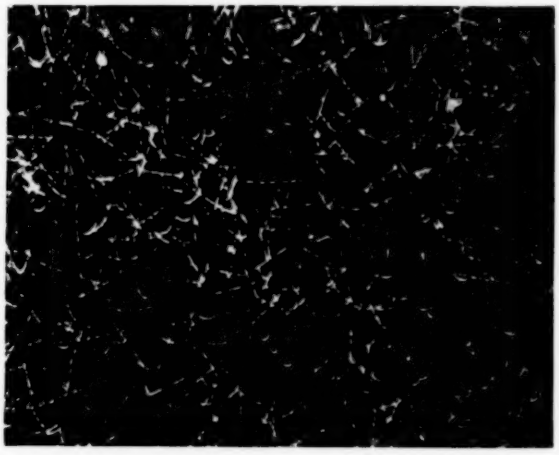

Fig. 1. ThC′ and ThC tracks in the Ilford R2 emulsion. (mag. 225 diam.)

[1] O. Mugge, Zentralbl. f. Mineralogie **71**, 144–147 (1909).
[2] W. Michl, Akad. Wiss. Wien Ber. IIa **121**, 1431–1447 (1912).
[3] E. Mühlestein, Arch. d. Sci. Phys. et Nat. **4**, 38–63 (1922). M. Blau, Mitt. d. Ra. Inst. Nr. 179 (1925); 208 (1927), 259 (1930); Zeits. f. Physik **34**, 285–295 (1925); Akad. Wiss. Wien Ber. IIa, **134**, 407–436 (1925); IIa, **136**, 469–480 (1927); IIa, **139**, 327–347 (1930). A. Jdanoff, J. de phys. et le rad. **6**, 233–241 (1935). H. J. Taylor, Proc. Roy. Soc. **A150**, 382–394 (1935).

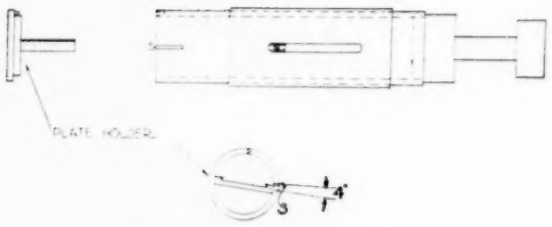

FIG. 2. Camera for cyclotron.

emulsion, and separated by a few thousandths of an inch. A button coated with the active deposit from thorium emanation gave a source of ThC and ThC′ alpha-particles. This button held immediately below the edge of the plates for about one minute gave several hundred quite flat tracks in the emulsions.

Protons and deuterons

The sources of protons and deuterons were the cyclotrons at the University of Rochester and Michigan, respectively. The plates were exposed in a simple sliding-tube "camera" shown in Fig. 2 which could be placed in the beam. The plateholder *P* fits into the camera tube so that the stream of particles which enters the camera from the side through the fine slot *s* strikes the plate at an angle of about four degrees to the surface of the emulsion. In this way flat tracks are secured. The outer tube provides a tight cover except during the instant of exposure. Because of the intensity of the cyclotron beams the exposures must be as short as possible.

PROCESSING AND VIEWING TECHNIQUE

The plates were processed in an Elon-hydroquinone process developer (Kodak formula D-11) for 3 min. at 65°F, and fixed in an acid hardening fixing bath (Kodak formula F-5). After washing and drying, the plates were mounted on a microscope equipped with a dark-field (cardioid) condenser, a 4 mm (N.A. 0.85) dry objective (uncorrected for cover-glass) and a 20× hyperplane eyepiece with an eyepiece scale of 100 divisions, each interval covering 2.35 microns on the microscope stage. The objective was equipped with a variable iris diaphragm which varied the illumination and the depth of field. The magnification of the complete system was 900 diameters. Tracks photographed through such a system are almost restored to air-ranges since the stopping power of this emulsion as compared with air for alpha-rays is about 1380. An oil-immersion objective increases the magnification about twice but its use necessitates the placing of oil on the surface of the emulsion. During the removal of this oil the emulsion tends to become scratched. The advantage that an oil-immersion objective has over an ordinary 4-mm objective with respect to differential focusing is almost completely overcome by the addition of the variable diaphragm in the tube of the 4-mm objective. A thin film of oil of cedar was used between the dark-field condenser and the glass side of the photographic plates.

If dark-field illumination is used the thickness of the plate must be such that the cone of light from the condenser comes to a focus in the emulsion. The emulsions were therefore coated for us by the manufacturer on glass about 1 mm thick.

EXAMINATION OF PLATES

The three types of tracks were examined under a magnification of 900 diameters. The variable diaphragm was set fairly wide open so that shallow focusing was obtained. Only those tracks which were entirely in focus under this condition were measured. The directions of the tracks were known from the method of exposure. All measurements were made from the slow end of the track. The number of grains in each five divisions of the eyepiece scale was counted. Data were obtained on approximately 260 tracks of each of the three radiations studied. All the data for the proton and deuteron tracks came from single plates while the data for the alpha-particles are from two plates exposed and processed together.

TABLE I. *Group data for alpha-particle tracks. Arithmetic means of grain number between scale divisions (1 eyepiece scale div. = 2.35 microns).*

GROUP	NO. OF TRACKS	NO. OF GRAINS IN SUCCESSIVE SECTIONS OF TRACKS 0–5	5–10	10–15	15–20	20–25	25–30	30–35
I	3	8.7						
II	60	8.5	7.0					
III	12	8.3	7.2	7.0				
IV	127	8.3	7.0	6.7	6.5			
V	58	7.9	7.0	6.6	6.6	6.8		
VI	0							
VII	1	7.0	6.0	4.0	5.0	5.0	4.0	7.0

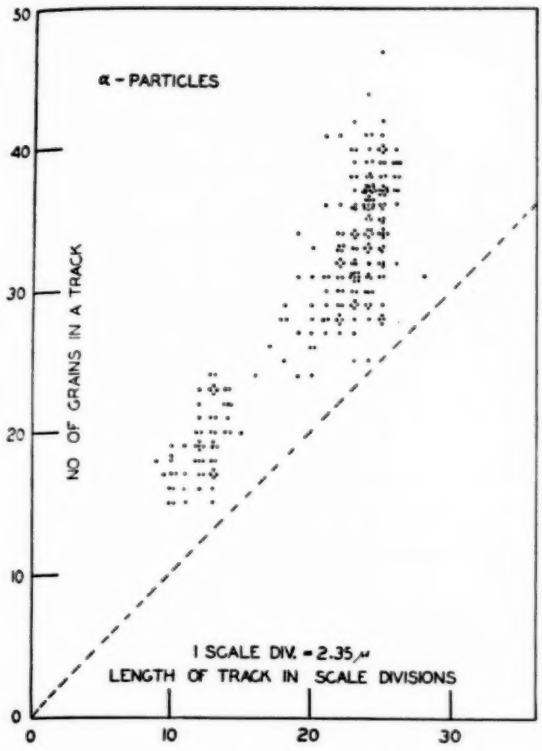

FIG. 3. Distribution of data for alpha-tracks.

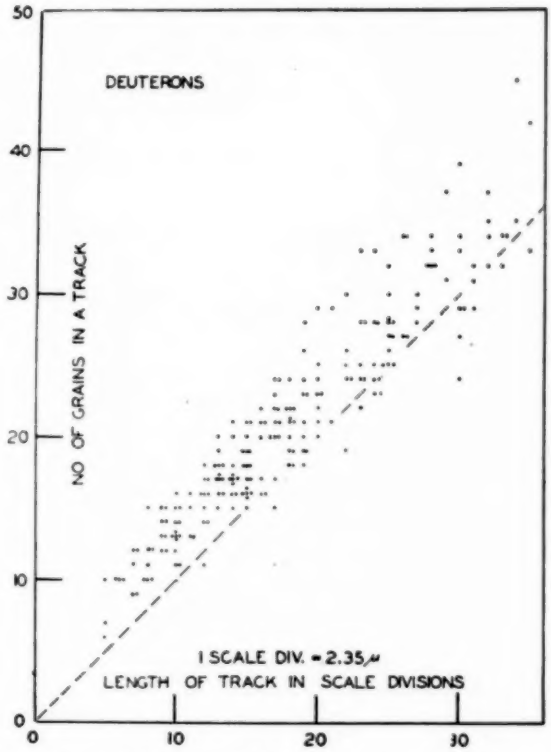

FIG. 4. Distribution of data for deuteron tracks.

RESULTS

The data are grouped according to the length of the tracks. Group I refers to those tracks whose lengths, l, satisfy the condition 5 div. $\leqq l < 10$ div. For Group II 10 div. $\leqq l < 15$ div., etc. The arithmetic means of the numbers of grains in each group were computed and are summarized in Tables I–IV. The distribution of the data is shown in Figs. 3, 4 and 5. A rather clear separation is shown for alpha- and proton tracks even in this distribution data. The data are averaged in Fig. 6 and well-separated curves are shown passing nicely through the observed values.

The average grain separations, obtained by dividing the track length by the number of grains minus one, are summarized in Table V.

TABLE II. *Group data on deuteron tracks.*

Group	No. of Tracks	No. of Grains in Successive Sections of Tracks							
		0–5	5–10	10–15	15–20	20–25	25–30	30–35	35–40
I	37	7.4							
II	60	7.3	5.7						
III	64	7.3	5.4	5.0					
IV	37	7.0	5.4	5.3	4.8				
V	32	7.1	5.6	5.0	4.4	5.3			
VI	23	7.2	5.4	4.7	4.4	4.7	4.9		
VII	5	7.2	5.4	5.2	5.6	4.8	4.4	5.0	
VIII	1	6.0	4.0	2.0	5.0	5.0	4.0	4.0	7.0

TABLE III. *Group data for proton tracks.*

Group	No. of Tracks	No. of Grains in Successive Sections of Tracks			
		0–5	5–10	10–15	15–20
I	60	5.8			
II	89	5.3	4.1		
III	76	5.2	3.7	4.2	
IV	36	5.2	3.6	3.5	3.5

TABLE IV. *The average number of grains in successive sections of tracks.*

	Av. No. of Grains in Successive Sections of Tracks							
	0–5	5–10	10–15	15–20	20–25	25–30	30–35	35–40
Alpha-Particles	8.3	7.0	6.7	6.5	6.8			
Deuterons	7.2	5.5	5.0	4.6	5.0	4.8	4.8	7.0
Protons	5.4	3.9	4.0	3.5				

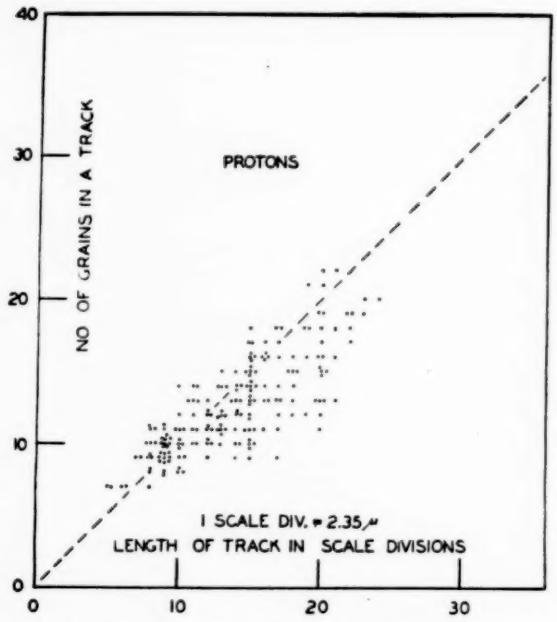

FIG. 5. Distribution of data for proton tracks.

SUGGESTED THEORY OF VARIATION IN GRAIN-SPACING

In his derivation of the equations for the photographic density produced by alpha-rays falling on a photographic emulsion, Wilkins[4] assumed that the alpha-particle rendered a grain developable if it came within a radius of action ρ and showed that this distance for the grains in the process emulsion used was about 0.6×10^{-4} cm at room temperature. The grain is pictured as becoming developable because the "impulse" (force × time) exerted on an electron in the halide grain is able to eject an electron and ionize the grain. The radius of action will thus be a function of the speed of the projectile. The decrease in grain spacing results because as the projectile slows down, the radius of action is increased. Thus surrounding the track of an atomic projectile we have a cone of action, smaller when the speed of the particle is large and increasing in radius as the particle slows down.

TEST OF THEORY

A. Comparison of alpha- and proton spacing

The equation given by Bloch for the rate of loss of kinetic energy T by a particle of charge e and velocity V passing through a medium consisting of atoms of nuclear charge Ze is

$$-\frac{dT}{dx}=\frac{4\pi e^2NZ^2e^2}{mV^2}\log\frac{4\pi mV^2}{kZRh},$$

where Z is the atomic number of the element, R the Rydberg constant, N the Loschmidt number, k an undetermined constant, and m the mass of the electron.[5] From this equation, it will be noticed: (1) that the rate of loss of energy by an alpha-particle will be four times as great as for a proton of the same speed; (2) that since an alpha-particle has four times as much energy as a proton of the same velocity, but loses this energy at four times the rate, the ranges will be equal. We can, therefore, compare alpha-particles and protons of the same residual range and assume that their speeds are the same.

Calculation of radius of action and relative grain-spacing.—The force exerted by a projectile of charge E on an electron of charge e at a distance ρ is Ee/ρ^2 and the impulse is Ft. At the limiting distances ρ_α, and ρ_p the impulses due to an alpha-particle and a proton are to be equal but since the speeds are equal, we write

$$2e\cdot e/\rho_\alpha{}^2=e\cdot e/\rho_p{}^2,$$

whence

$$\rho_\alpha{}^2=2\rho_p{}^2$$

and hence the number of grains per unit path (being proportional to ρ^2) will have the ratio

$$n_\alpha=2n_p.$$

The grain-spacing is not exactly the reciprocal of the number of grains per unit path but is obtained by dividing the length of path by $n-1$. Thus the grain-spacing of protons should

TABLE V. *The average grain separation (in microns) (1 eyepiece div. = 2.35 microns).*

	AV. GRAIN SEPARATION IN TRACKS OF LENGTH					
	5	10	15	20	25	30
Alpha-Particles	1.61	1.65	1.69	1.72	1.74	
Deuterons	1.90	2.0	2.12	2.23	2.26	2.33
Protons	2.68	2.89	2.98	3.17		

[4] S. E. Sheppard, T. R. Wilkins, E. P. Wightman, and R. N. Wolfe, Kodak Research Lab. Comm. No. 590; J. Frank. Inst. **222**, 417–460 (1936).

[5] See also M. S. Livingston and H. A. Bethe, Rev. Mod. Phys. **9**, 266 (1937).

be approximately double that for alpha-particles. This ratio will be more exact for very fine grain emulsions where the increase in radius of action is able to bring an observable increased number of grains into the cone.

Observed values for alpha-particles and protons.—The data of Table VI are taken from Fig. 6 showing the average number of grains as a function of track length. These results are in good qualitative agreement with the predicted value of 2.0. For better quantitative agreement finer grained emulsions would be required, but unfortunately proton tracks are not secured when the grain size gets much smaller. It must be remembered, too, that photographic grains have fairly wide fluctuations in size and irregularity in position.

B. Comparison of proton and deuteron spacing

The values in Table VII are taken or calculated from Fig. 21 of Livingston and Bethe. From this it is seen that the ratio of proton to deuteron velocities does not change rapidly and can be taken as 1.25 in the range of our measurements.

Using the impulse equation as above

$$ee/\rho_p^2 \cdot 1/V_p = ee/\rho_d^2 \cdot 1/V_d$$

whence

$$\rho_d^2/\rho_p^2 = V_p/V_d = 1.25.$$

Since the number of grains is proportional to ρ^2, it follows that

$$n_d = 1.25 n_p$$

and this will also be the approximate value for the relative grain-spacings. Again it will be noted that the observed values are in good qualitative agreement with the calculated ones. The theory has predicted that deuteron spacing should lie between the spacings for alpha-particles and protons, and this is in accord with the observations.

TABLE VI. *Average number of grains as a function of track length for alpha-particle and deuteron tracks.*

Range in Emulsion	n_α	n_p	Observed n_α/n_p	Calculated n_α/n_p	Percent Difference
23.5μ	15	9	1.7	2.0	15
35	22	13	1.7		15
47	28	16	1.8		10
59	35	(19)	1.8		10

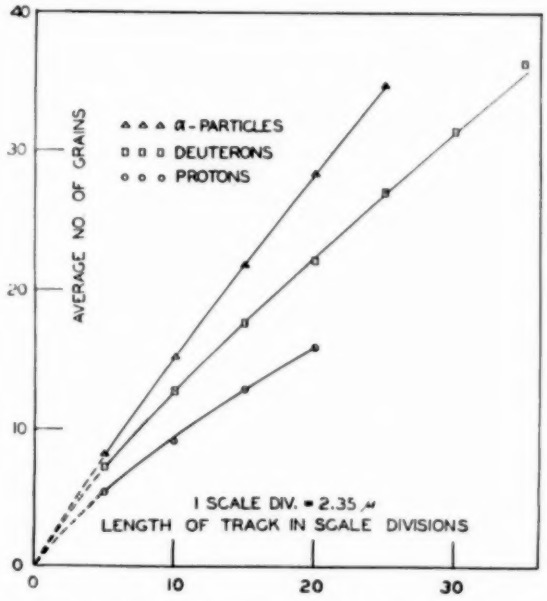

FIG. 6. Comparative spacing of alpha-, deuteron, and proton tracks.

Some examples of the use of the grain-spacing technique.—We have used grain-spacing in a number of cases to identify the nature of particles. For example, plates sent into the stratosphere were found to have numbers of very long tracks whose spacing showed them to be caused by alpha-rays presumably ejected in the emulsion by cosmic rays.[6] Fig. 7 shows a phe-

TABLE VII. *Ratio of proton and deuteron velocities at equal ranges.* (From Livingston and Bethe, reference 5, Fig. 21.)

Mean Range (Air)	Energy in Mev Protons	Deuterons	V_p/V_d
2 cm	0.91	1.12	1.28
3	1.19	1.50	1.26
4	1.42	1.82	1.25
5	1.62	2.11	1.24
6	1.81	2.37	1.24

TABLE VIII. *Average number of grains as a function of track length for deuteron and proton tracks. (Calculated value of n_d/n_p 1.25.)*

Range in Emulsion	n_d	n_p	Observed n_d/n_p	Difference
23.5μ	13	9	1.4	11%
35	18	13	1.4	11%
47	22	16	1.4	11%
59	27	(19)	1.4	11%

[6] T. R. Wilkins, Nat. Geog. Soc. Stratosphere Series 2, 37 (1936); T. R. Wilkins and H. J. St. Helens, Phys. Rev. **51**, 1026 (1937).

nomenon first reported by us for plates sent up in balloons and especially in plates exposed for some months at the high altitude cosmic-ray station at Mt. Evans, Colorado, in 1936. Groups of tracks whose spacing shows them to be due to protons are seen to originate in a common point below the emulsion (in the glass or the binder). These groups are probably identical with those observed by Brode, MacPherson and Starr[7] in a cloud chamber. Similar tracks have more recently been found by M. Blau and H. Wambacher.[8]

FIG. 7. Typical proton groups ejected by cosmic rays in plates exposed on Mt. Evans.

FIG. 8. A typical disintegration in a lithium impregnated emulsion exposed to neutrons. One track *B* has typical alpha-spacing; the other track *A* (only part of which is shown in the photograph) has greater spacing. (Mag. 900 diam.)

Many such groups have been found on our Mt. Evans plates. They have also been recently reported by Filippov, Gdanow and Gurevich.[9]

Figure 8 shows a typical disintegration of lithium (incorporated in a photographic emulsion) by neutron bombardment. The difference in the spacing of the alpha-particle track and the other (presumably H_3) is apparent.

In the case of tracks which do not lie flat in the emulsion, the correct grain spacing may be obtained by measuring the dip or by taking stereoscopic pictures. The theory for such orthostereoscopic photographs has been developed by Martin and Wilkins.[10]

Our thanks are due to Dr. J. M. Cork of the University of Michigan for his cooperation in the securing of the deuteron tracks and the neutron disintegrations.

[7] R. B. Brode, H. G. MacPherson and M. A. Starr, Phys. Rev. **50**, 581 (1936).
[8] M. Blau and H. Wambacher, Nature **140**, 585 (1937).
[9] A. Filippov, A. Gdanow and I. Gurevich, C. R. Acad. Sci. USSR, **18**, 181 (1938).
[10] L. C. Martin and T. R. Wilkins, J. Opt. Soc. Am. **27**, 340 (1937).

X-Ray Evidence on the Nature of the Surface Layers of Thin Ground Quartz Crystals Secured with the Cauchois Spectrograph

F. R. HIRSH, JR. AND J. W. M. DUMOND
California Institute of Technology, Pasadena, California

(Received August 15, 1938)

Spuriously doubled lines observed in spectra formed by the Cauchois transmission-type curved-crystal focusing spectrograph have been reported by several investigators. B. B. Watson has shown the varying separation of these doublets in several orders to be consistent with the assumption that they are caused by enhanced intensity of reflection in the front and back surface layers of the crystal lamina where its structure has been disturbed by grinding. The enhancement of x-ray reflection by grinding, polishing or other mechanical disturbance is already well known. The present authors note that the more roughly ground of two surfaces on the curved crystal gives rise to the more intense member of the spurious doublet and that heavy etching of the ground quartz surface with hydrofluoric acid suppresses the surface reflection. Cauchois has pointed out that an initially flat crystalline lamina subjected to elastic bending to a circular cylindrical curved form should (approximately) focus the selectively reflected radiation not only from various parts of the arc *but also for all regions of the finite thickness of the slab;* the second type of focusing is a result of the elastic change in grating constant at points off the neutral axis of the curved slab. The single lines we obtain with curved slabs that have been etched confirm the reality of this type of focusing. We draw the conclusion that the surface layer responsible for the enhanced x-ray reflection must have three interesting properties: (1) The mechanical stress and consequent strain, incident to bending, existing in the main body of the crystal is not shared by this surface layer which thus seems to be differentiated from the rest; (2) the surface layer is crystalline, however, and has the grating constant of unstrained quartz; (3) in spite of their disturbance the atomic planes in this surface layer must have with surprising accuracy the same average orientation as the planes in the main body of the supporting crystal. These properties differing from those to be expected for the amorphous glass-like layers first postulated by Sir George Beilby suggest a recrystallization of the displaced atoms on the underlying crystal foundation such as Finch has proposed.

THE SPURIOUSLY DOUBLED SPECTRAL LINES OBSERVED WITH THE CAUCHOIS FOCUSING SPECTROGRAPH

EARLY in 1934 in these laboratories B. B. Watson, in studies with a Cauchois transmission-type curved-crystal spectrograph, observed that all the lines exhibited a very fine doublet structure.[1] Watson's measurements on the different separations of these doublets in different orders and at different angles gave satisfactory quantitative proof that they result from enhanced intensity of reflection in the regions of the crystal very close to its front and back or exit and entry surfaces and the reader is referred to his paper[1] for this proof.

In conversations with Y. Cauchois last year in Paris one of us learned that she and her co-worker H. Hulubei have also observed these double lines. Interested in the many beautiful applications of this instrument in x-ray spectroscopy, Mlle. Cauchois said that they had merely rejected crystals giving such doubled lines as useless for their purposes. It is interesting to note that they succeeded in getting laminae which did not give the doubling. We have also found a crystal lamina ground at this Institute by Mr. Max Kelch which did not exhibit the double lines and we conclude that the method of grinding or polishing has much influence in this respect.

[1] Watson described his researches on these double lines in complete detail in his doctorate thesis (1935) and later gave a brief account of his measurements proving their origin in a paper "Development of a Curved Quartz Crystal X-Ray Spectrograph and a Determination of the Grating Constant of Quartz." B. B. Watson, Rev. Sci. Inst. **8**, 480 (1937).

FOCUSING OF RADIATION REFLECTED IN REGIONS OF THE CURVED CRYSTAL OFF ITS NEUTRAL AXIS

Cauchois was, we believe, the first to recognize a new type of focusing to be expected in the curved transmission-type lamina. Not only should the radiation selectively reflected in different regions of the curved arc focus to the same point [2] on the focal circle *but also radiation re-*

[2] This focusing is, of course, approximate subject to certain aberrations which can be minimized very satisfactorily.

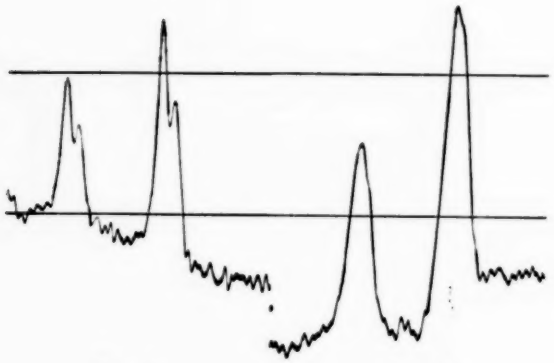

FIG. 1.

FIG. 2.

FIG. 1. Illustrating the spuriously doubled spectral lines caused by enhanced reflection in the disturbed surface layers of the crystal.

FIG. 2. Showing the result of etching the crystal heavily with hydrofluoric acid. This is otherwise the same crystal whose spectral lines were shown in Fig. 1.

flected throughout the entire finite thickness of the crystal should be similarly brought to a focus. This latter type of focusing is the result of the change in grating constant resulting from the elastic strain set up in regions of the crystal off its neutral axis when it is bent. The grating constant on the outside of the curve, increased by the tension, reflects with a slightly smaller Bragg angle, and the grating constant on the inside, diminished by compression, reflects with a slightly greater angle in just the right degree to focus the radiation reflected from all regions of the thickness of the lamina to the same point on the focal circle as does the crystalline structure on the unstressed neutral axis of the crystal.

Cauchois has obtained crystal laminae which give exceedingly fine single spectral lines, conclusively supporting her second type of thickness focusing by elastic strain, and the fact that the enhanced reflection from front and back surface layers of our ground crystals does not obey this focusing law, but on the contrary gives doubled lines in the position to be expected if the grating constant for the surface layers had its normal unstressed value becomes, therefore, very interesting.

THE EFFECT OF ROUGHNESS OF GRINDING

Recently with radiation from a molybdenum target tube we have noted in another curved-crystal spectrograph of similar design and 15-inch crystal radius of curvature, the same doubling of the spectral lines. (See Fig. 1.) This crystal sample gave the component of the doublet on the short wave-length side less intense than the other one (the two doublet components are, of course, of the same wave-length), and we noted that the concave side of the crystal was not as roughly ground as the convex side indicating that the enhanced reflection from the rougher surface layer was the more intense. The enhanced intensity of selective x-ray reflection from the surface of a crystal which has been disturbed by grinding or polishing is a well-known effect noted by many observers.[3]

THE EFFECT OF ETCHING

We next tried etching[4] the crystal slab with hydrofluoric acid and found that after heavy etching scarcely a trace of the double nature of the lines remained (50 percent H_2F_2 for 42 hours). See Fig. 2.

Lighter etching on another crystal slab gave lines with a broadened and serrated profile. Pre-

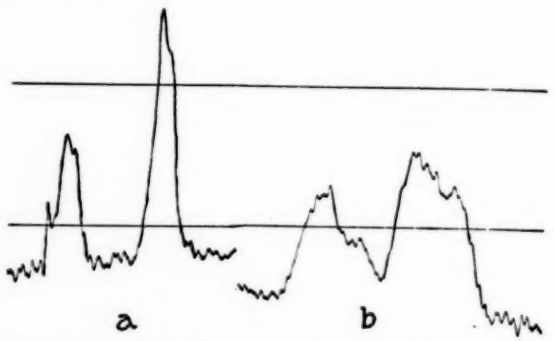

FIG. 3. (a and b) Showing the result of lighter etching on a different crystal slab from the one whose lines appear in Figs. 1 and 2.

[3] C. C. Murdock, Phys. Rev. **45**, 117 (1934), has reported *triple* Laue spots from plane unstressed quartz lamina which he attributed to two surface reflections and reflection from the interior of the slab. Sakisaka reports a similar finding regarding the surface reflections. I. Sakisaka *et al.*, Inst. Phys. and Chem. Res., Tokyo, Sci. Papers, No. 526, pp. 20–30 (1934). D. L. Webster reported in discussion having noticed the same phenomenon. DuMond and Bollman have found that even in cleaved calcite slabs with excellent cleavage surfaces untouched by grinding or polishing an analogous but not identical phenomenon of enhanced Laue reflection from regions near the surface occurs. DuMond and Bollman, Phys. Rev. **50**, 97 (1936); **50**, 524 (1936).

[4] It is well known that etching a disturbed crystal surface will remove the disturbed portions. K. V. Manning has given specifications for etching cleaved or polished calcite surfaces so as markedly to reduce the "rocking curve" width obtained with this crystal in the parallel position in the two crystal spectrometer. K. V. Manning, Rev. Sci. Inst. **5**, 316 (1934).

sumably the disturbance of the ground surface layer when the latter is incompletely removed by the acid may be seriously increased by undercutting and loosening. Fig. 3a shows the lines obtained with this slab before etching while Fig. 3b shows this broadening effect of the light etching.

Figure 4 shows the paths of the rays for the two types of reflection *viz.* reflection from a surface layer with normal grating constant and reflection from the interior of the crystal brought to a focus by the change in grating constant due to bending strain. This sketch idealizes the actual case, the focusing due to strain in the case of etched crystals is less sharp than here shown probably because of the large surface irregularities and pits formed by the etching action. These irregularities which are a decent fraction of the thickness of the slab in depth undoubtedly introduce local irregularities of strain; the peaks of the prominences are practically without strain while the valleys may be strained well in excess of the maximum value to be expected if the surface of the slab were smooth.

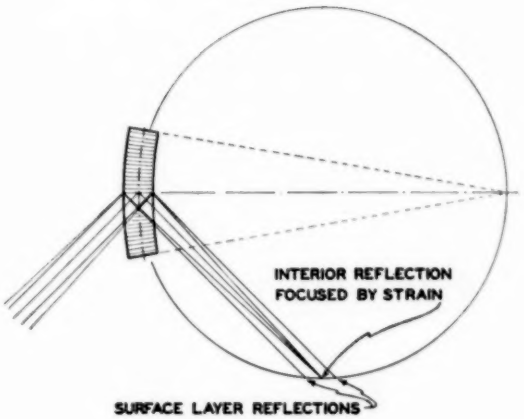

FIG. 4. Showing the paths of the x-rays for the interior reflection focused by strain and for the layers on the surface which apparently do not experience the strain and hence do not focus the radiation. Here the crystal thickness is greatly exaggerated.

USE OF OTHER CRYSTAL PLANES

The (310) planes of quartz have been recommended to one of us by Cauchois and Hulubei as having a very favorable combination of small grating constant and strong reflection and we also have tried a crystal lamina cut and bent to utilize these planes. This lamina gave similar results regarding the doubled lines. These planes are considerably superior to the basal planes for spectroscopic work although the ratio of intensity in the curved-crystal spectrograph is not as high for the two sets of planes as the structure factors might lead one to expect.

CONCLUSIONS

We believe that these observations warrant the following conclusions as to the nature of the material on the ground quartz surface:

1. The mechanical stress and consequent strain, incident to bending existing in the main body of the crystal, is not shared by this surface layer which seems thus to be physically differentiated from the remainder. Such a differentiation might be ascribable to a weaker attachment of the surface layer to the under structure or to a discontinuous nature of the surface layer or both.

2. The surface layer is nevertheless crystalline and has the grating constant of normal unstrained quartz.

3. In spite of their having been disturbed, the atomic planes in this surface layer must have with surprising accuracy the same orientation as the planes in the main body of the supporting crystal. (In so perfect a crystal as quartz a disturbance of orientation of only a few seconds of arc would suffice to cause considerable enhancement of reflected intensity.) Other Miller indices in quartz correspond to planes all of which have quite different grating constants from the basal planes and we conclude that the surface layer must have its crystalline axes orientated in just the same way as the main body of the crystal.

All this seems to indicate that the surface layer in our ground quartz responsible for the enhanced x-ray reflection is very unlike a liquid or an amorphous glass-like substance such as Beilby postulated. It *may*, however, have been rendered fluid or amorphous by the grinding or polishing action and then it may have recrystallized in the surface fields of the mother crystal during or immediately after the polishing process. These results are in excellent accord with the

conclusions of G. I. Finch[5] from his experiments with electron diffraction.

Quartz has no noticeable plasticity and great cohesive strength so that one would expect this crystal to have a strong aversion to the formation of amorphous or Beilby surface layers. It is even quite possible that the crystalline surface layers we observe are formed by recrystallization as fast as the grinding and polishing action can displace the quartz, either atom by atom, or at least in aggregates so small that cohesive forces are able to capture and orientate them correctly on the surface of the mother crystal.

[5] G. I. Finch, Nature **138**, 1010 (1936); Science Progress (April 1937); Sci. J., Royal College of Science **VII**, 32 (1937); Trans. Faraday Soc. No. 191, **XXXIII**, 425 (1937); Finch, Quarrel and Roebuck, Proc. Roy. Soc. **A145**, 676 (1934).

ACKNOWLEDGMENTS

The writers wish to acknowledge gratefully Mr. R. von Huene's skillful preparation of the thin ground quartz crystals. For the spectrograph used in the later work and one of the quartz lamina we are indebted to the work of Mr. Max Kelch, formerly of this Institute. We are also grateful for the able assistance of Mr. Paul Youtz.

The funds which made possible this research were the gift of Dr. Leon L. Watters of New York City and we are glad of this opportunity to express our appreciation for his aid.

NOVEMBER 15, 1938 PHYSICAL REVIEW VOLUME 54

Exploratory Study of Plural X-Ray Reflection Methods Applied to the Problem of the Diffraction Pattern of Calcite

V. L. BOLLMAN, H. H. BAILEY AND J. W. M. DuMOND
Occidental College, Los Angeles, and California Institute of Technology, Pasadena, California

(Received June 27, 1938)

An exploration of the possibilities and difficulties in the study of the x-ray diffraction patterns of crystals with the method of the plural reflection spectrometer is described. This method, first suggested to the present authors by P. Kirkpatrick, has been analyzed in a recent article[1] by one of us and the present article describes our first attempts to apply these ideas and to refine and extend the suggested methods of the first article. Diffraction patterns of calcite samples for Mo $K\alpha$-radiation were studied with three nearly parallel crystal faces reflecting x-rays in $(1,-1,1)$ order, Allison's notation, or $\{1,1,1\}$ order, DuMond's notation, and it was found that the fillets to be expected as approaches on the sides of the Prins diffraction pattern offer a serious obstacle to the direct use of this simple method. Two methods of circumventing the fillet difficulty are proposed, but not tried. A third method more readily adaptable to the equipment at hand, involving the use of three crystals and five successive reflections, was tried with a fair measure of success. Four successive reflections occur between two nearly parallel adjacent faces of a pair of large calcites. By adjusting these two calcites 1.5 seconds of arc off parallel there is good reason to believe that a narrower "tool" beam with reduced fillets was prepared with which the "object" crystal diffraction pattern was then explored. The observed diffraction patterns for the two calcite object crystals studied are shown. No asymmetry of the top of the pattern could be observed with reproducible certainty but this is to be expected since the theoretical asymmetry for Mo $K\alpha$-radiation in the first order on calcite is very small. An extension of present methods to longer wave-lengths in the vacuum region could quite possibly reveal such asymmetrical pattern shapes for at longer wave-lengths the asymmetry is more marked and the pattern is several times broader.

Our results make it appear very doubtful whether the ideal flat topped diffraction pattern of Prins really obtains at the wave-lengths we have studied, the indications being that the real diffraction pattern has a sharper peak.

INTRODUCTORY

General considerations and terminology

IN a recent paper[1] one of us has proposed a method of improving both the angular and the spectral resolving power of x-ray crystal reflection spectrometers by an extension of the

[1] DuMond, Phys. Rev. **52**, 872 (1937). F. Miller and L. G. Parratt have recently described in a "Letter to the Editor," Phys. Rev. **53**, 200 (1938), a method of determining crystal diffraction patterns with the two-crystal spectrometer which has attractive simplicity from an experimental standpoint. Miller and Parratt point out that for our method to be valid the effect of the wings or fillets must be negligible. The present article recounts how we have accomplished just this with the four-reflection tool. Renninger, Zeits. f. Krist. **A99**, 181 (1938) applying our transparency graph analysis proposes an arrangement $(1,1,\pm1)$ (Allison's notation) in which the first two reflections occur on "very sharply reflecting crystals" while the third crystal is the object of study.

two-crystal spectrometer principle to more than two successive x-ray reflections from two or more crystals. Following Paul Kirkpatrick who first suggested the method, we shall refer to such spectrometers as "plural reflection" spectrometers, or more simply "plural" spectrometers.

The "single crystal diffraction pattern" or simply the "diffraction pattern" of a crystal is an abstraction which we may think of as determined by the following ideal experiment. An extremely well-parallelized beam of highly monochromatized x-rays falls on the reflecting atomic planes of a crystal. The ratio of the reflected to the incident x-ray intensity expressed as a function of the slight angular deviation of the incident beam from the Bragg angle is then the diffraction pattern in the sense used in this paper. The degree of parallelism of the incident beam must be high relative to the angular width of the diffraction pattern so as to exert negligible influence on its shape. An important possibility must not be overlooked. The reflected beam may not be confined to the single direction prescribed by the laws of geometrical optics and dependent on the direction of the incident parallel beam, but will in all probability fill a somewhat larger cone than the latter as physical optics and the imperfect nature of the crystal lattice both lead us to expect. Thus if necessary we could express the intensity reflected (per unit solid angle) as a function not only of θ_1, the incidence angle, but also as a function of θ_2, the reflection angle, and ϕ, the angle of deviation of the plane of reflection from the plane of incidence. The "smearing effect" of such a departure from the ideal geometry of specular reflection, especially as regards θ_2, can, unless it is sufficiently small, invalidate many of our expectations for the plural spectrometer. We shall refer to such a defect as "blurring of the reflected beam" or simply "blurring."

The boundaries of the window on the transparency graph. Effect of using a spectral line

In the previous paper[1] it was pointed out that since there are many traces on the two or more superposed transparency graphs, there will, in general, be many intersections or "windows" corresponding to decidedly different angles and wave-lengths so that unless some means is used to exclude all but one of these windows the observed changes of intensity in the ionization chamber will be difficult to interpret.

In the work to be described we have made use of the Mo $K\alpha$ spectral lines to define the boundaries on the transparency graph. The spectral line in the transparency graph method is represented by a horizontal line source of light behind the entire system of superposed transparency graphs located at an ordinate corresponding to the wave-length of the line and having a vertical breadth and structure descriptive of the natural spectral structure of the line as emitted by the x-ray source. *Thus the use of a natural spectral line limits the utilized length of trace segment to a very short length indeed.*

One is accustomed to think of the energy of the continuous radiation emitted by an x-ray tube as far larger than the energy in the line spectrum and so it is when the entire continuous spectrum *is integrated*. If, however, we ask for the intensity per unit wave-length range, $d\lambda$, in say the core of a line compared to the intensity for the same $d\lambda$ in the adjacent background, the line may easily be many thousand times as intense, and a wave-length range of continuous spectrum very large indeed compared to the line width may well be included without having intensity in the continuous background comparable to the line intensity. We have made an empirical test of this using a horizontal beam width of 20 minutes of arc. The ratio of the intensity when set on the line to that when set on the adjacent background was 1100 : 1, which is notable when we consider the large angular range permitted by the stops so as greatly to favor the continuous spectrum intensity. It should be noted that the tube was running at 40 kilovolts, and the line was thus well excited.

First Trial with Three Crystals

Our first attempt was to study the diffraction pattern of calcite with Mo $K\alpha$-radiation and three successive reflections, {1,1,1} order[2] between nearly parallel calcite faces as explained in

[2] The braces are to indicate DuMond's order notation. In Allison's notation it would be (1,−1,1). The first notation is convenient for determining the resolving power, the second for determining dispersion. For a discussion of the two notations see Phys. Rev. **52**, 884 (1937).

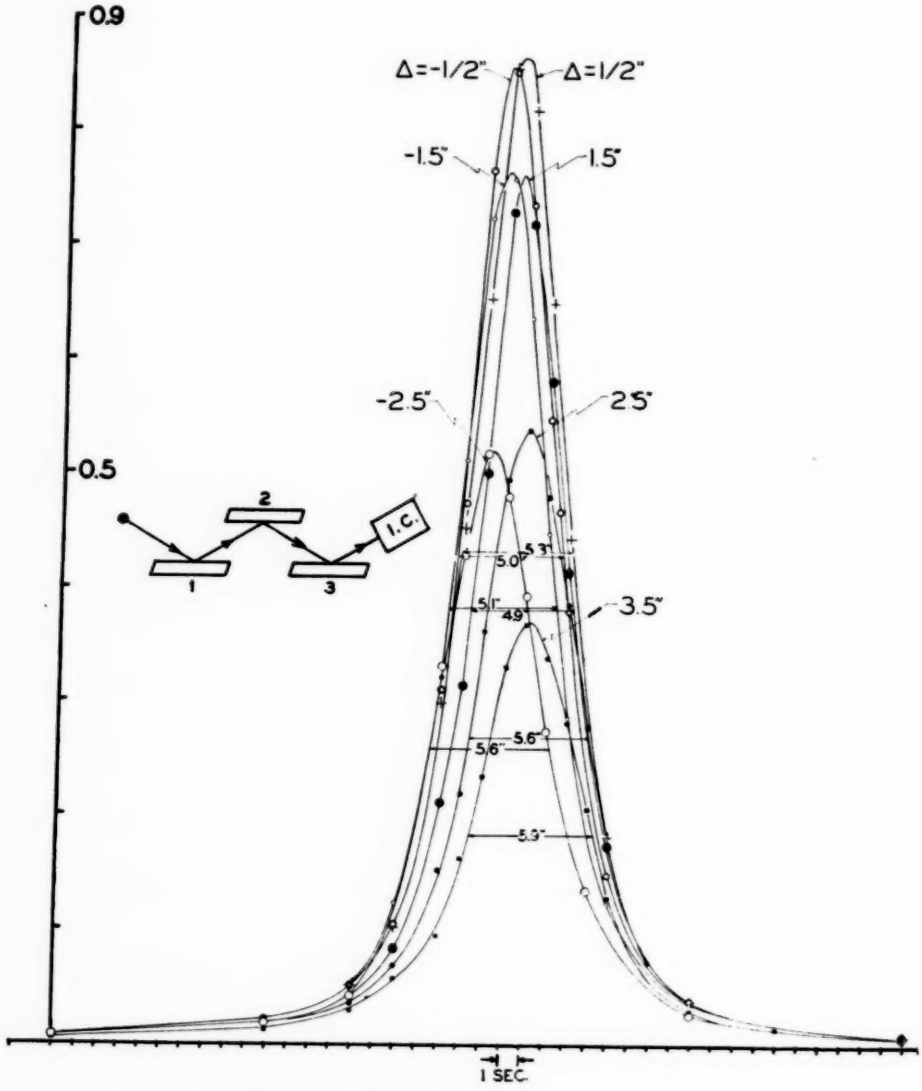

FIG. 1. Diffraction patterns obtained with a three-reflection three-crystal spectrometer. With the two tool crystals 1 and 2 set at seven different displacements Δ from exact parallelism, the third crystal was rocked in each of the seven resulting beams and the seven curves here shown were obtained. The abscissa scale refers to the angle through which the third or object crystal was turned in exploring each curve. The ordinate scale gives the ratio of the x-ray intensity in the beam after the first two reflections by the tool crystals to the intensity after the third reflection for the case of $\Delta = \frac{1}{2}$-second and $-\frac{1}{2}$-second tool displacement. The other curves show their correct observed intensity relative to these first two curves.

our previous paper under the heading "The Three Crystal Spectrometer" (see also Fig. 9 of that paper).

The rocking curve obtained by rocking the first crystal with respect to the second, the third crystal being removed from the beam, gave a very satisfactory symmetrical curve with a breadth at half-maximum of 7 seconds of arc. If we assume that the diffraction pattern is similar in shape to the prediction of Prins, but possibly somewhat broader on account of the crystal imperfection, then we can get an idea as to the degree of overlapping of the two Prins patterns for any particular displacement from parallelism by examining the rocking curve. From our rocking curve we found that a displacement of 3.5 seconds of arc away from exact parallelism reduced the twice reflected

intensity to one-half its value at exact parallelism. This indicates an overlapping of the core of the two diffraction patterns of much less than one-half their width because of the approaches or fillets of which we shall have more to say presently. Indeed it is likely that 3.5 seconds of arc displacement gives about as narrow and desirable a tool profile as can be obtained with two reflections under these conditions.

We next placed the third crystal or "object crystal" so as to reflect the beam from the two tool crystals and with the first of these set at varying displacements, $\Delta = 3.5, 2.5, 1.5, 0.5, -.5, -1.5$ and -2.5 seconds, we ran curves of the diffraction pattern of the object crystal exploring it with the sharpened tool thus formed. These curves shown in Fig. 1 have the following noteworthy features.

1. All the curves have blunter points than the ordinary two-crystal rocking curve and the bluntest is the one observed with the sharpest tool (formed by superposition with displacement of 3.5 seconds). This bluntest curve is evidently about the best that can be done in approaching a faithful delineation of the diffraction pattern with the method of three reflections in the parallel position. Further increase of the tool displacement would probably have suppressed the tall core in the tool profile entirely and thus the delineation of the diffraction pattern of the object crystal would have been spoiled.

2. The displacements of the curves of Fig. 1 to right and left fit our expectations very satisfactorily. If we think in terms of the transparency graphs and the horizontal profiles of the traces on them, we see that when the first tool crystal is shifted to give a displaced superposition (with the second crystal stationary), the center of the resulting tool displaces half this amount. The diffraction pattern observed with the tool will have this displacement also and the progressively increasing displacements coupled with the decreasing intensities show clearly in Fig. 1.

3. The intensity is gratifyingly strong after three reflections. In exploring the diffraction pattern of the third or object crystal the intensities obtained near the peak of its diffraction curve are only slightly weaker than the intensity coming directly from the tool with the object crystal removed from the beam. This again fulfills our expectations as to the Prins pattern which according to theory attains a maximum value of 98 percent for Mo $K\alpha$-radiation in the 1st order on calcite and stays above 90 percent over a range of some 3 sec. of arc. There is no reason why intensity alone should place a limit much below eight or ten on the number of successive reflections which can be used.

4. Practically no asymmetry is visible in the peaks of the curves of Fig. 1. By an extreme stretch of imagination some very slight asymmetry near the peak might be claimed for the curve observed with the tool at 3.5 sec. displacement but we do not feel that the precision of the ionization readings warrants giving this result much weight. Incidentally, it should be stated that Fig. 1 has been plotted with increasing Bragg angle in the direction to the right. The theoretical asymmetry then should throw the maximum a little to the left of the center of the main body of the curve.

These results, however, do not necessarily indicate that the real diffraction pattern has no flattened asymmetrical top as Prins predicts. It remains to be seen whether indeed the tool formed by two displaced Prins reflections is capable of adequately revealing a Prins pattern in a third reflection for our particular case and we are led to the conclusion that a serious difficulty comes from the fillets of the Prins patterns of the tool crystals.

The difficulty caused by the fillets of the diffraction pattern

The diffraction pattern for a "perfect" crystal, whether we consider the theoretical predictions of Ewald or Darwin neglecting absorption or those of Prins taking absorption into account, should have approaches, wings of "fillets" which decay at large distances from the center of the pattern inversely as the square of the distance.

In the Darwin pattern (which neglects absorption) only one-quarter of the total area is associated with the wings; the remainder is in the rectangular central core where the reflection is 100 percent. The effect of absorption lowers the reflection in the central region much more than in the wings.

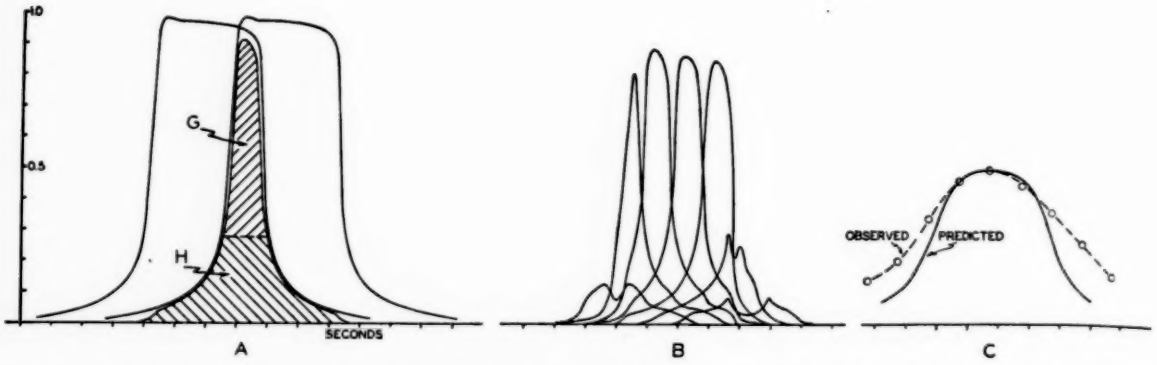

FIG. 2. Curves used in computing the results to be expected from an exploration of the Prins calcite diffraction pattern with a tool consisting of two Prins patterns mutually displaced 2.5 seconds of arc. The shaded portion at *A* shows the tool obtained by taking the product of the two displaced patterns. *B* is the product of this tool multiplied into a Prins pattern in successively displaced positions separated by one second of arc. *C* is the curve showing the areas of the curves *B* plotted against the position of the tool. *C* is thus the result of exploring a Prins pattern with the tool *A*. The dotted curve at *C* is the experimental curve taken from Fig. 1.

In the course of trying the suggested method of "displaced superposition" of diffraction patterns for sharpening the tool, this difficulty became clear, and it was demonstrated by computations of the curves to be expected in the three reflection case (assuming all three reflections to have ideal Prins patterns for Mo $K\alpha$ reflected on calcite) that it would be very difficult to reveal adequately the Prins pattern for any one of them regarded as the object. The difficulty is that when the core of the composite diffraction pattern of the two crystals constituting the tool has been narrowed down by displaced superposition the importance (relative area) of the fillets is so much increased as to necessitate a special procedure to remove their distorting effect. In Fig. 2 are shown the curves used in computing the results to be expected from an exploration of the Prins calcite diffraction pattern with a tool consisting of two Prins patterns mutually displaced 2.5 seconds of arc. The experimental curve (taken from Fig. 1) for this case is shown dotted in *C*. It is important to note that while the asymmetry of the Prins pattern of the object crystal is undetectable in the resulting ionization curve *C*, Fig. 2, the successive maxima of the curves *B* whose respective areas form the ordinates of *C* show this asymmetry clearly. A little study shows that the fillets on the tool cause this trouble. Indeed we can think of the tool curve at *A* as divided into two parts *G* and *H* of comparable areas. The part *H* is harmful, the part *G* good as an exploring tool. The contribution of *H* masks the detail which we seek. This way of looking at the matter suggested three promising methods of avoiding the difficulty.

One of these is to suppress the undesirable fillets on the tool by an application of the principle of undisplaced superposition. The ideal way to do this would necessitate the use of a spectrometer with four crystals to prepare the tool and a fifth crystal as object. Two successive reflections would occur between strictly parallel crystal faces from which the beam would pass to another entirely similar parallel pair of reflections. These two pairs, however, would not be mutually parallel but would be displaced the right number of seconds of arc (say 2.5 sec. for Mo $K\alpha$ on calcite) so as to give the requisite sharpening of the tool. The resulting tool (based on the Prins pattern) from the four reflections is almost completely devoid of fillets. This method requires a five spindle spectrometer of special design and was not used in this exploratory study. The second method consists in running two rocking curves on the same object crystal with two different tool pair displacements (e.g. 2.5 and 4 sec. of arc) multiplying the resulting curves by appropriate factors and *taking the difference* between these curves to eliminate the effect of *H*, the harmful part of the tool. However there enters the practical difficulty which is the weakness of this difference method, namely the uncertainty regarding the angular shift which the center of the tool may have suffered

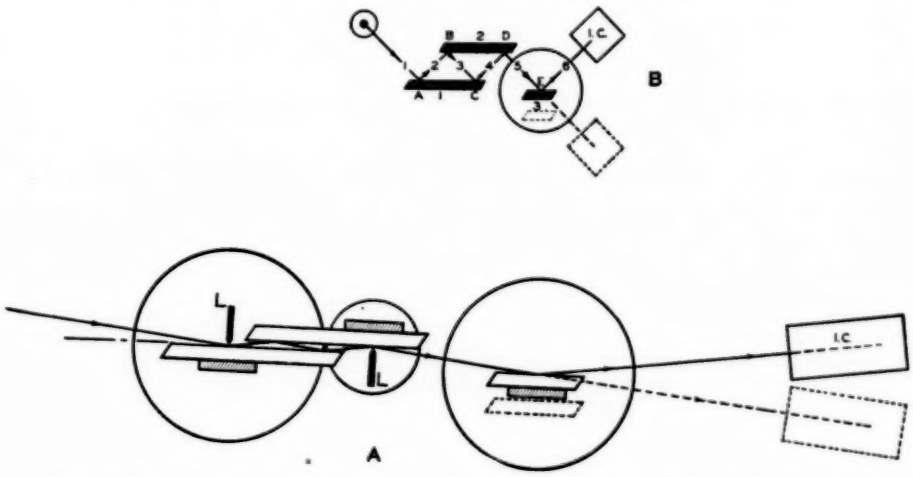

FIG. 3. Three-crystal five-reflection spectrometer. *A* shows the actual arrangement to scale. In its dotted position the third crystal is removed from the beam to permit study of the characteristics of the tool. The ion chamber is set in the dotted position for this purpose. *B* is a schematic view of the arrangement better adapted to reference labeling.

in passing from one displacement value to the other. This uncertainty implies *an uncertainty as to how the abscissa scales of the two curves are to be matched* before the process of subtraction is applied. It is an easy matter to show that the asymmetry of the difference curve can be given either sign by a slight error in this matching of the two abscissa scales so that one feels skeptical whether the asymmetry which such a procedure would reveal would reflect the real asymmetry of the diffraction pattern of the object crystal or merely the accidental errors of setting the tool. We encountered this difficulty in an attempt to use this method with our three-crystal arrangement. It should be emphasized however that these difficulties are not fundamental objections to the difference method but merely practical difficulties arising from the very small angles involved. An appropriate design of apparatus might obviate this difficulty.

THE QUINTUPLE REFLECTION STUDY

Three-crystal five-reflection arrangement used in the present study

It occurred to us to try a tool constituted by four repeated reflections between two large and very perfect calcite samples. Fig. 3 at *B* shows schematically the arrangement of crystals 1, 2 and 3 while Fig. 3 at *A* shows the actual geometry to scale. The spectrometer which has been previously described[3] provides two spindles together with accurate and appropriate motions for the arm supporting the x-ray tube and for the instrument as a whole relative to the ion chamber. These greatly facilitate its use for the present purpose. We were obliged to add a third spindle half-way between the two existing ones which, however, did not need to be rocked with precision. It was carefully designed according to the modern principals of kinematic design,[4] and instead of rotating on a taper pivot for which there would have been no room, it was made with three equally spaced ball bearings held between a plane surface and an annular *V* groove; the centering was accomplished with a third ball bearing and leaf spring which also furnished the necessary force to hold the assembly in contact. The design permits complete rotation so as to facilitate optical alignments.

Study of the tool by rocking crystal 1 relative to crystal 2

Crystal 3 could be removed from the beam by means of the slide carriage on which it was mounted. The whole instrument could then be swung so as to direct the beam after the fourth reflection straight into the ion chamber. In this

[3] Rev. Sci. Inst. **8**, 112 (1937).
[4] Pollard, *The Kinematical Design of Couplings in Instrument Mechanisms* (Adam Hilger, London, 1929). We are much indebted to Professor Wm. Hansen of Stanford for calling our attention to this book.

condition then crystal 1 was rocked minutely relative to crystal 2.

A good sample curve of x-ray intensity (after the quadruple reflection) as a function of the rocking angle of crystal 1 is shown in the curve of Fig. 4. *This curve must not be confused with the tool profile*, however. This distinctly triangular shaped curve with total width at half its maximum height of only 2.0 seconds of arc is just about what one should expect for the varying composite window area resulting from the superposition with varying degrees of displacement of four supposedly equally spaced Prins patterns. The width of the 4-reflection rocking curve indicates that the tool crystals somewhat exceed the Prins prediction for the width of their diffraction patterns. This might also be an effect of "blurring of the reflected beam" mentioned above.

Unsatisfactory distorted rocking curves were too frequently obtained by this rocking of crystal 1 with respect to crystal 2 in our study of the 4-reflection tool. A most annoying tendency which we have not been able to explain satisfactorily was the appearance of a double peak. The smaller member of this double peak always occurred quite reproducibly at the same setting of crystal 1 but the taller member was variable in position occurring everywhere from a position 8 or 9 seconds of arc counter clockwise away from the smaller stationary peak down to complete coincidence with the latter. The tall peak never crossed over, however, to the clockwise side of the short one.

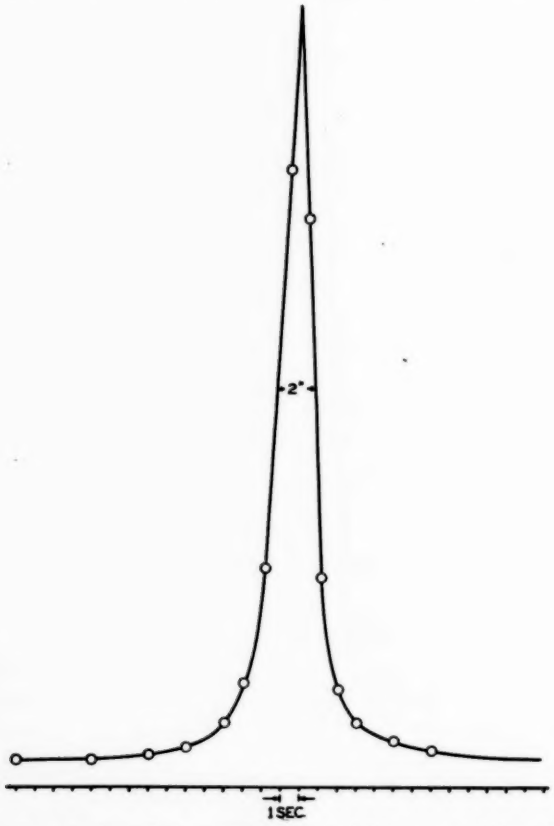

FIG. 4. Sample four-reflection rocking curve giving the intensity after the four reflections between the first two large crystals (Fig. 3) as a function of their displacement from parallelism.

Toward the latter part of our work the erratic double peaks were less troublesome. We took precautions to check the rocking curve of the tool for absence of double peak just *before* each study of the diffraction pattern of the object crystal and in the last three curves we also checked this just *after* each run. The stability of the tool both as to shape and angular position of its rocking curve was excellent for all the diffraction patterns reproduced in this report.

Computed profile of four-reflection tool with and without displacement of the pair

Figure 5 shows the composite four-reflection tool profiles, computed on the assumption of a Prins pattern, for the case of no displacement at U and for the case of a displacement of crystals 1 and 2 of 1 sec. of arc at D. These are not to be confused with the rocking curves we have just discussed above. In the case of zero displacement a notable diminution in the fillets is effected by the four reflections and the asymmetrical top of the core of the pattern is exaggerated. In the case of 1 sec. displacement the fillets are still quite effectively suppressed. The triangular shape of the profile with almost complete absence of any flat top is an accident of the choice of the displacement, the side slopes of the triangle being principally the result of the sloping sides of the single crystal Prins pattern. Fig. 5 also shows at P_U and P_D, respectively the computed result of exploring a Prins pattern with tools U and D as well as the successive product curves whose areas gave the ordinates of P_U and P_D.

Diffraction patterns of calcite observed with the four-reflection tool

Figure 6 shows the diffraction patterns of two different calcite object crystals (the crystal 3 in

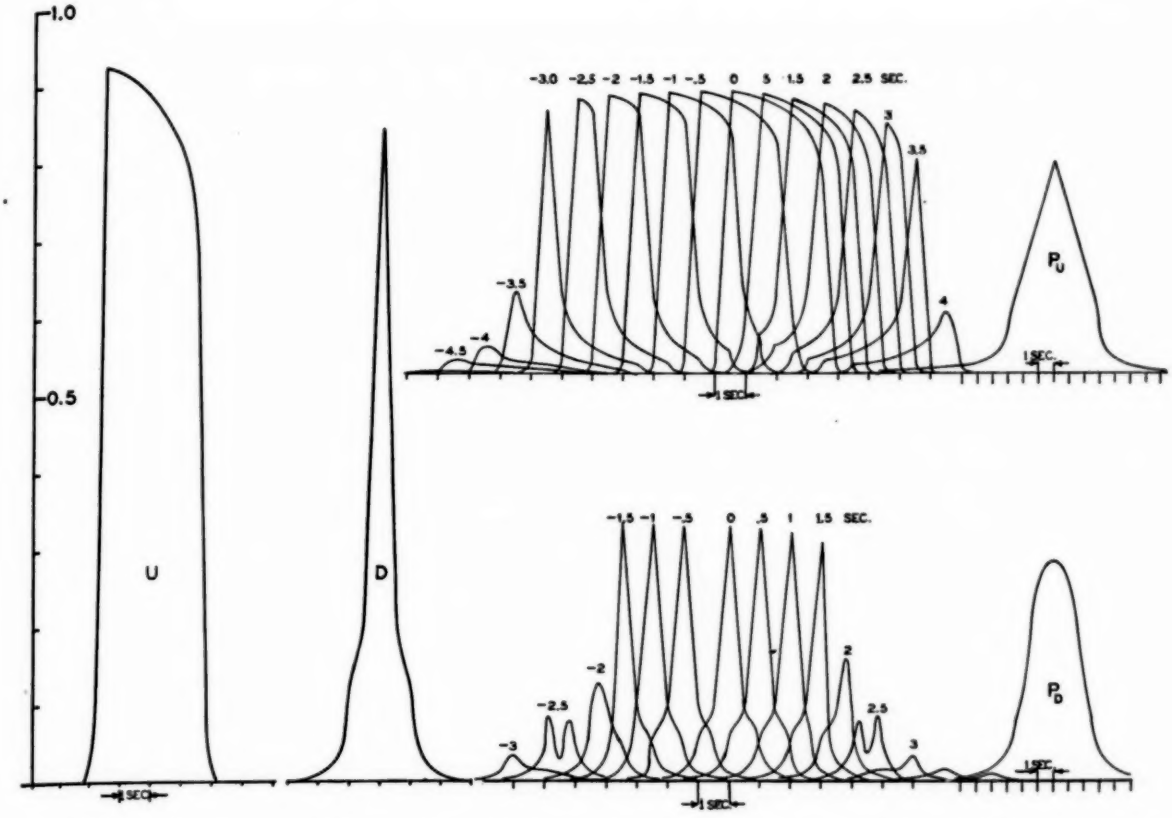

FIG. 5. On the assumption of a Prins profile for each reflection U and D are respectively the tools to be expected from the four-reflection arrangement for the parallel case and for a setting 1 second of arc off parallel. P_U and P_D are the curves to be expected as a result of exploring a fifth crystal having a Prins profile with tools U and D, respectively. Product curves computed at every half-second of the exploration are shown. Their areas give the ordinates of P_U and P_D.

Fig. 3 *B*) as observed with the four-reflection tool; the curve marked U was made with the undisplaced tool, the curve marked D with the displaced tool. The dotted curve of U is for our first calcite sample, the full lines for the second sample. *We think the pattern D* 1.5, Fig. 6, *obtained with the four-reflection tool in displaced superposition* (*crystals 1 and 2 set 1.5 sec. out of "parallel"*) *probably comes nearer to a direct observation of the x-ray diffraction pattern of a crystal than any other work we have done.* The assumption that Fig. 5 really represents faithfully the exploring tool profile (case of 1 sec. displacement) is the extreme of optimism. The other extreme of pessimism, we think, might be embodied in the assumption that the tool profile should be inferred from the result of Fig. 6 *D* itself, that is to say, on the assumption that the tool crystals have diffraction patterns for their individual reflections just like the observed object crystal pattern. In this case Fig. 7 shows the profile O_D of the four-reflection tool for 1.5 sec. displacement. This profile, like the theoretical tool profile of Fig. 5 *D*, is seen to be nearly an isosceles triangle with, however, a wider base than the latter. It seems almost certain that the actual tool must have had a profile lying somewhere between these two shapes and this fact gives us considerable confidence in the profile of Fig. 6 *D* as an approximation to the calcite diffraction pattern for Mo $K\alpha$-radiation in first-order reflection. In Fig. 7 at O_U is shown the tool computed under the same assumption but for four reflections with no displacement.

The following characteristics of these observed patterns are worth noting:

1. The experimental profiles D and U of Fig. 6 exhibit no such striking difference of

shape as the curves (P_U, P_D Fig. 5) computed from the assumption of a Prins profile lead one to expect. We are led to conclude that the Prins profile which is based on very ideal assumptions as to the perfection of the crystal and of its upper boundary surface is only very roughly approached in the real case.

2. The top of the curve shows no reproducible marked asymmetry. This is not very surprising when we see how little asymmetry the theoretical Prins pattern possesses for the case of Mo $K\alpha$-radiation, first order. In order to produce a marked asymmetry it would be necessary to repeat our experiments with much softer radiation, probably with a vacuum spectrometer.[5] This would have the advantage not only of giving more asymmetry to the pattern, but also of giving a broader pattern which would not put such severe requirements on the instrument as to angular sensitivity and freedom from thermal effects.

3. The curve has the right order of magnitude for its breadth exceeding only slightly the Prins prediction for breadth at half-maximum.

4. The curve has a noticeably different shape in the right- and left-hand fillets, the right-hand one falling off less abruptly than the left. This is suggestive of the same sort of double peak which seemed to be indicated by our study when rocking the two tool crystals. We are unable to explain this whether it be regarded either as a characteristic of the diffraction pattern of one or more reflections in the tool, or as a characteristic of the diffraction pattern of the object crystal.

These somewhat disappointing deviations of the observed diffraction pattern shape from the Prins prediction are probably caused by crystal imperfection. In order to minimize the effect of such imperfection it should be pointed out that

[5] An expedient to exaggerate the asymmetry of the diffraction pattern to be expected for Mo $K\alpha$-radiation might be resorted to as follows. The single object crystal would be replaced by a parallel pair of object crystals between which several successive reflections (say four reflections) could take place with undisplaced superposition of their diffraction patterns. The effect of undisplaced superposition increases the asymmetric slope of the top; four reflections give four times as great a slope when the slope is small, c.f. Fig. 5U. To combine such an expedient with a two-crystal, four-reflection tool, however, calls for a four-crystal spectrometer and eight successive reflections. Such an expedient goes beyond our present facilities.

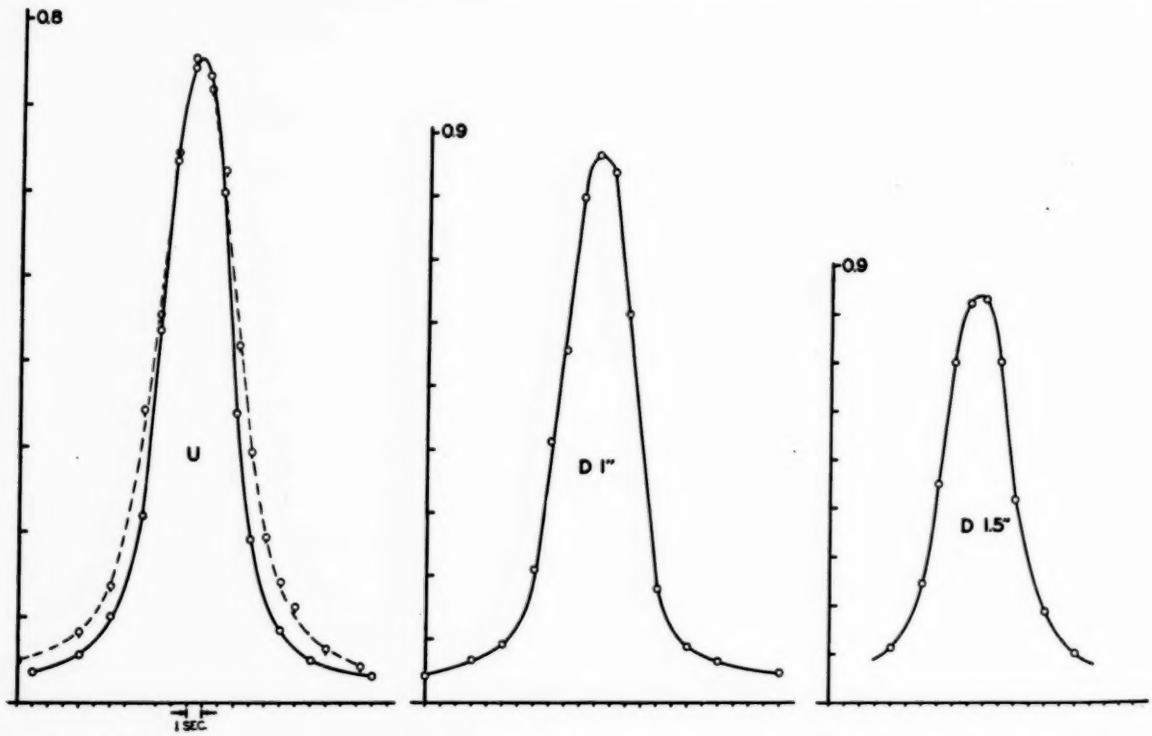

FIG. 6. Observed diffraction patterns of object crystal using four-reflection tool. The tool here was set with the crystals at zero displacement and with displacements of 1 and 1.5 seconds of arc off parallel. The dotted curve is for the first sample explored only with zero displacement.

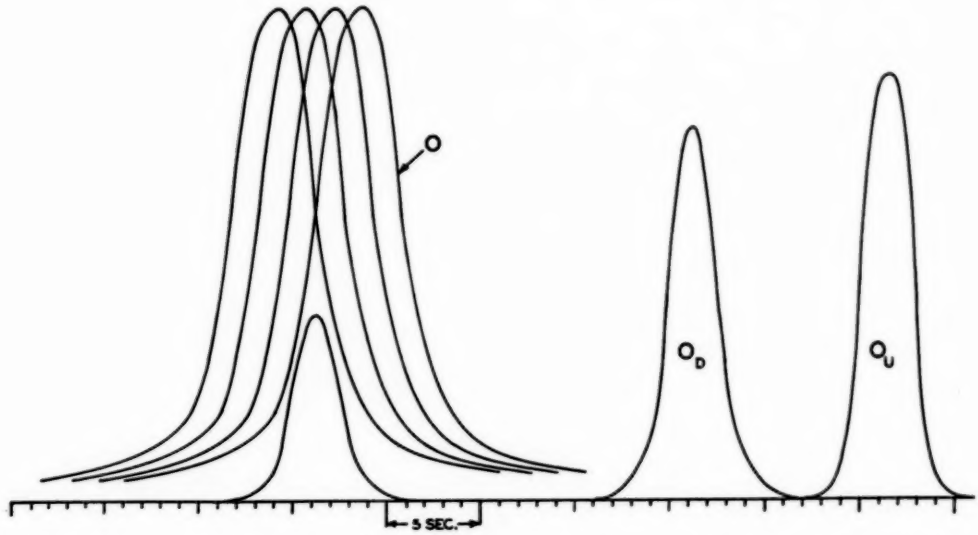

FIG. 7. Four-reflection tool shapes to be inferred on the assumption that each tool reflection has a pattern similar to that experimentally observed for the object crystal as shown at D 1.5 in Fig. 6. The tools O_D and O_U are computed for zero displacement and for 1.5 sec. displacement of the four-reflection pair.

the work was done *with a very limited area of the crystal* active in each reflection. In all the work with the four-reflection tool the *height* of the beam was limited to 2 mm at the point where it entered the lead snout leading to the ion chamber. The focal spot of the x-ray tube had a height of this same order. The horizontal dimension of the reflecting area is probably limited principally by the projection of the horizontal extension of the focal spot normal to the x-ray beam and this is of the same order again so that the reflecting areas were probably roughly rectangles 2 mm high and 16 mm long; the horizontal elongation was a result of the grazing incidence at about 7°.

CONCLUSIONS

The present work we must regard as an *exploration* of the possibilities of the plural spectrometer in the direction of the study of crystal diffraction patterns. As to the diffraction pattern profile for Mo $K\alpha$-radiation incident on calcite cleavage planes, probably the most we can say is that the work casts grave doubt on the applicability of the ideal flat-topped Prins pattern to the real case.

We feel no great surprise or disappointment to find no noticeable asymmetry in the peaks of the curves since the asymmetry to be expected on the Prins theory for a perfect crystal at this wave-length (about 1 percent per second of arc) is so small. Since we were not equipped with the necessary vacuum plural spectrometer, it was natural, of course, to attack the problem first in the wave-length region permitted by our apparatus. It is our hope that others better equipped than ourselves may feel encouraged to continue the work at longer wave-lengths.

ACKNOWLEDGMENTS

We wish to express our grateful appreciation for the funds which made possible the construction of the spectrometer used in this work. These funds are the gift of Dr. Leon L. Watters of New York City to the California Institute of Technology.

Shape of the Modified Compton Line for Hydrogen and Ceylon Graphite Scatterers

H. A. KIRKPATRICK
Occidental College, Los Angeles, California

AND

J. W. M. DUMOND
California Institute of Technology, Pasadena, California

(Received August 1, 1938)

Hydrogen under ten atmospheres pressure was used to scatter almost directly backward the characteristic K radiation of a molybdenum-target x-ray tube. After an exposure of 1914 hours in a focusing curved-quartz-crystal spectrograph the resulting modified line was studied with a microphotometer. The breadth of the composite modified line of the alpha-doublet was 15.2 x.u. This is ten percent greater than the breadth computed by B. Hicks from the electron momentum distribution. That the discrepancy is greater for H_2 than for the previously studied He is probably because the H_2 calculations were not carried to so high a degree of approximation. The unmodified line was completely absent. The shift as determined by fluorescence reference lines is less than that required for free electrons by an amount appropriate to the binding energy of electrons in the H_2 molecule.

A renewed search was made for evidence of any departure of the electron momenta from an isotropic directional distribution in Ceylon graphite, a diamagnetic crystal. This time the diamagnetic axis of the graphite was placed normal to the direction along which the experiment resolves the electron velocities. There was no indication of two lines or prominences symmetrically disposed on either side of the center of the Compton line corresponding to shifts for the directly approaching and receding electrons.

A small error in the previous determination of the shift defect for helium is noted.

I. INTRODUCTION

THE authors have previously shown by a comparison of experiment and theory that the modified line in the Compton effect has a broad structure whose shape reflects directly the velocity distribution of the electrons (their linear momenta) in the atoms of the scattering body; the broadening effect on the modified line is to a classical approximation (which in the present case is a very good one) simply a Doppler broadening caused by the quantum motions of the electrons scattering the radiation. Including the results of the present paper we may say that we have shown the breadth of the line to vary quantitatively as a function of all four of the available variables, scattering angle, primary wave-length, scattering material and physical state (solid or gaseous) in accord with the predictions of the above concept.[1]

Recently the authors[2] succeeded in obtaining for the first time[3] a direct spectrum of modified x-radiation scattered by a gas, helium. For the purpose of comparison with theory Mr. Bruce Hicks[4] of this Institute kindly consented to compute the momentum distribution to be expected in the helium atom[5] and the shape of the Compton "line" which should result from scattering of the radiation by electrons with such a distribution. At the same time Hicks also computed the momentum distribution and resulting line shape for the hydrogen molecule H_2 which latter turned out to be very appreciably narrower than the Compton line for a helium scatterer. Such a marked dependence of Compton line

[1] P. A. Ross, Proc. Nat. Acad. Sci. **9**, 246 (1923). G. E. M. Jauncey, Phys. Rev. **25**, 314 and 723 (1925). DuMond, Phys. Rev. **33**, 643 (1929); DuMond and Kirkpatrick, Phys. Rev. **37**, 136 (1931); **38**, 1094 (1931); DuMond and Hoyt, Phys. Rev. **37**, 1443 (1931); DuMond, Rev. Mod. Phys. **5**, 1 (1933); DuMond and Kirkpatrick, Phys. Rev. **52**, 419 (1937).

[2] DuMond and Kirkpatrick, Phys. Rev. **52**, 419 (1937).

[3] Kappeler, Ann. d. Physik **27**, 129 (1936). This author had studied the shape of the Compton line from a gaseous scatterer (neon) previous to our study of helium, but without obtaining a direct spectrum of the scattered radiation. Kappeler used a refinement of a method first proposed and used by P. A. Ross in which by varying the angle of scattering and hence the shift the modified line is made to cross an absorption discontinuity defined by a filter. The shape of the Compton line can be deduced from the results.

[4] B. Hicks, Phys. Rev. **52**, 436 (1932).

[5] A. L. Hughes, Phys. Rev. **53**, 50 (1938). This author, by the study of inelastically scattered electrons, has developed a very beautiful and precise method of experimentally observing the distribution of electron momenta in the atoms of a gas which furnished in the above reference a very satisfactory check on the theoretical predictions of Hicks as to helium.

breadth on the scattering atom furnishes a valuable check on the validity of our concept of the Doppler broadening of the line, and we have therefore undertaken the present study with a gaseous hydrogen scatterer.

II. Hydrogen Scattering Experiment

The reader is referred to our previous article[2] on the Compton line with helium gas as scatterer for details of the experiment, apparatus and procedure which were identical in the present work save for the scattering chamber. This latter we moved somewhat with respect to the primary and the scattered beams and we lengthened it from one meter to 1.5 meters. These improvements permitted us to reduce the pressure from 14 to 10 atmospheres with still an appreciable gain in scattered intensity for a given exposure time.

The characteristic K-line radiation from a molybdenum target was scattered almost directly backward by the hydrogen for 1914 hours; the voltage and current supplied to the tube were 60 kv and approximately 20 milliamperes. As before, test films behind the film proper in the focusing curved crystal spectrograph were used to test the progress of the exposure.

The reference spectrum on the edges of our film was accidentally fogged. Fortunately certain fluorescence lines which always appear on our film from the lead backing in the scattering chamber could still be used in conjunction with other spectra previously made in the same instrument to establish the exact position of the unshifted lines.

Thus we were able, in spite of the mishap, to determine the exact shift of the Compton line scattered by hydrogen. This was done in the same manner as we did for the case of helium.[2]

III. Results of Hydrogen Scattering Experiment and Their Interpretation

Computation of Predicted Line Profile

We have used, because of its intensity, the alpha-doublet of the molybdenum K spectrum as the primary radiation. The profile of each of the two shifted lines resulting from the two members of this doublet is so much broader than the doublet separation that the doublet character

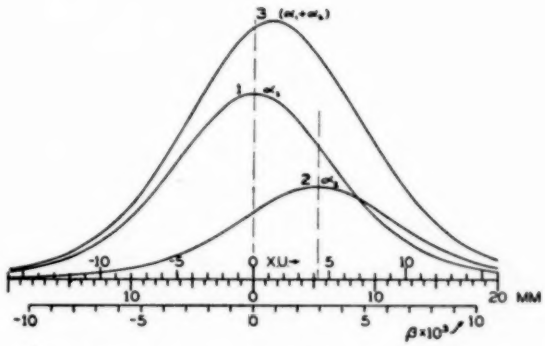

Fig. 1. Hicks' computed curve for the Compton line as broadened by his theoretically computed electron momentum distribution in the hydrogen molecule is here shown as curves 1 and 2 plotted to correct wave-length scale for the cases of Mo $K\alpha_1$ and $K\alpha_2$ as primary radiation and for our scattering angle. Curves 1 and 2 are plotted with relative intensities in the ratio (2 : 1) and with a wave-length separation of 4.27 x.u. (the separation of the alpha-doublet in the Mo K spectrum). Thus curve 3, which is the sum of 1 and 2, gives the correct shape to be compared with our observed shifted line. These curves show that the doublet nature of the primary radiation has but a slight distorting effect on the line shape.

of the primary radiation disturbs the shape of the profile but little even for the case of hydrogen scattering which gives the narrowest shifted line we have yet observed. Fig. 1 shows how we have corrected the theoretical shape for the doublet nature of the source by plotting Hicks theoretical curve to correct wave-length scale in the two positions corresponding to shifted α_1 and shifted α_2 with the appropriate relative intensities (2 : 1) and adding the two resulting curves. This gives us a master theoretical curve for comparison of the profile with our experimental results. This master comparison curve on which appear the positions of the centers of shifted α_1 and α_2 also serves to determine the shift very conveniently. This is done by sliding the master curve horizontally along the wave-length scale until it coincides for best fit with the observed microphotometer trace and then measuring the shift from the position of either member of the unshifted alpha-doublet to the line center of the same member marked on the shifted master curve.

In every case the vertical or ordinate scales of theoretical and experimental curves have been adjusted so as to normalize these curves to the same area.

Figure 2 shows a few sample microphotometer traces, nine of which were averaged by reading

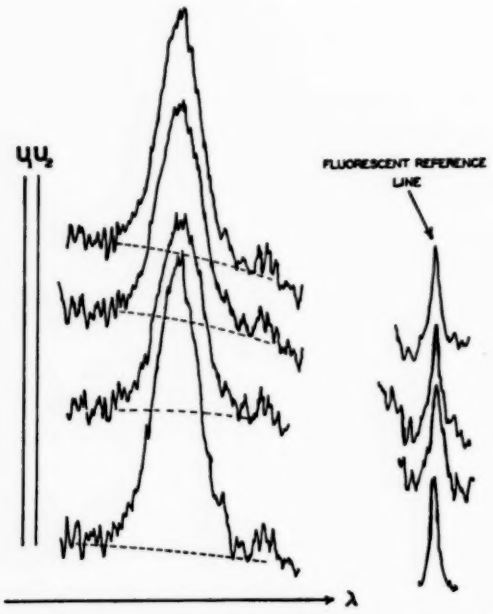

FIG. 2. Samples of single microphotometer traces of the Compton line with gaseous hydrogen as the scatterer. The unshifted wave-length positions are marked as U_1 and U_2. Nine such traces were numerically averaged to obtain the final results for comparison with the theoretical curves.

some eighty ordinates (every millimeter), taking the numerical average of these readings, and replotting these averaged results. As usual the background of the spectrum is found to have a slight slope and we are obliged to determine the average slope for all our microphotometer traces and subtract from the final averaged trace a straight line background having this slope.

The abscissa scale of Hicks' computed profiles is given by him in terms of the variable $\beta=v/c$, where v is the electron velocity responsible for the broadening of the Compton line. This is transformed into wave-length units by the formula

$$l=2\beta\lambda^*, \tag{1}$$

where l is the abscissa of the shifted line measured from its center in wave-length units and λ^* is given by

$$\lambda^*=\tfrac{1}{2}(\lambda_1^2+\lambda_c^2-2\lambda_1\lambda_c\cos\theta)^{\frac{1}{2}}, \tag{2}$$

where θ is the scattering angle, λ_1 is the primary wave-length, $\lambda_c=\lambda_1+(h/mc)(1-\cos\theta)$ is the shifted wave-length for initially stationary electrons.

The abscissa scale of the computed theoretical profile must next be transformed into centimeters on the microphotometer plate to facilitate comparison with the microphotometer curves. This involves a knowledge of the dispersion which the geometry of the transmission-type focusing curved-quartz-crystal spectrograph imposes on the original film and also the ratio of abscissa magnification imposed by the recording microphotometer. This latter has been determined as 10.0024 ± 0.001 uniform over its entire range to the indicated precision which is far higher than necessary for our present purposes. As for the dispersion of the spectrograph the method of its determination and the errors involved have been treated at length in our paper on helium scattering to which the reader is referred.[2]

In Fig. 3 the full line gives the theoretical Compton line profile derived from Hicks' computations while the dots are the observed values obtained by averaging the microphotometer traces. Experiment thus indicates that the Compton line is here about ten percent broader than Hicks' theory predicts. Our helium results supported Hicks' predictions with much better agreement than this. Hicks is of the opinion that his results for molecular hydrogen might well be in error by this amount as the approximation to which these somewhat more difficult calculations were carried out was not as high as in the case of his helium calculations. Also in the hydrogen case it was difficult for him to estimate the error committed at a given stage of approximation. Hicks points out that for his helium calculations at one of his earlier stages of approximation which gave an error of 2 percent in the energy levels he found an error of 10 percent in the momentum (breadth of the Compton line at half-maximum height). Hicks' calculations for H_2 were only carried to a stage of approximation which yielded about 2 percent error in the energy levels (owing to the rapidly increasing difficulties for this molecule) and it is interesting to note that our experimental results seem to indicate the error in momentum here to be about 10 percent again as in the case of helium.

A. L. Hughes[6] has also observed this slight excess (11 percent) for the actual momentum breadth in the H_2 distribution (as compared to

[6] A. L. Hughes, Phys. Rev. **54**, 189 (1938).

Hicks' predictions) by his method of inelastically scattered electrons.

In order to make quite sure that the excess observed over Hicks' calculated breadth might not be an instrumental effect, we narrowed the exploring slit of our recording microphotometer until it admitted less than half the intensity used in making our traces of the line profiles and we ran another profile with this new slit. The breadth of this curve was identical with that obtained before and we conclude therefore that this cannot explain the excess breadth.

This shifted line for a hydrogen scatterer is the narrowest so far observed at this scattering angle and primary wave-length in accord with the lower electron velocities to be expected for hydrogen. Our observed breadth at half-maximum height for the shifted composite $\alpha_1+\alpha_2$-line is 15.2 x.u. which corresponds to a breadth at half-maximum for a strictly monochromatic primary line of 14 x.u. We arrive at this correction on the assumption that the ratio of breadth of the composite shifted line to breadth of the pure shifted line will be the same in the actual case as in the case of the Hicks' theoretical curves which approximate the observed curves. This ratio is 1.09.

For comparison we list below the breadths at half-maximum of Compton lines for two gases and one solid used as x-ray scatterer, all corrected as above to give the breadth for a strictly monochromatic primary line of wave-length 710 x.u. at scattering angles approximately 180°.

H_2, 14 x.u.; He, 18.6 x.u.; Graphite, 21.4 x.u.

Determination of the Shift

Our exposure shows no unmodified line so we have determined the shift directly and separately from each of our microphotometer records as follows: The positions on the microphotometer recording plate of the center of shifted α_1 and α_2 were found by fitting to the actual microphotometer curve of the Compton line a plotted composite curve (like the one in Fig. 1) on which the center lines of the shifted α_1- and α_2-bands appear. These positions were next measured with reference to a fluorescence line which appears on our spectra whose position is accurately known relative to the unshifted α_1- and α_2-lines from previous work.

The average shift so measured turns out to be 59.12 mm on our microphotometer plates or 5.912 mm on the original film and the deviations of the nine individual measurements on the nine plates from the mean indicate the probable error of the mean as ±0.08 mm on the microphotometer plate or ±0.008 mm on the original film (±0.13 percent). From the average dispersion of the spectrometer (in Siegbahn wave-length units) for the range of wave-lengths between Mo $K\alpha_1$ and shifted Mo $K\alpha_1$, which is 80.622 x.u./cm, we compute the shift to be 47.66 x.u. and correcting this slightly to express it in terms of absolute or grating wave-lengths we obtain finally for the observed shift 47.75±0.06 x.u. where the error is based only on the internal consistency of the nine observations.

The Shift of Initially Stationary Free Electrons

We have recomputed the mean effective value of $(1-\cos\theta)$ averaged over the scattering volume with appropriate weighting for distance from source and from the spectrometer (see our article on helium scattering[2]) and we obtain

$$(1-\cos\theta)=1.9933.$$

Taking a value of 24.15×10^{-11} cm for h/mc we obtain 48.13×10^{-11} cm for the shift to be expected at our mean effective scattering angle for free initially stationary electrons on the simple Compton theory.

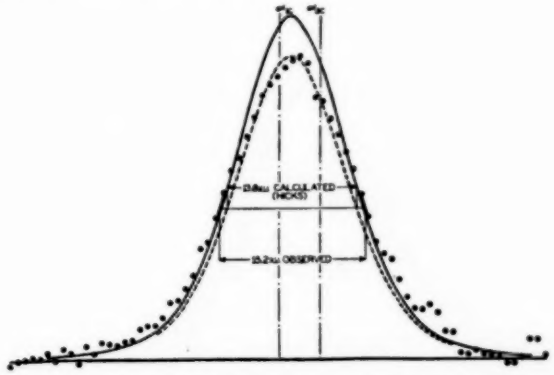

FIG. 3. Comparison of calculated and observed Compton line profiles for a gaseous hydrogen scatterer. The dots are the averages of measurements made on nine microphotometer traces. The full and dashed lines are each Hicks' calculated curve corrected for the doublet nature of the primary radiation. The vertical scale of the full line curve has been normalized to the same area as the observed curve while the dashed curve has been adjusted to have the same maximum ordinate as the observed curve.

The Defect in the Shift

As Ross and Kirkpatrick have shown both theoretically and experimentally[7] x-ray scattering by bound electrons should take place with slightly less shift than for free electrons. The recoiling electron ejected from the atom by the Compton effect may be thought of as slightly "loaded" with a small fraction of the mass of its parent atom through the agency of the binding forces and the greater effective m in the expression h/mc calls for a smaller shift. Our present results seem to support this defect in the shift, our value for the defect for hydrogen being $48.13-47.75=0.38$ x.u. This should be compared with a defect we obtained for the case of helium scattering of 0.53 x.u. The lower binding energy of hydrogen as compared with helium leads one to expect a lower value for the defect in the shift and our results seem consistent with this. We do not wish however to attach undue faith to our shift-defect measurements which may well be in error by considerably more than the "probable" value ± 0.06 x.u. indicated by the application of the theory of errors to our shift measurements.

Correction of a Slight Error in our Shift Defect for Helium

In the present computations we have discovered a small error which we committed in computing the mean effective value of $(1-\cos\theta)$ for our paper on the Compton effect with a helium scatterer.[2] We find that the mean value of $(1-\cos\theta)$ should have been, for that work, 1.994 instead of 1.997.

This has no effect whatever on any of the conclusions of that paper except the computed value of the shift to be expected for free stationary electrons and the resultant shift defect. Those should be corrected to 48.16 x.u. and 0.53 x.u., respectively.

Internal Evidence That Our Shifted Line Was Scattered by Hydrogen Only

The absence of unmodified scattering for weakly bound electrons is well understood. When the energy imparted to the electron by the radiation (recoil energy) is large compared to the binding energy there is a high probability that the electron will be ejected from the atom and the energy balance then requires a change of wave-length. For hydrogen even more so than for helium the unmodified scattering is utterly negligible and no unshifted lines whatever could be observed on our film. Every other substance which could conceivably be present in our scattering chamber would have an atomic number equal to or greater than carbon which for our primary radiation and scattering angle gives unmodified lines of the same height approximately as the modified line. The absence of unmodified lines is thus conclusive evidence that our Compton line was scattered by the hydrogen alone. The lead lining and back wall of our chamber can easily be shown to scatter negligibly in comparison to the hydrogen because its fluorescence absorption so greatly limits the thickness of the layer from which scattering can occur.

IV. Experiment with Ceylon Graphite Scatterer

Reason for the Experiment

Five conditions influence the breadth and shape of the Compton modified line, and of these we believe we have experimentally verified the effects of four. The five are: the scattering angle, the primary wave-length, the material of the scatterer, the physical state (solid, liquid or gaseous) of the scatterer, and finally an effect which might be expected if the electrons in the scatterer do not on the average have their linear momenta isotropically directed in the crystalline lattice of the scatterer. The fifth condition would make the shape of the Compton line dependent on the orientation of the crystalline structure of the scatterer with reference to the incident and scattered beams of radiation. So far we have been unable to reveal the fifth effect.

For radiation observed under a given scattering angle θ we have shown[8] that there exists a natural reference axis in space (which is very nearly the bisector of the supplement of the

[7] Ross and Kirkpatrick, Phys. Rev. **45**, 223 (1934); **46**, 668 (1934).

[8] This "natural reference axis" is "the vector change in light momentum for scattering at angle θ by an initially stationary electron." See DuMond and Kirkpatrick, Phys. Rev. **37**, 142, 143 (1931); **38**, 1094, 1100 (1931); DuMond, Kirkpatrick and Alden, Phys. Rev. **40**, 168, 170 (1932); DuMond, Rev. Mod. Phys. **5**, 1 (1933).

scattering angle and lies in its plane) such that it is the component electron momentum resolved along this axis which is responsible for the Doppler broadening of the Compton line. As Jauncey[9] has later pointed out, the shape of the Compton line is a picture of the component electron momentum distribution. It is along this natural axis that the momenta are to be resolved.

Our first attempt to reveal the existence of anisotropic electron momenta was made with Ceylon graphite crystals[10] which exhibit marked diamagnetic anisotropy and which occur in small thin hexagonal flakes the diamagnetic axis being normal to the flakes. If the diamagnetism could be attributed to a fairly numerous class of electrons in the crystal lattice executing thin, flat, approximately circular orbits these we thought might have no component momentum normal to the plane of the orbit. We therefore tried the experiment with the axis of diamagnetic anisotropy of the crystals directed along the above mentioned "natural reference axis" for our incident and scattered beams of radiation. Scattering from a sufficiently populous class of electrons having no component momentum along this natural reference axis should contribute a sharp shifted line in the center of the broad band from the remaining electrons. Nothing of the sort was observed. This might have been either because such a class of electrons existed but was insufficiently populous or because the electrons responsible for the diamagnetism did not behave as we pictured them. Oppenheimer pointed out that electrons spatially restricted in the axial direction in thin flat orbits would by the uncertainty principle be required to have a wide spread in momentum in the corresponding (axial) direction.

The scattering blocks we used, and which we still have, are built up out of the tiny crystal flakes orientated by the combined action of settling in a fluid and of a superposed magnetic field. The flakes are held together by a very tiny quantity of gum binder.[11] Very recently it has occurred to us to try placing these blocks with

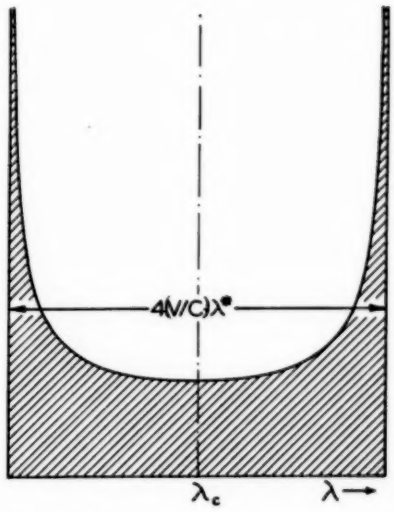

FIG. 4. Ideal modified spectrum to be expected from a class of electrons revolving at speed, v, in circular orbits with their axes normal to the natural reference axis for the scattering experiment.

the diamagnetic axis *normal* to the natural reference axis of the scattering experiment. In this new position if there exists a class of electrons responsible for the diamagnetic anisotropy executing approximately circular orbits at roughly one constant tangential velocity one should expect the radiation scattered by such a class to exhibit two peaks symmetrically disposed on either side the center of the Compton line and corresponding to the shifts for the electrons approaching and receding parallel to the natural reference axis. Fig. 4 is a sketch of the intensity distribution to be expected ideally for a class of circular orbits with uniform tangential speed. Some rough approach to this might perhaps be anticipated in the form of two bumps or a mere flattening at the top of the shifted lines.

Experimental Results and Interpretation

Figure 5 shows a microphotometer record from our scattered spectrum with the orientated Ceylon graphite scatterer. The diamagnetic axis of the graphite was normal to the natural reference axis of the scattering experiment and the plane of the graphite flakes was parallel to the plane of the scattering angle. The effective value of the scattering angle was approximately 137° with a range of inhomogeneity of about ±4°. The exposure of 54 hours with the molyb-

[9] G. E. M. Jauncey, Phys. Rev. **46**, 667 (1934).
[10] DuMond, Kirkpatrick and Alden, Phys. Rev. **40**, 165 (1932).
[11] We are much indebted to Messrs. A. Goetz, A. B. Focke and A. Faessler (see Phys. Rev. **39**, 168 (1932)) for purifying the graphite and preparing the orientated blocks.

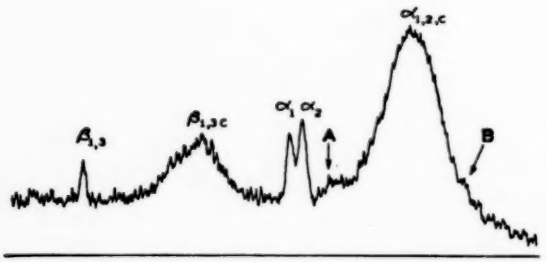

FIG. 5. Microphotometer curve of Mo K radiation scattered by orientated Ceylon graphite with its diamagnetic axis normal to the natural reference axis of the scattering experiment.

denum target tube running at 60 kv and 20 ma served to give a very clear scattered spectrum.

Examination of Fig. 5 shows nothing which we feel inclined to interpret as an effect of anisotropically directed electron momenta. Near the unshifted α-lines to their right there is a shelf, A, with a region of less intense blackening separating it from the α-lines themselves. This less intense region is distinctly visible on the original negative as a white line. There is the bare possibility of interpreting B as a companion shelf to A. However the fact that A and B are not symmetrically disposed around the center of the Compton line argues conclusively against these prominences as maxima corresponding to the velocities of approach and recession of a class of electrons in circular orbits responsible for the diamagnetic anisotropy. The Doppler spread between A and B (if we assume momentarily that these *are* approach and recession maxima) indicates an orbital velocity referred to light velocity of $\beta=v/c=0.0178$ corresponding to a kinetic energy of 80 volts. This is too low for the K electrons in graphite and too high either for L electrons or structure electrons.

The shelves A and B may correspond to double or multiple scattering inside our scatterer which was rather large and of more or less the same dimensions in all directions. This configuration would be such as to favor multiple scattering whose importance relative to single scattering increases with the size of the scatterer.[12] The spread between A and B is somewhat too broad for the band due to multiple scattering at a primary scattering angle of 137°, however.

[12] For a theoretical discussion of the effects of multiple scattering see DuMond, Phys. Rev. **36**, 1685 (1930).

The shelf at A might be an effect predicted by a number of authors in which one expects to find the continuous modified Compton band sharply limited on its short wave-length side by a discontinuity corresponding to a loss in quantum energy (relative to the primary frequency) equal to the binding energy of the scattering electrons.[13] The position of A calls for a binding energy of over 200 volts which may represent the binding energy of the K electrons in carbon.

The absence of the effect sought may again mean either or both of two things. The class of electrons responsible for the diamagnetic anisotropy in graphite may not have a sufficiently sharply defined momentum distribution approximating the kind we have postulated (circular orbits with uniform tangential velocity) or the class may be insufficiently populous to scatter an observable amount of shifted radiation.

The faintness of the unshifted α_1-line on this exposure is its most curious feature. The intensity of unshifted α_2 relative to the modified doublet corresponds well with our previous experience for graphite scatterers but the unshifted α_1-line should be more than twice as intense as it is. It is difficult to explain this as a vagary of the photographic negative because the line has this faintness over its entire length. We are totally at a loss to understand this weak α_1-line.

ACKNOWLEDGMENTS

We are indebted to Dr. A. Goetz of this Institute for furnishing the purified hydrogen which he pumped under pressure into our scattering chamber.

It is a pleasure to express our gratitude for the financial assistance which supported this research received through the generosity of Dr. Leon L. Watters of New York City.

[13] P. A. Ross, Proc. Nat. Acad. Sci. **9**, 246 (1923). G. E. M. Jauncey, Phys. Rev. **24**, 204 (1924); **25**, 314 (1925); **25**, 723 (1925). Jauncey assumes that an electron must receive in the scattering process enough energy from the radiation to be set free from the atom if the scattering is to be of the modified type. Thus the continuous distribution of shifted radiation which constitutes the Compton modified band must be limited on its short wave-length side at a shift for which the quantum energy lost by the radiation equals the electron binding energy. See also Compton, *X-Rays and Electrons*, page 286, 287; Wentzel, Zeits. f. Physik **43**, 1 (1927); **43**, 779 (1927); **58**, 348 (1929) and Sommerfeld, Ann. d. Physik [5] **29**, 715 (1937).

Symmetry Effects in the Spacing of Nuclear Energy Levels

JOHN BARDEEN,* *Harvard University, Cambridge, Massachusetts*

AND

EUGENE FEENBERG, *New York University, New York City*

(Received June 27, 1938)

The results of Wigner on mass defects and stability relations make possible a calculation of level density for intermediate nuclei ($A<60$) which takes properly into account the dependence of nuclear energies on symmetry character. In general, a configuration of neutrons and protons in single-particle orbits contains many different types of symmetry compatible with the exclusion principle. The various symmetry types arising from one configuration all have the same kinetic energy, but differ in potential energy; decreasing symmetry (increasing number of nodes) is associated with decreasing potential energy. Level densities for the different nuclear types are tabulated. The results indicate a marked increase of density for increasing isotopic number in an isobaric series. Transmutation experiments on isobars should make possible a test of the theory.

INTRODUCTION

TO discuss the problem of nuclear level density Bethe[1] and also Lier and Uhlenbeck[2] utilized the model of noninteracting particles in a potential well. The single-particle energy levels may be ϵ_1, ϵ_2, $\cdots$ arranged in ascending order. The total energy

$$E=\sum \epsilon_i n_i \tag{1}$$

is simply a sum of single-particle energies. Since no more than two neutrons and two protons can occupy a single orbit, the occupation numbers n_i are restricted to the values 0, 1, 2, 3, 4. Let δX designate the number of E's which fall in the energy interval E, $E+\delta E$. If δX is large in comparison with unity, and the average level spacing does not change appreciably over δE, we can define the density of levels $\rho(E)$ by the relation $\rho(E)\sim\delta X/\delta E$; the average spacing between levels is given by $1/\rho(E)\sim\delta E/\delta X$. For excitation energies $Q=E-E_0$ which are much smaller than the normal state energy E_0, Bethe and Lier and Uhlenbeck found the asymptotic formula

$$\rho(Q)\sim\tfrac{1}{4}(\Delta_\nu^2\Delta_\pi^2/54Q^5\Delta^3)^{\frac{1}{4}}\exp 2\pi(2Q/3\Delta)^{\frac{1}{2}},$$
$$2/\Delta=1/\Delta_\nu+1/\Delta_\pi. \tag{2}$$

Here Δ_ν and Δ_π are the average spacings between adjacent single-particle levels at the tops of the neutron and proton distributions for the normal state; these quantities have the values

$$\Delta_\nu\sim 31.6/B^2A^{\frac{1}{3}}(2N)^{\frac{1}{3}}\cdot mc^2,$$
$$\Delta_\pi\sim 31.6/B^2A^{\frac{1}{3}}(2Z)^{\frac{1}{3}}\cdot mc^2, \tag{3}$$
$$\Delta\sim 31.6/B^2A\cdot mc^2$$

for a system of Z protons and $N=A-Z$ neutrons in a spherical box of radius $R=BA^{\frac{1}{3}}e^2/mc^2$. Separate density functions for each value of the orbital angular momentum have also been computed.[1,3]

Certain properties of the density function are readily understood if the general distribution ϵ_1, ϵ_2, $\cdots$ is replaced by a system of uniformly spaced single-particle levels with the spacing Δ. It is clear that the addition or removal of an even number of neutrons or protons does not alter the number of ways in which a given excitation energy can be obtained provided only that the excitation energy is not large enough to raise a particle from the bottom of the single-particle distribution. However, the proportion of excited states in which a single particle obtains a large fraction of the excitation energy is negligible for large values of Q. Consequently the density function will not depend explicitly on Z or N within an even-even,

* Society of Fellows.

[1] H. A. Bethe, Phys. Rev. **50**, 332 (1936); Rev. Mod. Phys. **9**, 69 (1937).

[2] C. van Lier and G. E. Uhlenbeck, Physica **4**, 531 (1937).

[3] J. Bardeen, Phys. Rev. **51**, 799 (1937).

even-odd, or odd-odd series of nuclei; actually the asymptotic expression for $\rho(Q)$ does not involve explicitly even the odd-even character of the nucleus.

To extend the analysis of the independent particle model we have computed separate density functions $\rho_S(Q)$ for each value of the total spin in the nuclear series $4k\pm1$.

If the nuclear Hamiltonian H were known and a complete set of simple approximate wave functions $\psi_1, \psi_2, \cdots$ were available, an approximate evaluation of the density could be obtained by computing the diagonal matrix elements of H and identifying the level spacing with the separation of adjacent diagonal matrix elements. One of the authors[3] has made a calculation in this manner using exchange forces in the Hamiltonian and determinants constructed from products of single-particle wave functions for ψ_i. The problem can be reduced to that of a system of independent particles in a velocity dependent[4] potential well. At the top of the normal state distribution, the spacing between adjacent single-particle levels is about double that given in (3). Thus, for a given nuclear radius and excitation energy, this model yields a much smaller density than the true independent particle model.

The theory could be improved further by a first-order perturbation calculation. Generally a number of determinantal wave functions can be constructed from one configuration of single-particle orbits. In place of the determinants ψ_i, one should use the "correct" zero*th* order normalized and orthogonal linear combinations defined by the two conditions: (a) φ_i is a linear combination of determinants belonging to a single configuration, (b) $\int\cdots\int \varphi_i^* H \varphi_j d\tau = 0$ if $i \neq j$ and the two functions belong to the same configuration. With exchange forces the diagonal matrix elements $\int\cdots\int \varphi_i^* H \varphi_i d\tau$ arising from a single configuration would be spread generally over a wide range in the manner required by the observed dependence of nuclear energies on symmetry character. Because of computational difficulties this calculation has not been attempted. We present, in the following sections, an alternative attack on the problem which avoids the difficulties and some of the inaccuracies of perturbation and variational calculations.

[4] J. H. Van Vleck, Phys. Rev. **48**, 367 (1935).

Dependence of Potential Energy on Symmetry Character

The empirical mass defects and stability relations reveal a strong dependence of nuclear binding energy on symmetry character. A semi-empirical theory of this effect has been developed by Wigner[5] under the assumptions (a) the particles interact in pairs, (b) the spin dependent and Coulomb interactions are effectively small in comparison with the part of the Hamiltonian operator which is invariant under permutations of the space coordinates of the particles. The diagonal matrix elements of the potential energy then contain a symmetry dependent term having the form

$$V' = \tfrac{1}{2}A(A-1)\chi(P)/\chi(1)\cdot L(A), \qquad (4)$$

where $\chi(P)$ is the character of a transposition and $\chi(1)$ the character of the identity in the irreducible representation of the symmetric group to which the state in question belongs. The coefficient $L(A)$ is a matrix element involving the density functions for symmetrically and antisymmetrically coupled particles and the magnitude and range of the interaction operator between pairs of particles. The values of $L(A)$ required to fit the experimental material fall on a smooth curve with the correct asymptotic behavior. In this paper we take

$$L(A) \sim \Delta \sim 31.6/B^2 A \cdot mc^2, \qquad (5)$$

which is sufficiently close to Wigner's semi-empirical determination and convenient for the discussion of level density. Since energy differences only are involved in the theory of level density (5) may be replaced by a more convenient form

$$V'' = V'(\lambda) - V'(\lambda_0) = \omega(\lambda, \lambda_0) L(A),$$
$$\omega(\lambda, \lambda_0) = \tfrac{1}{2}A(A-1)\{(\chi(P)/\chi(1))_\lambda - (\chi(P)/\chi(1))_{\lambda_0}\} \geqq 0. \qquad (6)$$

Here λ_0 and λ are quantum numbers (partition symbols) describing the symmetry character of the normal and excited states respectively.

[5] E. Wigner, Phys. Rev. **51**, 106 (1937), (A); **51**, 947 (1937), (B).

The unsymmetrical part of the Coulomb interaction,

$$\sum_{1\leq i<j\leq Z} e^2/r_{ij} - Z(Z-1)/A(A-1)\cdot \sum_{1\leq i<j\leq A} e^2/r_{ij}, \quad (7)$$

eventually becomes large enough to destroy the symmetry character as a good quantum number by mixing together states belonging to different irreducible representations of the symmetric group; this effect probably accounts for the failure of Wigner's theory beyond mass 54. However, the usefulness of (5) and (6) in a calculation of level density should extend somewhat beyond $A=54$, because a quantity defined as an average over a number of levels should not be sensitive to a lack of sharp definition in some of the quantum numbers.

Level Densities with Constant and Symmetry Dependent Potential Energies

By using (6) to compute potential energy differences, one avoids the approximations and special assumptions involved in an actual calculation of the potential energy matrix elements. Kinetic energy differences are presumably given with reasonable accuracy by the model of noninteracting particles in a spherical box with a constant spacing Δ of single-particle levels at the top of the normal state distribution.

The symmetry properties of a configuration are completely determined by the distribution of particles in singly, doubly, triply, and quadruply occupied orbits. For the discussion of symmetry properties the configuration may be represented by a partition symbol $\mu=(\mu_l, \mu_{l-1}, \cdots \mu_1)$ with as many μ's equal to m as there are orbits containing m particles. Note that $A=\mu_l+\mu_{l-1}+\cdots+\mu_1$. To avoid ambiguity the μ's are ordered so that $\mu_l \geqslant \mu_{l-1} \geqslant \cdots \geqslant \mu_1 \geqslant 1$.

TABLE I. *Constant potential energy. $\rho_S(K\Delta)\Delta$ and $\rho(K\Delta)\Delta$ for the nuclear type $4k\pm1$.*

	$\rho_S(K\Delta)\Delta$					
K	$S=1/2$	$S=3/2$	$S=5/2$	$S=7/2$	$S=9/2$	$\rho(K\Delta)\Delta$
0	1					2
1	4	1				12
3	37	17	1			148
6	496	316	54	1		2590
9	4290	3220	812	55		26760
12	28500	23780	7510	850	18	204200
15	158200	142200	52300	8000	370	1266800

Let $P(\mu; K)$ denote the number of modes of excitation associated with the partition symbol μ and the kinetic energy $K\Delta$, and $M(S, T_z; \mu)$ the number of times the state with $T_z=\frac{1}{2}(N-Z)$ and total spin S occurs in a configuration belonging to μ.[6] Assuming a constant potential energy, the level densities $\rho_S(K\Delta)$ and $\rho(K\Delta)$ are given by the expressions

$$\begin{aligned}\rho_S(K\Delta)\Delta &= \sum_\mu M(S, T_z; \mu)P(\mu; K),\\ \rho(K\Delta)\Delta &= \sum_\mu \{\sum_S (2S+1)M(S, T_z; \mu)\}P(\mu; K).\end{aligned} \quad (8)$$

The set of functions generated from a single configuration by permutations of coordinates subtends a linear manifold in function space; with respect to the transformations of the symmetric group this manifold, $\Delta(\mu)$, is either irreducible or a linear combination of invariant subspaces which are irreducible. The invariant subspaces are denoted by the symbols $[\lambda]$ $[\lambda_k, \lambda_{k-1}, \cdots, \lambda_1]$, $\lambda_k \geqslant \lambda_{k-1} \geqslant \cdots \geqslant \lambda_1 \geqslant 1$, $\lambda_k+\lambda_{k-1}+\cdots+\lambda_1=A$ and the number of times the irreducible representation $[\lambda]$ occurs in $\Delta(\mu)$ by

$$(\lambda/\mu)=\begin{pmatrix}\lambda_k\lambda_{k-1}\cdots\lambda_1\\ \mu_l\mu_{l-1}\cdots\mu_1\end{pmatrix}.$$

To compute the level density when the dependence of potential energy on symmetry character is given by (6), we introduce two new quantities:

$$P'(\lambda, K)=\sum_\mu (\lambda/\mu)P(\mu; K),$$

the number of times the irreducible representation $[\lambda]$ occurs in the various modes of excitation, and $M'(S, T_z; \lambda)$, the number of ways in

TABLE II. *Symmetry dependent potential energy. $\rho_S'(K\Delta)\Delta$ and $\rho'(K\Delta)\Delta$ for the nuclear types $4k\pm1$, $|N-Z|=1$.*

	$\rho_S'(K\Delta)\Delta$				
K	$S=1/2$	$S=3/2$	$S=5/2$	$S=7/2$	$\rho'(K\Delta)\Delta$
0	1				2
1	2				4
3	11				22
6	104	8			240
9	695	105			1810
12	3890	833	9		11160
15	18850	5140	133		59000
18	82200	26700	1260	1	278000

[6] Methods used for computing the multiplicities are given in the appendix, part B.

TABLE III. *Symmetry dependent potential energy.* $\rho_S'(K\Delta)\Delta$ *and* $\rho'(K\Delta)\Delta$ *for the nuclear types* $4k\pm1$, $|N-Z|=3$.

K	$\rho_S'(K\Delta)\Delta$ $S=1/2$	$S=3/2$	$S=5/2$	$S=7/2$	$\rho'(K\Delta)\Delta$
0	1				2
1	3				6
3	20	1			44
6	194	24			484
9	1330	258	1		3690
12	7420	1880	34		22550
15	35700	10980	390		117600
18	153800	54700	2970	4	544300

TABLE IV. *Symmetry dependent potential energy.* $\rho_S'(K\Delta)\Delta$ *and* $\rho'(K\Delta)\Delta$ *for the nuclear types* $4k\pm1$, $|N-Z|=5$.

K	$\rho_S'(K\Delta)\Delta$ $S=1/2$	$S=3/2$	$S=5/2$	$S=7/2$	$\rho'(K\Delta)\Delta$
0	1				2
1	3				6
3	23	1			50
6	252	34			640
9	1831	387	3		5230
12	10570	2900	73		33160
15	51900	17080	747		176700
18	226500	85500	5400	14	827000

which the total spin S can be associated with the irreducible representation $[\lambda]$ to yield a completely antisymmetric function in the space, spin and charge spin coordinates of the particles. For the densities $\rho_S'(K\Delta)$ and $\rho'(K\Delta)$, which replace $\rho_S(K\Delta)$ and $\rho(K\Delta)$, we obtain

$$\begin{aligned}\rho_S'(K\Delta)\Delta&=\sum_\lambda M'(S,T_z;\lambda)P'(\lambda;K-\omega(\lambda,\lambda_0))\\&=\sum_\lambda\sum_\mu M'(S,T_z;\lambda)(\lambda/\mu)\\&\qquad\times P(\mu;K-\omega(\lambda,\lambda_0)),\\\rho'(K\Delta)\Delta&=\sum_\lambda\{\sum_S(2S+1)M'(S,T_z;\lambda)\}\\&\qquad\times P'(\lambda;K-\omega(\lambda,\lambda_0))\\&=\sum_\lambda\sum_\mu\{\sum_S(2S+1)M'(S,T_z;\lambda)\}\\&\qquad\times(\lambda/\mu)P(\mu;K-\omega(\lambda,\lambda_0)).\end{aligned}\tag{9}$$

Evidently

$$M(S,T_z;\mu)=\sum_\lambda M'(S,T_z;\lambda)(\lambda/\mu)\tag{10}$$

and the primed and unprimed densities are identical if ω is omitted in the argument of $P'(\lambda;K)$. Since $P'(\lambda;K)$ is a rapidly increasing function of K, the substitution of $K-\omega$ for K results in a considerable decrease in level density.

Numerical results from the evaluation of (8) and (9) are exhibited in Tables I–VIII. The method of calculation is described in the appendix.

The tables reveal a striking *dependence of level density on* $|N-Z|$ *in an isobaric series.* This consequence of the theory can be tested directly by transmutation experiments on isobars. The computed level spacing may very well be considerably in error because of the unavoidable oversimplification in the model and because of uncertainty in the correct value of the energy unit Δ. However the ratios of level densities at a definite excitation energy in a series of isobars should be free from much of the inaccuracy and uncertainty which affects the computed spacing of levels.

The essential reason for the increase in level density with increasing $|N-Z|$ in an isobaric series is that when $|N-Z|$ is small the lowest state belongs to a representation of very high symmetry and states belonging to practically all other representations have much higher energies. Thus most of the low-lying levels belong to a comparatively few representations which have high symmetry. On the other hand, if $|N-Z|$ is large, even the lowest state cannot have high symmetry and states belonging to many other representations have nearly as low an energy.

TABLE V. *Symmetry dependent potential energy.* $\rho_S'(K\Delta)\Delta$ *and* $\rho'(K\Delta)\Delta$ *for the nuclear types* $4k\pm1$, $|N-Z|=7$.

K	$\rho'(K\Delta)\Delta$ $S=1/2$	$S=3/2$	$S=5/2$	$S=7/2$	$\rho'(K\Delta)\Delta$
0	1				2
1	3				6
3	24	1			52
6	278	37			704
9	2120	457	4		6100
12	12700	3570	98		40290
15	64100	21710	1030	1	221200
18	284500	110700	7500	27	1057000

TABLE VI. *Nuclear type* $4k$. $\rho(K\Delta)\Delta$ *and* $\rho'(K\Delta)\Delta$ *as functions of* $|N-Z|$.

K	$\rho(K\Delta)\Delta$ N,Z EVEN	N,Z ODD	$\rho'(K\Delta)\Delta$ $\lvert N-Z\rvert=0$	$\lvert N-Z\rvert=2$	$\lvert N-Z\rvert=4$	$\lvert N-Z\rvert=6$	$\lvert N-Z\rvert=8$
0	1	4	1	4	1	4	1
1	8	16	1	12	2	16	2
3	112	192	6	76	21	124	22
5	856	1330	30	352	124	664	141
7	4820	7170	134	1716	589	2890	734
9	22320	31990	535	5040	2380	10880	3210
11	90140	100340	1970	16610	8580	37140	12320
13	327700	446200	6660	50720	28320	116730	42750
15	1095300	1439000	20970	146500	86600	344700	136600

Appendix. Part A

Calculation of $P'(\lambda; K)$

We are interested in finding $P'(\lambda; K)$, the number of times the irreducible representation $[\lambda]$ occurs for a given (kinetic) excitation energy K. (To simplify the notation the energy unit is taken equal to Δ). Some of the calculations have been made by using the equation

$$P'(\lambda; K)=\sum_{\mu}(\lambda/\mu)P(\mu; K). \qquad (11)$$

We first find $P(\mu; K)$, the number of configurations which have the energy K, multiply by (λ/μ), the number of times the irreducible representation $[\lambda]$ occurs in the manifold $\Delta(\mu)$, and finally sum over all configurations. For this purpose we have prepared tables of the numbers (λ/μ) for configurations of interest which include as many as twenty particles outside of closed four-groups.[7]

In many cases it is simpler to calculate $P'(\lambda; K)$ by a direct method; in the following sections we indicate how this may be done. In a sense, our problem is a generalization of Fermi-Dirac and Einstein-Bose statistics. In the former we want to know the number of times the antisymmetric representation occurs for a given energy; in the latter the number of times the symmetric representation occurs. In the present case we are interested in representations of intermediate symmetry types.

Table VII. *Nuclear type 4k+2. $\rho'(K\Delta)\Delta$ as a function of $|N-Z|$.*

K	$\rho'(K\Delta)\Delta$ $\|N-Z\|=0$	$\|N-Z\|=2$	$\|N-Z\|=4$	$\|N-Z\|=6$	$\|N-Z\|=8$
0	4	1	4	1	4
1	8	2	16	2	16
3	56	18	112	22	128
5	256	88	564	138	704
7	1008	378	2332	696	3150
9	3610	1460	8480	2980	12200
11	11780	5120	28180	11340	42520
13	36160	16770	86500	39370	136000
15	104800	51000	250300	127200	406300

[7] For a discussion of methods which may be used to compute the numbers (λ/μ) see F. D. Murnaghan, A. J. of Math. **59**, 437 (1937). Tables of (λ/μ) for values of n up to and including nine are given in this paper. We have prepared tables of these numbers for configurations of interest with values of n extending to twenty. We will be glad to supply the tables we have computed to any one who has use for them.

Table VIII. *Summary of level density dependence on nuclear type and $|N-Z|$. Ratio of $\rho'(K\Delta)$ to the level density for the nuclear type 4k, $|N-Z|=0$.*

K	$\|N-Z\|=0$	$\|N-Z\|=2$	$\|N-Z\|=4$	$\|N-Z\|=6$	$\|N-Z\|=8$
			Nuclear Type $4k$		
2	1	10.7	2.3	16.0	2.3
5	1	11.7	4.1	22.1	4.7
10	1	8.8	4.4	19.2	6.0
15	1	7.0	4.1	16.4	6.5
			Nuclear Type $4k+2$		
2	8.0	2.0	14.7	2.3	16.0
5	8.5	2.9	18.8	4.6	23.5
10	6.2	2.6	14.7	5.6	21.7
15	5.0	2.4	11.9	6.1	19.4
			Nuclear Type $4k\pm1$		
K	$\|N-Z\|=1$	$\|N-Z\|=3$	$\|N-Z\|=5$	$\|N-Z\|=7$	
2	3.3	5.3	6.0	6.0	
5	3.8	7.3	9.7	10.5	
10	3.2	6.5	9.4	11.1	
15	2.8	5.6	8.4	10.5	

A similar problem, which occurs in the case of electrons, is to determine the number of states of a given energy with a given total spin S. The procedure which is generally followed is to determine first the number of states $\rho_M(M_z)$ with a z component of spin equal to M_z. The number of levels, $\rho(S)$, with spin S, is then found from the familiar equation:

$$\rho(S)=\rho_M(S)-\rho_M(S+1). \qquad (12)$$

A similar procedure may be followed in the present case. Instead of a two-valued spin we must now consider a spin with four components $(\eta_1, \eta_2, \eta_3, \eta_4)$ which, according to Wigner,[8] we may define as follows:

η_1 = number of protons with $-$ spin
η_2 = " " neutrons " $-$ "
η_3 = " " protons " $+$ "
η_4 = " " neutrons " $+$ " .

The number of states, $N(\eta_1, \eta_2, \eta_3, \eta_4; K)$, of energy K and with spin components $(\eta_1, \eta_2, \eta_3, \eta_4)$ may be found by some standard method such as that of Sommerfeld.[9] The number of levels, $P'(\lambda; K)$, belonging to a given representation

[8] Reference 5, (A).
[9] A. Sommerfeld, Zeits. f. Physik **47**, 1 (1927). See also H. A. Bethe, Rev. Mod. Phys. **9**, 69 (1937).

$[\lambda]$ of the symmetric group may be obtained from a generalization of (12). While the equation is simple in form, it is rather difficult to use, so that we give only the result.

Let us define operators x_1, x_2, x_3, x_4 such that

$$x_1 N(\eta_1, \eta_2, \eta_3, \eta_4; K) = N(\eta_1 - 1, \eta_2, \eta_3, \eta_4; K),$$

$$x_2 N(\eta_1, \eta_2, \eta_3, \eta_4; K) = N(\eta_1, \eta_2 - 1, \eta_3, \eta_4; K), \text{ etc.}$$

The appropriate generalization of (12) is

$$P'(\lambda; K) = (x_4 - x_3)(x_4 - x_2)(x_4 - x_1) \times (x_3 - x_2)(x_3 - x_1)(x_2 - x_1) \times N(\Lambda_1, \Lambda_2 + 1, \Lambda_3 + 2, \Lambda_4 + 3), \quad (13)$$

where $[\Lambda_1, \Lambda_2, \Lambda_3, \Lambda_4]$ is the representation associate to $[\lambda_k, \lambda_{k-1}, \cdots \lambda_1]$. If in the representation $[\lambda]$ there are n_1 ones, n_2 twos, n_3 threes, and n_4 fours,

$$\begin{aligned} \Lambda_4 &= n_4 + n_3 + n_2 + n_1, \\ \Lambda_3 &= n_4 + n_3 + n_2, \\ \Lambda_2 &= n_4 + n_3, \\ \Lambda_1 &= n_4. \end{aligned} \quad (14)$$

In general, there may be as many as 2^6 or 64 terms to sum in (13), so that the expression is not very suitable for numerical work. We have found that simpler equations are obtained if, instead of considering the spin, we deal directly with the space functions.

Generating function for $P(\mu; K)$

Let us return to Eq. (11). The various quantities in which we are interested can be computed from generating functions. Let us first consider $P(\mu_l, \cdots \mu_1; K)$, the number of modes of excitation of energy K associated with the partition $(\mu_l, \cdots, \mu_1)$. In the partition there are γ_1 singly occupied orbits, γ_2 doubly occupied orbits, etc. The total number of particles $n = \gamma_1 + 2\gamma_2 + \cdots + h\gamma_h$. For the application to nuclei, we are interested in the case where no orbital is occupied by more than four particles, but we will carry through the analysis for the general case. Let us define the quantities*

$$U_i = y^{\epsilon_i}, \qquad (i = 1, 2, \cdots m),$$

where y is an indeterminant. In order to avoid dealing with an infinite number of U_i's, we take m finite but so large that $\epsilon_m > K$. It is easily seen that $P(\mu; K)$ is the coefficient of y^K in the symmetric function

$$\sum (U_1 \cdots U_{\gamma_1})(U_{\gamma_1+1} \cdots U_{\gamma_1+\gamma_2})^2 \times (U_{\gamma_1+\gamma_2+1} \cdots U_{\gamma_1+\gamma_2+\gamma_3})^3 \cdots. \quad (15)$$

The sum is over all $m!/(m - \sum \gamma_i)!\gamma_1!\gamma_2! \cdots \gamma_h!$ combinations of the subscripts which lead to different products.

There are no simple general expressions for the numbers (λ/μ) and the generating function (15) for $P(\mu; K)$ is rather complicated. Nevertheless, a rather simple expression can be obtained for the generating function for $P'(\lambda; K)$. In order to derive this expression, we make use of the method of characteristics.

Method of characteristics

Since the method of characteristics is perhaps not very familiar, we will give in outline the results which we will need later. For further details, the reader is referred to a recent article by Murnaghan.[10] The characteristic of an irreducible representation (p) of a finite group is defined by:

$$\phi_p(s) = \frac{1}{N} \sum_q N_q \chi_p^{(q)*} s^{(q)}, \quad (16)$$

where N is the total number of elements in the group; N_q is the number of elements in the class (q); $\chi_p^{(q)}$ is the character of the irreducible representation p going with the class q; and the $s^{(q)}$ are indeterminants. The sum is over all classes. The asterisk represents the complex conjugate.

The characteristic of a reducible representation which contains the irreducible representation (p) c_p times is simply

$$\phi(s) \equiv \sum_q a_q s^{(q)} = \sum_p c_p \phi_p(s) = \frac{1}{N} \sum_p \sum_q c_p N_q \chi_p^{(q)*} s^{(q)}. \quad (17)$$

* The ϵ_i are the individual particle energies defined in the introduction.

[10] Reference 7. The complete theory of the representations of the symmetric group is given in this article. We have attempted to follow Murnaghan's notation wherever possible.

From the orthogonality of the characters, we have

$$c_p=\sum_q \chi_p{}^{(q)}a_q. \tag{18}$$

If the characteristic of a reducible representation is known, this equation enables one to obtain the number of times a given irreducible representation is contained in the reducible representation.

Application to the symmetric group

The method of characteristics is particularly suitable for application to the symmetric group. All permutations having the same cyclic structure belong to the same class, which may be denoted by the symbol $(\alpha)=(\alpha_1, \alpha_2, \cdots, \alpha_r)$. The permutations of the class contain α_1 unary cycles, α_2 binary cycles, α_3 ternary cycles, etc. Note that $\alpha_1+2\alpha_2+3\alpha_3+\cdots+r\alpha_r=n$, the total number of particles on which the permutations act. The number of permutations in the class (α) is

$$N_{(\alpha)}=n!/1^{\alpha_1}2^{\alpha_2}\cdots r^{\alpha_r}\alpha_1!\alpha_2!\cdots\alpha_r!. \tag{19}$$

The indeterminant $s^{(q)}$ going with the class (α) may be expressed in the form:

$$s^{(q)}=s_1{}^{\alpha_1}s_2{}^{\alpha_2}\cdots s_r{}^{\alpha_r}. \tag{20}$$

The principal characteristic of the permutation group of order n (i.e., the characteristic of the identity representation) is:

$$q_n(s)=\sum_\alpha 1/\alpha_1!\alpha_2!\cdots\alpha_r! \cdot(s_1/1)^{\alpha_1}(s_2/2)^{\alpha_2}\cdots(s_r/r)^{\alpha_r}. \tag{21}$$

The sum is over all values of $\alpha_1, \alpha_2, \cdots, \alpha_r$ subject to the restriction $\alpha_1+2\alpha_2+\cdots+r\alpha_r=n$. The characteristic of the irreducible representation $[\lambda_k, \lambda_{k-1}, \cdots, \lambda_1]$ is:

$$\phi_\lambda(s)=\sum_\alpha \chi_{(\lambda)}{}^{(\alpha)}/\alpha_1!\alpha_2!\cdots\alpha_r! \cdot(s_1/1)^{\alpha_1}(s_2/2)^{\alpha_2}\cdots(s_r/r)^{\alpha_r} \tag{22}$$

$$=\begin{vmatrix} q_{\lambda_k}(s) & q_{\lambda_k+1}(s) & \cdots & q_{\lambda_k+k-1}(s) \\ q_{\lambda_{k-1}-1}(s) & q_{\lambda_{k-1}}(s) & \cdots & q_{\lambda_{k-1}+k-2}(s) \\ \cdot & \cdot & \cdot & \cdot \\ \cdot & \cdot & \cdot & \cdot \\ \cdot & \cdot & \cdot & \cdot \\ q_{\lambda_1-k+1}(s) & q_{\lambda_1-k+2}(s) & \cdots & q_{\lambda_1}(s) \end{vmatrix} \tag{22'}$$

Here $q_\lambda(s)$ is the principle characteristic of the permutation group of order λ. By convention, $q_0(s)=1$ and $q_\lambda(s)$ vanishes if λ is negative. The fact that (22′) gives a characteristic of an irreducible representation was first pointed out by Frobenius, although the above form is due to Schur. It is this expression which gives the justification for the characterization of an irreducible representation of the symmetric group in terms of a partition of the integer n.

It is sometimes convenient to express the indeterminants s_i in terms of other indeterminants $z_1, z_2, \cdots, z_{m'}$, by means of the relations:

$$s_i=z_1{}^i+z_2{}^i+\cdots+z_{m'}{}^i, \tag{23}$$

where m' is some large number ($\geqslant n$). The principle characteristic, $q_n(s)$, when expressed in terms of the z's, is the complete homogeneous symmetric function $p_n(z)$. Thus $q_n(s)=p_n(z)$, and in particular,

$$p_0(z)=1; \quad p_1(z)=\sum z_1; \quad p_2(z)=\sum z_1{}^2+\sum z_1z_2;$$
$$p_3(z)=\sum z_1{}^3+\sum z_1{}^2z_2+\sum z_1z_2z_3; \quad \text{etc.}$$

The $p_n(z)$ may be obtained from the generating function

$$f(z, t)=\{(1-z_1t)(1-z_2t)\cdots(1-z_{m'}t)\}^{-1} =p_0(z)+p_1(z)t+p_2(z)t^2+\cdots. \tag{24}$$

Generating function for $P'(\lambda; K)$

The expression (20) for the indeterminants $s^{(\alpha)}$ going with the different classes of the symmetric group is very suitable for our purpose because of the following theorem[11] which is based on this expression: the characteristic $\phi_{(\mu)}(s)$ of the reducible representation given by the manifold $\Delta(\mu)$ composed of γ_1 singly occupied orbits, γ_2 doubly occupied orbits, etc. is given by the product:

$$\phi_{(\mu)}(s)=(q_1(s))^{\gamma_1}(q_2(s))^{\gamma_2}\cdots(q_k(s))^{\gamma_k}. \tag{25}$$

The characteristic of the (reducible) representation given by the manifold of all functions with a given kinetic energy K is therefore:

$$\phi(s; K)=\sum_\mu P(\mu; K)(q_1(s))^{\gamma_1} \times(q_2(s))^{\gamma_2}\cdots(q_k(s))^{\gamma_k}. \tag{26}$$

[11] For a proof of this theorem, see Murnaghan, reference 7.

Let us now substitute the generating function (15) for $P(\mu; K)$ and replace $q_i(s)$ by $p_i(z)$. Then $\phi(s; K)$ is the coefficient of $y^K t^n$ in the following function:

$$g(U, z, t)=\sum_{\gamma}\{(U_1\cdots U_{\gamma_1})\times(U_{\gamma_1+1}\cdots U_{\gamma_1+\gamma_2})^2\cdots\}\times p_1^{\gamma_1}p_2^{\gamma_2}\cdots p_h^{\gamma_h}t^{\gamma_1+2\gamma_2+\cdots+h\gamma_h}. \quad (27)$$

The sum is over all values of the γ's. This function may be written in the form:

$$g(U, z, t)=\prod_{i=1}^{m}\prod_{j=1}^{m'}(1-U_iz_jt)^{-1}, \quad (28)$$

as is shown most easily by expanding the product for each value of i into a power series in t and then multiplying the resulting series together. From (28) we have:

$$\log g(U, z, t)=-\sum_i\sum_j\log(1-U_iz_jt)=\sum_i\sum_j(U_iz_jt+U_i^2z_j^2t^2/2+U_i^3z_j^3t^3/3\cdots). \quad (29)$$

Let us now express the U's in terms of new variables x_β defined by:

$$x_\beta=\sum_i U_i^\beta=\sum_i y^{\beta\epsilon_i}, \quad (\beta=1, 2, 3, \cdots). \quad (30)$$

From (23) and (30) we obtain

$$g(U, z, t)=\exp\{x_1s_1t+x_2s_2t^2/2+x_3s_3t^3/3\cdots\}=\sum_\alpha 1/\alpha_1!\alpha_2!\cdots\alpha_r!\cdot(x_1s_1/1)^{\alpha_1}(x_2s_2/2)^{\alpha_2}\cdots\times(x_rs_r/r)^{\alpha_r}t^{\alpha_1+2\alpha_2+\cdots+r\alpha_r}. \quad (31)$$

The generating function for $P'(\lambda; K)$ is obtained by finding how often the irreducible representation $[\lambda]$ is contained in the representation defined by the above characteristic. From the general equation (18), we find that $P'(\lambda; K)$ is the coefficient of y^K in

$$F(\lambda; y)=\sum_\alpha\chi_{(\lambda)^{(\alpha)}}/\alpha_1!\alpha_2!\cdots\alpha_r!\cdot(x_1/1)^{\alpha_1}(x_2/2)^{\alpha_2}\cdots(x_r/r)^{\alpha_r}, \quad (32)$$

where the summation is over all values of $\alpha_1, \alpha_2, \cdots, \alpha_r$ subject to the restriction $\alpha_1+2\alpha_2+\cdots+r\alpha_r=n$. In (32), $\chi_{(\lambda)^{(\alpha)}}$ is the character of the irreducible representation $[\lambda]$ going with the class $(\alpha)=(\alpha_1, \alpha_2, \cdots, \alpha_r)$.

Now the simple characteristic (22) of the irreducible representation $[\lambda]$ of the symmetric group on n particles has exactly the same form as (32). We need merely identify x_i with s_i. Since the equivalence of (22) and (22′) is an algebraic identity, the generating function (32) can also be expressed in the determinantal form (22′). This form is to be preferred because it does not involve the characters.

Generating function for evenly spaced levels

In the special case that the individual particle levels are evenly spaced, the generating function for $P'(\lambda; K)$ is particularly simple. We first obtain an expression for the function $q_n(y)$ defined by substituting x_i for s_i in $q_n(s)$ and then replacing x_i by its value in terms of y. For simplicity, as already remarked, we take the spacing between the individual particle levels as the unit of energy, so that

$$x_i=\sum_{k=0}^{\infty}y^{ki}=1/(1-y^i). \quad (33)$$

From Eqs. (23) and (24)

$$f(s, t)=q_0(s)+q_1(s)t+q_2(s)t^2+\cdots$$

and

$$\log f(s, t)=s_1t+s_2t^2/2+s_3t^3/3+\cdots.$$

The logarithm of the generating function for $q_n(y)$ is therefore

$$\begin{aligned}\log f(y, t)&=t/(1-y)+t^2/2(1-y^2)+t^3/3(1-y^3)+\cdots\\&=t(1-y)/(1-y)+yt/(1-y)+t^2(1-y^2)/2(1-y^2)+y^2t^2/2(1-y^2)+\cdots\\&=-\log(1-t)+\log f(y, yt),\end{aligned} \quad (34)$$

so that

$$(1-t)f(y, t)=f(y, yt). \quad (35)$$

Written out in full, Eq. (35) becomes

$$q_0+(q_1-q_0)t+(q_2-q_1)t^2+\cdots=q_0+ytq_1+y^2t^2q_2+\cdots.$$

Equating coefficients of t^n, we obtain the recurrence relation

$$q_n(y)=q_{n-1}(y)/(1-y^n). \tag{36}$$

Since $q_0=1$, repeated applications of (36) yield

$$q_n(y)=1/(1-y)(1-y^2)\cdots(1-y^n). \tag{37}$$

There remains to substitute expressions of this form into the determinant corresponding to (22′) and to evaluate this determinant, which can be reduced to the Vandermonde form. We give only the final result. $P'(\lambda;K)$ is the coefficient of y^K in

$$\begin{aligned}F(\lambda;y)&=y^{-k(k-1)(k-2)/6}\cdot q_{\lambda_k+k-1}(y)q_{\lambda_{k-1}+k-2}(y)\\&\quad\cdots q_{\lambda_1}(y)\prod_{i<j}(y^{\lambda_i+i-1}-y^{\lambda_j+j-1})\\&=y^{\lambda_{k-1}+2\lambda_{k-2}+\cdots+(k-1)\lambda_1}q_{\lambda_k+k-1}(y)\\&\quad\times q_{\lambda_{k-1}+k-2}(y)\cdots q_{\lambda_1}(y)\\&\quad\times\prod_{i<j}(1-y^{\lambda_j+j-\lambda_i-i}).\end{aligned} \tag{38}$$

It may be noted here that, except for a possible factor of a power of y, the generating functions of a given representation and its associate representation are the same.

Application to nuclear levels

In the application to nuclei of heavy or intermediate mass, we are interested in representations for which most of the λ_k's are equal to four; only a few have values less than four. In this case it is simpler to use the notation for the associate representation, which is defined by (14). The generating function for $P'(\lambda;K)$ is then

$$\begin{aligned}F(\lambda,y)&=y^{\frac{1}{2}[\Lambda_1^2+\Lambda_2^2+\Lambda_3^2+\Lambda_4^2]-\frac{1}{2}n}\\&\quad\times G(y)\prod_{i<j}(1-y^{\Lambda_j+j-\Lambda_i-i}),\\&\quad(i,j=1,2,3,4),\end{aligned} \tag{39}$$

where

$$G(y)=q_{\Lambda_4+3}(y)q_{\Lambda_3+2}(y)q_{\Lambda_2+1}(y)q_{\Lambda_1}(y).$$

In case the number of four-groups is large (Λ_1 large), we have, approximately,

$$G(y)\sim\prod_{i=1}^{\infty}(1-y^i)^{-4}. \tag{40}$$

This form has been used in the calculation of the tables given in the text. Eq. (39) may be used to calculate asymptotic formulae for the $P'(\lambda;K)$.

Appendix. Part B.

Multiplicities

The single-particle space orbits u_{j_1}, u_{j_2}, $\cdots$, with the j's equal in groups containing μ_l, μ_{l-1}, $\cdots$, μ_1 orbits, can be combined with single-particle spin functions g_1, g_2, g_3, g_4 to form a set of determinantal wave functions

$$|u_{j_1}g_{k_1}\,u_{j_2}g_{k_2}\cdots|, \tag{41}$$

which subtends an invariant subspace in the linear manifold $\Delta(\mu)$. Each determinant has definite S_z and T_z quantum numbers. Suitable linear combinations of the determinants with definite S_z, T_z describe states with definite values of S, the total ordinary spin, and T, the total charge spin. We wish first to compute $M(S,T;\mu)$, the number of times the state with given S, T values and $S_z=S$, $T_z=T$ occurs in the manifold $\Delta(\mu)$. One sees immediately that this quantity depends only on the number of two-groups and the total number of one and three-groups. Thus

$$M(S,T;\mu)\equiv M(S,T;\gamma_1+\gamma_3,\gamma_2). \tag{42}$$

Obviously the multiplicity is symmetrical in S and T. If $M(S,T;\gamma_1,\gamma_2)$ is known we compute $M(S,T;\gamma_1+1,\gamma_2)$ and $M(S,T;\gamma_1,\gamma_2+1)$ by means of the recurrence formulae

$$\begin{aligned}M(S,T;\gamma_1+1,\gamma_2)&=M(S-\tfrac{1}{2},T-\tfrac{1}{2};\gamma_1,\gamma_2)\\&\quad+M(S-\tfrac{1}{2},T+\tfrac{1}{2};\gamma_1,\gamma_2)\\&\quad+M(S+\tfrac{1}{2},T-\tfrac{1}{2};\gamma_1,\gamma_2)\\&\quad+M(S+\tfrac{1}{2},T+\tfrac{1}{2};\gamma_1,\gamma_2),\end{aligned} \tag{43}$$

$$\begin{aligned}M(S,T;\gamma_1,\gamma_2+1)&=M(S-1,T;\gamma_1,\gamma_2)\\&\quad+M(S,T-1;\gamma_1,\gamma_2)+M(S+1,T;\gamma_1,\gamma_2)\\&\quad+M(S,T+1;\gamma_1,\gamma_2)+2M(S,T;\gamma_1,\gamma_2).\end{aligned} \tag{44}$$

Terms with negative S or T must be omitted. These relations follow from the usual rules for combining angular momenta together with the starting values

$$\begin{aligned}M(S,T;1,0)&=1,\quad S=T=\tfrac{1}{2},\\&=0,\quad\text{for all other } S,T.\\M(S,T;0,1)&=1,\quad(S=1,T=0),\\&\qquad\qquad(S=0,T=1),\\&=0,\quad\text{for all other } S,T.\end{aligned} \tag{45}$$

The multiplicity $M'(S, T; \lambda)$ associated with the irreducible manifold $[\lambda]$ is related to $M(S, T; \mu)$ by the equation

$$M(S, T; \mu) = \sum_{\lambda} (\lambda/\mu) M'(S, T; \lambda). \quad (46)$$

Eq. (46) can be used as a recurrence formula for the computation of $M'(S, T; \lambda)$; since $(\lambda/\lambda) = 1$,

$$M'(S, T; \mu) = M(S, T; \mu) - \sum_{\lambda \neq \mu} (\lambda/\mu) M'(S, T; \lambda). \quad (47)$$

One needs also the starting values

$$M'(S, T; 4\cdots4) = 1, \quad S = T = 0,$$
$$= 0, \quad \text{for all other } S, T.$$

$$M'(S, T; 4\cdots41) = M'(S, T; 4\cdots43) = M(S, T; 1, 0). \quad (48)$$

$$M'(S, T; 4\cdots42) = M(S, T; 0, 1).$$

Finally

$$M'(S, T_z; \lambda) = \sum_{T \geqq |T_z|} M'(S, T; \lambda) \quad (49)$$

and

$$M(S, T_z; \mu) = \sum_{T \geqq |T_z|} M(S, T; \mu). \quad (50)$$

NOVEMBER 15, 1938 PHYSICAL REVIEW VOLUME 54

The Focusing of Charged Particles by a Spherical Condenser

EDWARD M. PURCELL
Harvard University, Cambridge, Massachusetts

(Received August 12, 1938)

The paths of charged particles traversing a portion of an ideal spherical condenser are worked out. The section of the condenser considered is bounded by two rays, enclosing an angle Φ, from the common center of curvature, O, of the equipotential surfaces. It is shown that a group of particles, homogeneous in energy, leaving a point P on a normal to one of these boundaries and entering the condenser along this normal as a diverging bundle, will be brought to a focus at a point Q lying on the line PO extended, if the proper potential is applied to the condenser. This permits the whole condenser gap to be used as a focusing energy analyzer, or monochromator, of very large useful aperture. The velocity dispersion and reduced velocity dispersion are calculated for the most general case, and are found to take the same simple form as do the corresponding expressions for the limited homogeneous magnetic field spectrograph. The expressions for the reduced velocity dispersion are identical in the two cases. Compensation for edge effect is discussed. The relativistic modification of the theory required for high speed particles is discussed and results are presented which indicate that the simple theory of the electrostatic spectrograph may be inadequate even for fairly low values of v/c. It is suggested that this difficulty may be avoided by the choice of suitable instrument parameters.

An analyzer is described which has a useful aperture of 0.210 steradians, a theoretical reduced dispersion of 1010, and which requires a total focusing potential of 0.315 E, where E is the particle energy in equivalent volts. The operation of the analyzer in focusing electrons accelerated by a field designed to furnish an equivalent point source is described.

INTRODUCTION

THE possibility of deflecting and focusing a slightly diverging beam of charged particles by means of a cylindrical condenser was first demonstrated by Hughes and Rojansky.[1] In Fig. 1(a), a beam of particles of the same charge and initial energy, diverging from P and traveling between the plates C and D of a cylindrical condenser, will be approximately focused at Q, if the circular arc PBQ, subtending an angle of $\pi/\sqrt{2}$ or 127° 17′, is the trajectory of those particles which leave P in a direction perpendicular to OP. This device is essentially an *energy*-analyzer, for the trajectory of a (nonrelativistic) particle in any given electrostatic field depends only on its initial position and direction and the ratio of its charge to its initial kinetic energy. Such analyzers have been incorporated in successful mass spectrographs.

[1] A. L. Hughes and V. Rojansky, Phys. Rev. **34**, 284 (1929).

A similar focusing effect is obtained in a uniform magnetic field, after traversal of 180°, for particles with the appropriate ratio of charge to momentum, a result so well known and widely applied as to make further description superfluous. Certain properties of the more general case, in which the extent of the magnetic field is limited, may be recalled, however. In Fig. 1(b), the homogeneous magnetic field (normal to the figure) in the shaded area is assumed to be cut off sharply at the boundaries OA and OB. Particles of the proper charge-to-momentum ratio leaving P and traveling near the normal PA, are approximately focused at Q, the intersection of the normal to the OB boundary and PO extended. The fact that the conjugate points lie on a line through O was pointed out by Barber.[2] In the corresponding general case of the cylindrical condenser, which has been investigated by Herzog,[3] no such simple rule holds, of course.

It will be noted that the focusing analyzers mentioned above are all two-dimensional, that is, they are analogous to optical systems composed of prisms and cylindrical lenses.

In the work to be described here, the focusing properties of the spherical condenser were investigated. The possibility of using a portion of a spherical condenser as an analyzer was suggested by Aston[4] in 1919. He remarked that particles of the proper energy entering the condenser in the proper direction would follow great circles and be united on the axis of the figure. The fact that there would also be a focusing action in a plane through the axis was not brought out, and no proof or further details were given. Our analysis will show that such a focusing effect does exist, and that it is described by formulas remarkably similar to those obtained for the general case of the homogeneous magnetic field spectrograph. Moreover it will be shown that the conjugate points are determined by a rule exactly corresponding to the relation found by Barber for the magnetic spectrograph; this result is particularly important here, for it permits the construction of a three-dimensional analyzer of very large useful aperture.

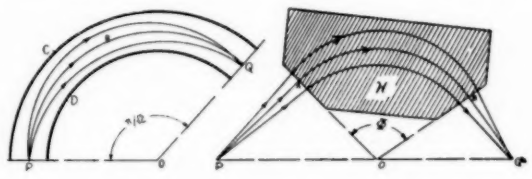

(a) (b)

FIG. 1.

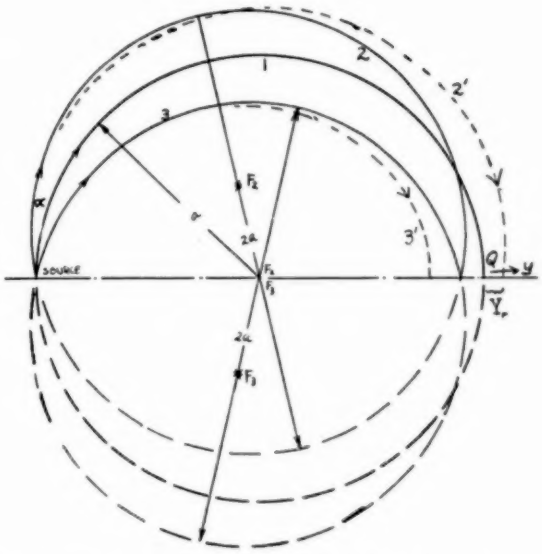

FIG. 2. The partial re-focusing of orbits of equal energy in an inverse square field.

THEORY

If one recalls that Kepler orbits of the same total energy in a given field have the same major axis, it appears from the construction in Fig. 2 that approximate re-focusing of orbits passing through a given point, the "source," and grouped about the circular orbit through that point, is obtained after a revolution of 180°. Clearly, from the symmetry of the figure, the intercept, y, measured from Q, is an even function of α, the angular separation of a trajectory at the source from the circular trajectory, and hence vanishes to the order of αa in the neighborhood of $\alpha=0$. A slightly diverging bundle of trajectories through P will therefore be nearly focused at the "receiving slit," Q. The similarity to the homogeneous magnetic field spectrograph, in which all trajectories are circular, is here first evident. It is this point which encourages one to attempt the analysis of the more general case,

[2] N. F. Barber, Proc. Leeds Phil. Soc. **2**, 427 (1933).
[3] R. Herzog, Zeits. f. Physik **89**, 447 (1934).
[4] F. W. Aston, Phil. Mag. **38**, 710 (1919).

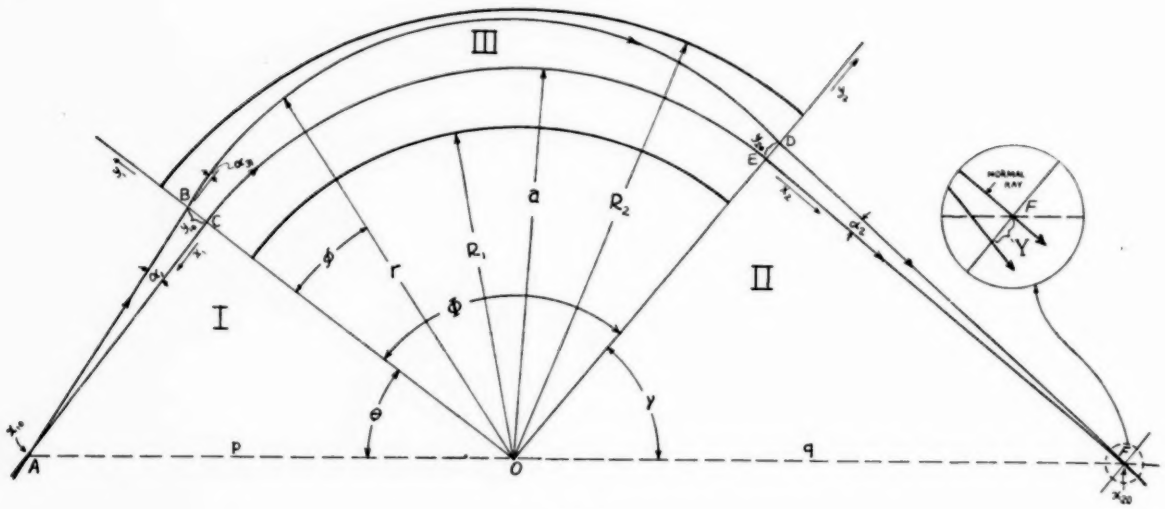

FIG. 3.

in which a section of the inverse-square field is considered; the "source" or "receiving slit" or both are permitted to lie in a field-free region outside, as in Fig. 3.

The problem will be treated as one of two dimensions. Only trajectories lying in a plane through the axis of symmetry of the condenser will be considered. Practically, this means that in the spectrograph finally suggested the source is supposed to be confined to this axis. Space charge will, of course, be neglected, as will, for the present, any modification required by relativity. The fringing field at the condenser edge will be ignored; the effect of this rather drastic simplification will be discussed later. The procedure, which is standard, is to calculate the trajectories approximately, by assuming α, the angle at the source between the trajectory in question and the "normal" trajectory, $ACEF$, to be small. Most of the results in which we shall be interested are obtained from a simple calculation carried only to the first power in α.

A particle of specific charge e/m travels along the trajectory $ABDF$ in Fig. 3. The first part of the trajectory, in the field-free region I, is defined by x_{10} and y_{10}, the intercepts on the x_1, y_1 axes. At the boundary $x_1=0$, the particle enters the electrostatic field between the spherical surfaces R_1 and R_2, which differ in potential by V_f. The original velocity, v_1, of the particle in region I, is: $v_1=v_0(1+\beta)$ if the circle of radius a is the proper orbit for a particle velocity v_0 entering along the x_1 axis. β is small, and represents a possible spread in velocity of the rays from the source. It is not necessary to consider a spread in mass as well, for the mass need not appear explicitly in the calculation. The particle leaves the field (again abruptly) at the boundary $x_2=0$ between the region III and the field-free region II. The problem is to find the path DF of the particle in II.

The radial field is $\mathcal{E}(r)=V_f R_1R_2/(R_2-R_1)r^2$, and the condition on the circular orbit requires that $\mathcal{E}(r)=amv_0^2/er^2$. It follows that, if $mv_0^2=2eE$, that is, if E is the energy in equivalent volts of the normal particle in I, and if $a=(R_1+R_2)/2$, the focusing potential must be given by:

$$V_f=E(R_2/R_1-R_1/R_2). \tag{1}$$

From the equations of motion, $\ddot{r}-r\dot{\varphi}^2=-\mathcal{E}e/m=-k^2/r^2$, and $r^2\dot{\varphi}=A$. where $k^2=av_0^2$, we obtain, by making the substitution $u=1/r$, $d^2u/d\varphi^2+u=k^2/A^2$, the integral of which is:

$$u=P\cos\varphi+Q\sin\varphi+k^2/A^2. \tag{2}$$

The boundary conditions are now applied and the powers of α_1 and β higher than the first are neglected. The equation of the trajectory in I is, $y_1=\alpha_1(x_{10}-x_1)$. Upon entering the field at $(0, y_{10})$ the particle experiences a change in kinetic energy which is: $ey_{10}\mathcal{E}(a)$, to the first order, or $v_{31}=v_0(1+\beta-y_{10}/a)$; v_{31} here means the velocity of the particle just after entering region III. The angular deflection of the path

at the boundary is clearly of the second order. Now $A=r^2\dot{\varphi}=av_{31}(1+y_{10}/a)=av_0(1+\beta)$. If we define z by $u=1/a(1+z)$, we can write the equation of the trajectory in *III*, to the present approximation, as

$$z=2\beta-aP\cos\varphi-aQ\sin\varphi. \quad (3)$$

Determining P and Q by the position and direction of the trajectory at the *I–III* boundary we find that,

$$z=\alpha_1\sin\varphi+(\alpha_1x_{10}/a-2\beta)\cos\varphi+2\beta. \quad (4)$$

The particle enters the region *II* at y_{20} given by:

$$y_{20}=az(\Phi)$$
$$=a[\alpha_1\sin\Phi+(\alpha_1x_{10}/a-2\beta)\cos\Phi+2\beta].$$

The angle $\alpha_2=-dz/d\varphi$ (at $\varphi=\Phi)=-\alpha_1\cos\Phi+(\alpha_1x_{10}/a-2\beta)\sin\Phi$. Then in the region *II*,

$$y_2=y_{20}-\alpha_2x_2$$
$$=a[\alpha_1\sin\Phi+(\alpha_1x_{10}/a-2\beta)\cos\Phi+2\beta]$$
$$+x_2[\alpha_1\cos\Phi-(\alpha_1x_{10}/a-2\beta)\sin\Phi]. \quad (5)$$

A bundle of "rays" from a source at $(x_{10}, 0)$ will be brought to convergence in *II* if y_2 can be made independent of α_1 for some value of x_2, say x_{20}. From (5), this requires that:

$$a(x_{10}+x_{20})=\tan\Phi(x_{10}x_{20}-a^2). \quad (6)$$

It will now be shown that the conjugate points, which we may conveniently call the "source" and the "slit," lie on a line through O. In Fig. 3, $\tan\gamma=x_{20}/a$; $\tan\theta=x_{10}/a$; $\tan(\theta+\gamma)=a(x_{10}+x_{20})/(a^2-x_{10}x_{20})=-\tan\Phi$, by (6). This is the property found by Barber for the case of the homogeneous magnetic field. It is fortunate that it holds here, for it permits one to make a three-dimensional spectrograph, using the whole gap between the spherical shells for focusing. Our actual analyzer, then, would be formed like the surfaces generated by rotating Fig. 3 about AOF, and all particles of the proper energy leaving A in a hollow cone would be focused at F. If the above result did not hold, the source at A would project as a *ring* in region *II*.[5]

[5] One might wonder whether a similar spectrograph of large aperture could not be made by a modification of the magnetic analyzer of Fig. 1 (*b*), in which the field would be "bent around in a ring." This was suggested by Stephens, Phys. Rev. **45**, 513 (1934), who was one of the first to study in detail the focusing by a sector of a magnetic field. This is not possible however, without modifying the shape of the field boundaries, for the requirement curl $H=0$ in the space through which the particles pass introduces an inhomogeneity which is necessarily large enough to invalidate Barber's rule. It is essentially an additional inhomogeneity of this order which makes our results here so different from those for the cylindrical condenser.

The velocity dispersion may now be obtained from (5). At x_{20} determined by (6) we have:

$$Y_2=2\beta a(1-\cos\Phi+(x_{20}/a)\sin\Phi). \quad (7)$$

Y_2 is the distance, measured from the normal ray, EF, by which a particle with velocity $v_0(1+\beta)$ misses F, the focal point for particles of velocity v_0. If we call AO, the "source distance," p, and OF, the "slit distance," q, (7) reduces to: $Y_2=2\beta a(1+q/p)$. The velocity dispersion proper, D_v, is defined as Y_2/β. We then have:

$$D_v=2a(1+q/p). \quad (8)$$

This is just twice the dispersion found for the case of the limited homogeneous magnetic field spectrograph.[6] It is perhaps more appropriate to speak of the *energy* dispersion of an electrostatic spectrograph. Since the energy dispersion D_e is just one-half the velocity dispersion, it will be given by exactly the same expression as is the velocity dispersion of the magnetic spectrograph.

A better figure of merit for an analyzer than the dispersion alone is represented by the *reduced dispersion*. This takes into account the broadening of the image of the source due to the fact that the focusing is only approximate, and that rays at an inclination α_1 to the normal ray will miss the focus by a small amount proportional to $(\alpha_1^2+\cdots)$. If B is the "trace width" so caused, then the reduced dispersion, Δ, is defined by $\Delta=|D/B|$. This is equivalent to the *resolving power* (for complete separation of lines) for an analyzer with an infinitely small receiving slit. It will be the energy resolution if D_e is used, the velocity resolution if D_v is used.

In order to obtain B we must carry the previous calculation to the order of α_1^2. Let $\delta=y_{10}/a$; that is, $\delta=\alpha_1x_{10}/a$. For convenience, the subscript will be dropped from α_1. Starting from (2), we wish to apply the boundary conditions with an accuracy of α^2. We are here considering only particles with $v_1=v_0$, or $\beta=0$.

[6] Brüche and Scherzer, *Geometrische Elektronenoptik* (J. Springer, 1934). See especially p. 142. Their z is the same as p/q here.

At the boundary *I–III* we must take into account not only the deflection of the path, but also the variation of the field with r. The change in kinetic energy at the boundary is $-mv_0^2\delta/(1+\delta)$. Then $v_{31}=v_0[1-2\delta/(1+\delta)]^{\frac{1}{2}}$. Now $v_{0r}=v_{31r}$. That is, the radial component of the velocity is not changed for the particle merely crosses the boundary suddenly into a region of different potential. Thus we can find $v_{31\varphi}$ from:

$$v_{31}^2=v_0^2[1-2\delta/(1+\delta)]=v_{0r}^2+v_{31\varphi}^2,$$

which yields:

$$v_{31\varphi}=v_0[1-2\delta/(1+\delta)-\alpha^2]^{\frac{1}{2}}.$$

Since

$$A=rv_{31\varphi}=av_0(1+\delta)[1-\alpha^2-2\delta/(1+\delta)]^{\frac{1}{2}}$$

the equation of the trajectory in *III* is:

$$1/(1+z)=aP\cos\varphi+aQ\sin\varphi+1/(1-\delta^2-\alpha^2). \quad (9)$$

Determining P and Q at the *I–III* boundary, we find: $aP=-(\delta+\alpha^2)$. $aQ=-(dz/d\varphi)/(1+z)^2=-\tan\alpha_{31}/(1+\delta)$, at $\varphi=0$. But $\tan\alpha_{31}=v_{31r}/v_{31\varphi}=\alpha[1-\alpha^2-2\delta/(1+\delta)]^{-\frac{1}{2}}$, which yields:

$$Q=-\alpha/a.$$

Writing δ' for y_{20}/a, or $z(\Phi)$, we obtain, after inserting the above values of P and Q in (9),

$$\delta'=(\alpha\sin\Phi+\delta\cos\Phi)+(\alpha\sin\Phi+\delta\cos\Phi)^2+\alpha^2(\cos\Phi-1)-\delta^2.$$

But, as one can easily show, $(\alpha\sin\Phi+\delta\cos\Phi)=\alpha x_{20}p/aq=\alpha\sin\gamma/\cos\theta$, so that we have finally for δ':

$$\delta'=\alpha\sin\gamma/\cos\theta+\alpha^2\sin^2\gamma/\cos^2\theta+\alpha^2(\sin\theta\sin\gamma-\cos\theta\cos\gamma-\sec^2\theta). \quad (10)$$

The angle α_{32} must now be determined from $\tan\alpha_{32}=(dr/d\varphi)/r$ at $\varphi=\Phi$ and from this α_2 must be found, taking into account the velocity change at the boundary, which will, of course, involve δ'. After some calculation, in which the appropriate approximations are made, one obtains: $\tan\alpha_2=\alpha\cos\gamma/\cos\theta+\alpha^2\sin\Phi$, to the order of α^2. Now Y_2, the amount by which the trajectory misses F, will be given by: $Y_2/a=\delta'-\tan\gamma\tan\alpha_2$. Using the results above for δ' and $\tan\alpha_2$, and the identities arising from $\theta+\gamma+\Phi=\pi$, one finally arrives at:

$$Y_2/a=-\alpha^2(\cos^2\gamma/\cos^2\theta+\cos\theta/\cos\gamma)=-\alpha^2(p^2/q^2+q/p). \quad (11)$$

The trace width, B, is then $-a\alpha^2(p^2/q^2+q/p)$. The minus sign indicates that the rays on the outside of the bundle are bent too much and pass underneath F in Fig. 3. Now the expression above is just twice the corresponding expression for the homogeneous magnetic field case, and hence, from the result expressed in (8), the reduced velocity dispersions of the two types of spectrograph are identical. For each:

$$\Delta=\left|\frac{D}{B}\right|=\frac{2(1+q/p)}{\alpha^2(p^2/q^2+q/p)}=\frac{2/\alpha^2}{1-p/q+p^2/q^2}. \quad (12)$$

The maximum value of Δ is attained for $q=2p$ and is $8/3\alpha^2$. For the symmetrical case, $p=q$, $\Delta=2/\alpha^2$. For comparison we note[6] that the reduced dispersion for the cylindrical condenser is $3/2\alpha^2$.

The effect of finite source-width on the trace is also of practical interest. The path of a ray emerging from a point near the source, and traveling in a plane through the axis of the system, can be constructed if one makes use of the general expression (11) for Y_2, the expression (10) for δ', and the fact that the conjugate points are on a line through O. (The intersection of the ray in question with the normal ray from the source is taken as a new source.) It is hardly profitable to carry this analysis out unless one has settled on definite values for Φ and p/q. However the following statement can be made: If the source width is not much greater than α^2a, where α is the maximum divergence of rays from the normal ray at the source, the spreading of the trace due to source-width will be of the same order as the spreading due to the aberration expressed in (11). One can justify this statement most readily by recalling that any given trajectory is *reversible*. A spreading of this order will also be caused by those rays which do not travel in a plane through the axis of the condenser, when the source has finite extent.

The detailed calculation of these second-order effects is of doubtful value because of the uncertainty introduced by our neglect of the fringing field of the condenser. If the gap is small compared to the total path in the condenser, the

first-order results should still be valid, and one can go further and use a grounded guard-diaphragm of the proper proportions, as suggested by Herzog,[7] to compensate for the edge effect as far as possible. This course was followed in the design of the present analyzer. Herzog's calculations were made for a plane condenser, and one cannot rely on the compensation to the order of α^2 because of the variation of the field strength across the spherical (or even the cylindrical) condenser. Thus strict validity cannot be claimed for the expression for the reduced dispersion, in a practical case; this is true, of course, for any kind of particle spectrograph except the 180° focusing magnetic spectrograph.

Correction for Relativity

In certain possible applications, involving high speed electrons, the modification of the above theory required by relativity may be important.[8] The extent to which the theory of the electrostatic spectrograph is affected by relativity does not seem generally to be appreciated. One might at first suppose that, since the trajectories with which one is concerned are nearly circular, and only small changes in the energy of the particles as they traverse the condenser are involved, the effect of the relativistic change in mass would first be felt in the second-order calculation, at least for reasonably small values of v/c. It turns out, however, that there will be, at the nonrelativistic focus, a spreading of the relativistic beam of the order αa, even when v/c is only a few tenths.

It is fortunately fairly easy to understand and to calculate what happens in the spherical condenser spectrograph, for we have essentially the problem of the relativistic Kepler orbits which arises in the calculation of the relativistic fine structure in the quantum theory. It is well known that the effect of the relativistic correction is to introduce a precession of the orbits,[9] essentially replacing the argument φ in (2) by $\gamma\varphi$, where, for orbits near the circular orbit, $\gamma \approx 1/(1+E)$, E being the particle kinetic energy, now measured in mc^2 units. In Fig. 2 the dotted trajectories, 2′ and 3′, have been roughly sketched in to show the modification of 2 and 3 caused by such a precession. It will be noted that although the orbits 2 and 3 are *very nearly* circular, the precession nevertheless shifts the intercept by a rather large amount, for the precession is about the appropriate focus, and not about the center of the orbit.

If we let Y_r represent the distance by which a relativistic trajectory misses the nonrelativistic focus, it is of interest to calculate k_1 in $Y_r/a = k_1\alpha + k_2\alpha^2 + \cdots$. In Fig. 2, k_1 is seen to be positive for the 180° case. The calculation is too long to be reproduced here. It has been carried out to the first order in α, but without any restriction on $\beta = v/c$. The result can be written in the following form:

$$k_1 = \frac{1+\beta^2}{1-\beta^2}(x_{10}/a)\cos\gamma\Phi + \frac{\sin\gamma\Phi}{\gamma} - \frac{2\beta^2(x_{10}/a)}{1-\beta^2} + (x_{20}/a)[\cos\gamma\Phi - (x_{10}\gamma/a) \times \sin\gamma\Phi(1+\beta^2)/(1-\beta^2)], \quad (13)$$

where $\gamma^2 = 1-\beta^2-2\beta^4\alpha$, $\beta = v/c$, and the other quantities have their former meaning.

The general symmetrical case, $x_{10}/a = x_{20}/a = \cot(\Phi/2)$ was investigated in some detail; k_1 was calculated numerically for $E = 0.2$ (100 kev electrons) for several values of Φ, including 90° and 180°. The interesting result of this calculation is that k_1 changes sign between these limits of Φ. For $\Phi = 90°$, k_1 is -0.48, and for $\Phi = 180°$, k_1 is 0.60, representing in each case a very serious departure from focusing. By trial, the zero of k_1 was found to lie very near $\Phi = 131°$. For 131°, $k_1 = 0.003$, for a 100 kev electron. k_1 is even less for lower energies, and is small clear up to 500 kev, the value for this energy is 0.064, and does not yet represent a serious spreading of the beam.

There is still one parameter available for adjustment, namely the ratio of x_{10} to x_{20}, or, what amounts to the same thing, p/q. It may be that a more favorable case could be found in which the coefficient of relativistic spreading is small by exploring the dependence of k_1 on this parameter as well. One would expect the same

[7] R. Herzog, Zeits. f. Physik **97**, 596 (1935).

[8] F. T. Rogers, Rev. Sci. Inst. **8**, 22 (1937) has calculated the effect of relativity on the *dispersion*, but not on the *focusing itself*.

[9] See, for example, Sommerfeld, *Atombau und Spektrallinien*, fifth edition, p. 272ff.

difficulty to arise in the cylindrical condenser spectrograph, but there, unfortunately the analysis, especially that of the general case, is more difficult.

The Construction and Operation of a Spherical-Condenser Spectrograph

The results of the preceding analysis seemed to warrant the construction of an experimental analyzer. The case $\Phi=90°$, $p=q=\sqrt{2}a$, was chosen for its simplicity. The construction is easier because of the symmetry, and the reduced dispersion is still high ($\Delta=2/\alpha^2$). The radius of the inner spherical surface was 8.69 cm, of the outer surface, 10.16 cm, making the total source-to-slit distance 21.65 cm. These dimensions yield a value of 0.315 for the theoretical ratio, V_f/E, of focusing potential to particle energy. The width of the annular aperture of the guard-diaphragm, i.e., the width of the beam at the entrance to the condenser, is limited by the requirement of clearance for the whole beam inside the condenser. Ideally, the maximum width of the beam inside is $\sqrt{2}$ times its width at the entrance to the condenser. After the aperture width (8 mm) has been chosen, the separation of the guard diaphragm from the condenser edge was adjusted according to Herzog's[7] curves.

Figure 4 is a cross section of the analyzer. It will be noted that the focusing electrodes, *1* and *2*, which are of spun copper, are supported between two heavier, pie-pan shaped plates (the grounded guard diaphragms) in which the entrance and exit apertures, *5*, are cut. The lavite blocks, *6*, insulate and space the parts. The analyzer, including the accelerating electrode structure beneath, is supported as a mechanical unit by the lavite feet, *11*, resting on the wall of the glass bulb. The entire instrument has threefold rotational symmetry.

It was desired to test the operation of the analyzer with electrons, and for this purpose a source was needed which, while acting effectively as a point source, would yield a hollow cone (semi-angle 45°) of electrons of the same energy. The problem is somewhat similar to the one which arose in the e/m measurement of Busch.[10] It was here solved by the use of accelerating electrodes arranged as shown in Fig. 5, which also shows the internally heated cathode in cross section. The latter is a nickel tube carrying an oxide-lined cup at one end. From the mouth of this cup electrons are accelerated in the desired directions if the potential V_b is near that of the cathode V_c, V_a is the plate potential. The central pin is maintained at the potential V_b by a wire which the electrons never "see." The alignment of the cathode is assured by two pins, *13*, in Fig. 4. The lens action of the accelerating electrodes was not a serious difficulty, and the source was entirely satisfactory.

At the other end of the spectrograph a Faraday cage collects the beam current through a 1.4-mm diameter slit. The Faraday cage assembly, which can be moved about from the outside, carries a small fluorescent screen, and during part of the work this whole assembly was replaced by a larger screen. The position of the slit can quickly be determined to 0.1 mm by the settings of the three tilting screws. The collector and the filament, and also, when desired, the whole accelerating electrode assembly, from *9* on down in Fig. 4, can be removed and replaced through the respective ends of the tube.

The glass envelope of the analyzer was an 11-liter flask, cut along the equator and sealed together again on the glass lathe. All leads are flexible and it will be noted that the lead to the inner sphere lies in one of the three narrow segments of the condenser which are closed to the beam; its presence did not disturb noticeably the adjacent parts of the beam. The analyzer was mounted with its axis along the earth's field and care was taken to avoid other magnetic disturbances. A weak field along the axis has a small and symmetrical effect on the focusing which can easily be estimated.

All potentials applied to the analyzer were tapped off a line of stable bleeder resistances connected across a 3000-volt rectifier. This is a convenient and satisfactory supply, for the operation of an electrostatic analyzer depends only on the ratios of the various potential differences. Fluctuations in the over-all voltage do not matter. Tapped resistors in the bleeder line allowed one to vary the electron energy by small, known steps, with the focusing potentials on the spheres held constant.

[10] H. Busch, Physik. Zeits. **23**, 438 (1922).

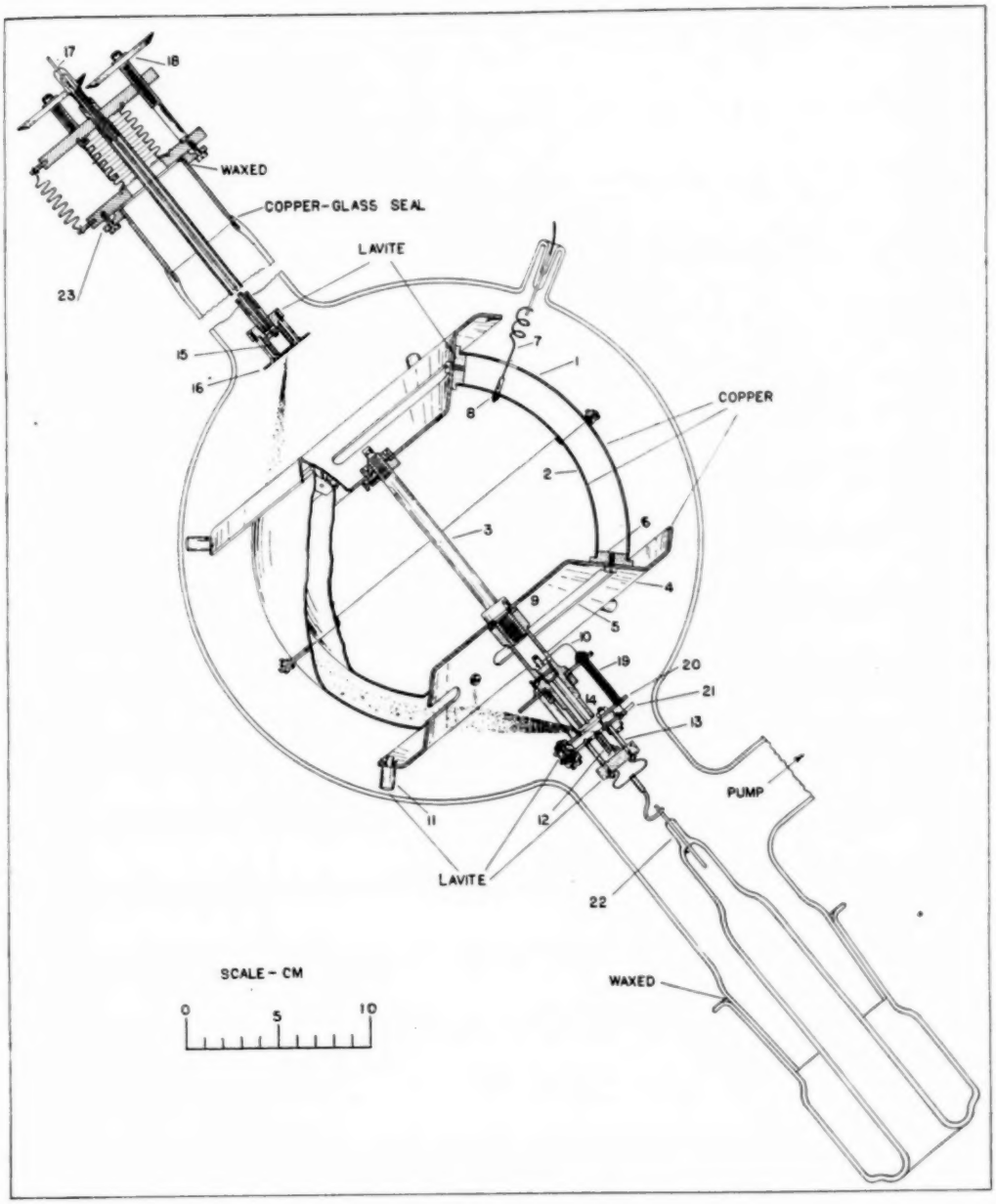

FIG. 4.

The analyzer was operated with the cathode about 2000 volts below ground, the inner and outer spheres being then about 300 volts above and below ground, respectively. Under these conditions a pattern was observed on the screen, but it did not have the simple form expected. For a given focusing potential one would expect to observe at approximately the correct plate potential, a ring, or rather three segments of a ring, which should shrink down to a spot as the electron energy is adjusted to exactly the right value. Instead, the different parts of the ring appeared to shrink into focus at somewhat different accelerating potentials. The resulting asymmetry of the pattern was rather simple, suggesting, at first, a source off the axis. It was finally shown, however, after several experiments, to have its origin in an asymmetry of the

condenser itself; it became clear that the two spheres were not concentric. It is believed that an accidental dislocation of the parts during their rather severe ordeal in the glass lathe caused the trouble. A departure of about 1 mm from concentricity is indicated. One cannot get at the condenser to remedy this, and this lack of the flexibility which was sacrificed in favor of clean vacuum conditions in the present apparatus, was keenly felt at this stage. It was possible, however, to check the theory.

It should be remembered that an analyzer of this type is really "many spectrographs in parallel." If the spheres are not quite concentric it is, to the first order, as if the various spectrographs were not adjusted to focus at the same V_f/E value. By moving the receiving slit along a chosen perpendicular to the axis of the system at the focal point we can confine our attention, as we did in developing the theory, to one of the spectrographs, i.e., to a plane through the axis.

The current through the slit at successive steps of the accelerating potential was measured, for various positions of the slit off the axis. From the shifting of the current peaks one can find the dispersion, and from the narrowing of the peaks as the slit nears the theoretical focal point the focusing action can be observed. The results thus obtained agreed satisfactorily with the indications of the theory. The width of the trace at the focus was not appreciably greater than the width of the source itself, confirming the conclusions drawn in the discussion of second-order effects. Both from visual and electrical studies of the pattern it seemed likely that, had the condenser not been distorted, the entire beam leaving the exit aperture of the condenser would have entered the 1.4-mm diameter receiving slit when the focusing and accelerating potentials were in the indicated ratio of 0.315.

Conclusion

In the design of a charged particle spectrograph the particular compromise between resolution and useful aperture which is finally reached will depend on the use to which the instrument is to be put. The particular merit of the spherical condenser spectrograph is that, being in effect a three-dimensional instrument, it offers, for any desired resolving power, a very large aperture. This advantage is well illustrated by the constants of the instrument described above. The theoretical reduced dispersion is 1010; the actual useful aperture, measured in solid angle at the source, is 0.210, or 1/60 of the whole sphere. The results of the experimental work indicate that a considerably larger aperture could be used without serious trouble from edge effect and other second-order disturbances. The allowable aperture is governed to some extent also by the practical limitations on V_f/E.

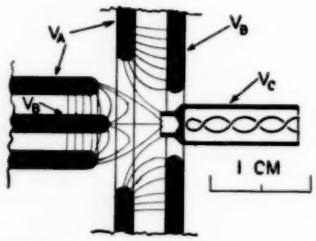

FIG. 5. Arrangement of cathode and accelerating electrodes, showing lines of force.

A disadvantage of the complete three-dimensional spectrograph is its inherent difficulty of construction. However, it is believed that in the light of experience a considerably better design than the present one can be evolved. This problem is being attacked at present with a view to some possible applications of the instrument. The simplicity and generality of the results of the theoretical analysis permit one to choose fairly easily the most practical form of the spectrograph for a particular application.

To Professor Bainbridge, who suggested this problem, the author is deeply indebted for advice and encouragement. The difficult task of assembling the glass envelope of the analyzer was accomplished by Mr. H. W. Leighton.

The Magnetic Scattering of Neutrons*

PHILIP N. POWERS
Columbia University, New York City
(Received September 22, 1938)

The interaction of neutrons with ferromagnetic materials has been investigated through a number of experiments. Because of the dependence of the interaction upon the spin orientation of the neutron relative to the magnetic field of the atom, and the effect of this spin dependent perturbation on the nuclear scattering, a beam of neutrons transmitted through or scattered from a magnetized iron plate becomes polarized by selective scattering.

This resultant neutron polarization has been studied most thoroughly through the increase in intensity of a neutron beam transmitted through a single iron plate when magnetized. The dependence of observed polarization on thickness of iron has been shown to agree within the limits of error with the theories of Bloch and Schwinger. The dependence of magnetic interaction on neutron energy was studied by the use of an effective "howitzer" for the production of low energy neutrons. The interaction increased rapidly for lower energy neutron energies, as would be expected, since the form factor for the interaction increases for longer neutron wave-lengths. The effective cross sections of iron for neutrons of spin $+\frac{1}{2}$ and $-\frac{1}{2}$ have been determined to be 13.7×10^{-24} cm² and 10.3×10^{-24} cm² for ~300°K neutrons, and 14.1×10^{-24} cm² and 9.9×10^{-24} cm² for ~120°K neutrons. Considering the uncertainty in the values to be expected theoretically, these cross sections are probably in reasonable agreement with the theories.

The intensity of neutrons scattered from a single iron plate has been shown to decrease when the plate is magnetized. Neutron polarization has also been studied through the change in neutron intensity when a beam of neutrons partially polarized by transmission through one plate of magnetized iron is scattered from or transmitted through a second iron plate magnetized parallel or antiparallel to the first. (Polarizer-analyzer action.)

These experiments show definitely the existence of nonadiabatic transitions of the magnetic spin quantum numbers of the neutron in rotating or precessing magnetic fields whose frequency is of the same order as the Larmor precession frequency, $g\mu H/h$, for the neutron.

The sign and the approximate magnitude of the neutron's magnetic moment have been determined by an experiment which depended on measuring the probability of nonadiabatic transitions in a controlled precessing magnetic field. This experiment was dependent only on the neutron properties in free space. The neutron magnetic moment has been shown to be negative in sign, and to be 2 ± 1 nuclear magnetons in magnitude.

INTRODUCTION

ON the assumption that the neutron has a magnetic moment, Bloch's original investigations[1] showed that there should be an appreciable magnetic interaction between a neutron and an atom of ferromagnetic material. This interaction arises from the atomic magnetic forces which, though small, are of long range in comparison with nuclear forces. Bloch made his calculations treating the atomic magnetic field as that due to an equivalent dipole of the electron currents and showed that the interaction should depend upon the relative orientation of the neutron with respect to the atomic magnetic field; i.e., it should be spin dependent. Schwinger[2] carried out a similar calculation in which he treated the atomic magnetic field as that due to the Dirac electron currents.

The calculations indicate that if σ is the total neutron cross section of demagnetized iron for "slow" (strongly absorbed in Cd) neutrons, then for magnetized iron the cross section becomes $\sigma(1+p)$ and $\sigma(1-p)$ for neutrons which have spin components of $+\frac{1}{2}$ and $-\frac{1}{2}$ in the direction of the field (or vice versa), where p is a constant whose predicted value is of the order of 0.07 to 0.3.[1-4] If a beam of neutrons passes through a magnetized iron sheet of thickness x_1, and atomic density n, the fraction P transmitted (i.e., I/I_0) should be:

$$P=\tfrac{1}{2}e^{-nx_1\sigma(1+p)}+\tfrac{1}{2}e^{-nx_1\sigma(1-p)} \qquad (1)$$
$$=e^{-nx_1\sigma}\cosh n\sigma x_1 p \quad \text{—magnetized}$$

and $$P=e^{-nx_1\sigma} \quad \text{—demagnetized.} \qquad (2)$$

For p different from zero, i.e., $\cosh n\sigma x_1 p>1$, a beam of neutrons transmitted through magnetized iron should not only become "polarized,"

* Publication assisted by the Ernest Kempton Adams Fund for Physical Research of Columbia University.
[1] Bloch, Phys. Rev. **50**, 259 (1936).
[2] Schwinger, Phys. Rev. **51**, 544 (1937).
[3] Schwinger, Phys. Rev. **52**, 1250 (1937).
[4] Hoffman, Livingston and Bethe, Phys. Rev. **51**, 214 (1937).

but should also have greater intensity than with the iron demagnetized, since the transmission in that case would be only $e^{-n x_1 \sigma}$. This increase in neutron transmission through magnetized iron provides one of the simplest methods for observing neutron polarization. In principle the difference between the two cross sections for the two states arises from the interference between the nuclear scattering and the electronic scattering.

If a partially polarized neutron beam be allowed to pass through a second magnetized plate of thickness x_2, then, depending on whether the magnetization in the second plate is parallel or antiparallel to that in the first plate, the transmitted intensities should be, respectively:

$$P = e^{-n\sigma(x_1+x_2)} \cosh pn\sigma(x_1+x_2) \quad \text{—magnetized parallel} \quad (3)$$

and

$$P = e^{-n\sigma(x_1+x_2)} \cosh pn\sigma(x_1-x_2) \quad \text{—magnetized antiparallel} \quad (4)$$

or

$$P = e^{-n\sigma(x_1+x_2)} \quad \text{—if } x_1 = x_2.$$

It is evident that if $x_1 = x_2$, the antiparallel case should give the same transmitted intensity as with the iron plates demagnetized. Thus one should expect the maximum intensity when two plates are magnetized in the same direction and the minimum intensity when they are magnetized antiparallel; however, the latter should be the same as if both plates were demagnetized. The second plate may be considered to be an "analyzer."

A variety of configurations are possible in which measurements of intensities may be used to study neutron polarization. These may be grouped into six general types.

1. *Single transmission.* Change in number of neutrons transmitted through a single plate of iron when magnetized.

2. *Single scattering.* Change in number of neutrons scattered from iron when magnetized.

3. *Double transmission.* Change in number of neutrons transmitted successive'y through two iron plates when the plates are magnetized parallel and antiparallel to each other.

4. *Transmission scattering.* Change in number of neutrons which are first transmitted through one plate and then scattered from a second iron plate whose directions of magnetization are parallel or antiparallel to that in the first.

5. *Scattering transmission.* Change in number of neutrons which are first scattered from one iron plate and then transmitted through a second iron plate whose magnetization directions are parallel or antiparallel.

6. *Double scattering.* Change in number of neutrons which are scattered successively from two iron plates when they are magnetized parallel or antiparallel to one another.

Quantitative experiments of types 1, 2 and 3 have been performed and will be separately discussed. Types 4 and 5 have been performed with less accuracy because of the low intensity of the scattered neutron beam. Regardless of the intensity of the primary neutron beam, the slow neutrons are always superimposed on an ever-present background of faster neutrons for which Cd does not have a large absorption cross section; i.e., neutrons above the Cd resonance level (above ~0.3 ev) which are also detected by the boron trifluoride ion chamber. Type 6, involving double scattering, has been found impossible to perform satisfactorily with the present neutron sources.

Single Transmission Experiments

Dependence of neutron polarization on (a) thickness of iron, and (b) neutron energy

The most complete investigations of neutron scattering in magnetized iron have been made with experiments of the single transmission type, since they are simpler and involve less possibility of disturbing effects. Fig. 1 shows the essential experimental arrangement used to study the magnitude of the observed neutron polarization as a function of (*a*) thickness of iron, and (*b*) neutron energy. Preliminary results were reported earlier.[5–7]

Neutron source for ~300°K and ~120°K neutrons.—For measurements with neutrons with an energy distribution corresponding to ~300°K, mean energy ~0.037 ev,[8–10] Rn–Be sources of

[5] Powers, Carroll and Dunning, Phys. Rev. **51**, 371 (1937).
[6] Powers, Carroll and Dunning, Phys. Rev. **51**, 1112 (1937).
[7] Dunning, Powers and Beyer, Phys. Rev. **51**, 382 (1937).
[8] Dunning, Pegram, Fink, Mitchell and Segrè, Phys. Rev. **48**, 704 (1935).
[9] Fink, Dunning, Pegram and Mitchell, Phys. Rev. **49**, 103 (1936).
[10] Fink, Phys. Rev. **50**, 738 (1936).

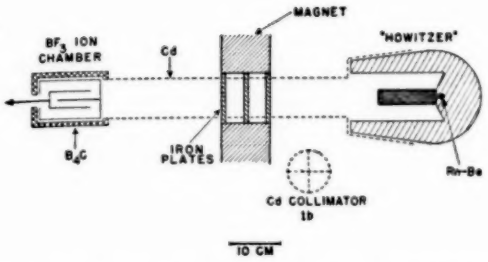

FIG. 1. Schematic arrangement of apparatus for investigation of magnetic scattering in iron as a function of thickness of iron and neutron energy. For measurements with low energy neutrons, the "howitzer" shown in Fig. 2 was used.

300 to 650 mC strength were placed in a paraffin "howitzer" of the usual type, as shown in Fig. 1. For measurements with lower energy neutrons, the special "howitzer" shown in Fig. 2 was constructed in a Dewar flask. The paraffin could be continuously and uniformly cooled by the circulation of liquid nitrogen through the imbedded copper tubing and a minimum amount of material was placed in the neutron beam. The Rn—Be source was placed in a small Dewar with a heater element and thermocouple so that it might be kept at room temperature and thus prevent changes in neutron intensity due to nonuniform condensation of the radon in the various parts of the source.

The temperature of the paraffin was normally maintained at approximately 105°K as measured by two thermocouples imbedded at different points. The "effective temperature" of the neutrons under these conditions was determined by a measurement of the absorption of the neutrons in boron, first with the "howitzer" at ~300°K and then at ~105°K. On the basis of the $1/v$ law for boron,[11] the absorption cross section should increase by $(300/105)^{\frac{1}{2}}$ or 1.70 for the low temperature if complete equilibrium were obtained. The average observed increase for a number of measurements was 1.60, hence from $(300/T_{\text{eff}})^{\frac{1}{2}}=1.60$, $T_{\text{eff}}=\sim 117$°K. The average energy then corresponds to ~0.015 ev. This approach to equilibrium is the most complete yet obtained.[12]

Detection system.—The sensitivity necessary for these experiments was obtained by a boron-trifluoride pressure ion chamber (see Fig. 3), connected to a linear amplifier system and scale-of-two thyratron recorder.[17]

This chamber represents nearly the maximum feasible size because of the difficulty in achieving sufficiently small collection time and sufficiently small recombination of the ions produced in BF_3 under pressure. The type of collector system shown makes possible the effective collection of ions throughout the large volume, but the increasing capacitance sets an upper limit on the usable size. A pressure of two atmospheres of BF_3 was the maximum which could be used and still give ionization pulses which were sufficiently large and sharp for proper recording with a collection potential of 1650 v. Under these conditions, a maximum of 35 percent of the incident slow neutrons were detected. With quartz insulation, this type of chamber has an indefinite life, some chambers having been in service over two years.

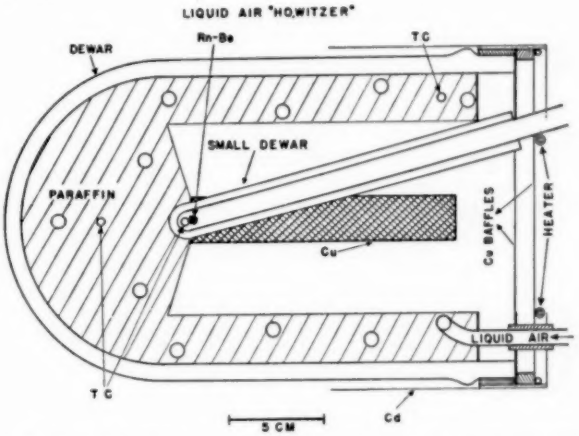

FIG. 2. Neutron source arrangement for lower energy neutrons. The paraffin was cooled by circulating liquid nitrogen through the imbedded copper tubing. An average temperature of ~105°K was maintained, and the "effective temperature" of the neutrons approximated ~120°K, corresponding to an average energy of ~0.015 ev.

[11] Rasetti, Mitchell, Fink and Pegram, Phys. Rev. **49**, 777 (1936).

[12] A series of measurements of the cross sections of a number of other elements with this "howitzer" has already been reported.[13] The "howitzer" was also used by Dunning, Brickwedde, Manley and Hoge in the experiments on the scattering of neutrons by ortho- and parahydrogen.[14–16]

[13] Powers, Goldsmith, Beyer and Dunning, Phys. Rev. **53**, 947 (1938).

[14] Dunning, Manley, Brickwedde and Hoge, Phys. Rev. **52**, 1076 (1937).

[15] Dunning, Hoge, Manley and Brickwedde, Phys. Rev. **53**, 205 (1938).

[16] Brickwedde, Dunning, Hoge and Manley, Phys. Rev. **54**, 266 (1938).

[17] Dunning, Rev. Sci. Inst. **5**, 387 (1934).

The ionization chamber was magnetically shielded with 0.65 cm iron. Tests showed that under the conditions of the experiments the effects of stray magnetic fields on the detection of the neutrons was not larger than 0 ± 0.20 percent.

The ionization chamber was also shielded by 0.5 cm Cd, and by a 1 cm layer of B_4C, to eliminate the slow neutrons and a large fraction of the faster neutrons just above the Cd absorption limit (i.e., above $\sim$0.3 ev). The neutron beam was well collimated by Cd from source to detector so that the probability of a scattered neutron reaching the chamber was small.

Magnetization of the iron samples.—As shown in Fig. 1, the neutron beam was usually transmitted through one or more plates of unannealled Armco iron, each 10×12.5 cm in area, which were placed between the pole pieces of a large electromagnet.[18] The plates were accurately machined and surface ground so that an excellent magnetic circuit was maintained, and because of the large ratio of core area to plate cross-sectional area, high values of magnetization were attained. The value of the magnetizing field corresponded to approximately 1600 oersteds. The flux density within the iron was measured by a coil which was wrapped around one of the plates and connected to a fluxmeter or ballistic galvanometer. B−H averaged approximately 21,000 to 21,500 gauss for the Armco iron samples.

Procedure and results.—The magnetic interaction was investigated by the change in transmitted neutron intensity first with the plates magnetized and then with the plates carefully demagnetized.

The collected results for a large series of runs are shown in Table I. A series of runs were taken with 0.80, 1.30 and 1.95 cm total thickness of iron for $\sim$300°K neutrons and with 1.30 and 1.95 cm thickness of iron for $\sim$120°K neutrons. The final result for the 1.95 cm thickness and $\sim$300°K neutrons also includes additional data obtained under the same conditions in other experiments in the laboratory and hence has higher precision. A total of about 3,000,000 neutrons were counted

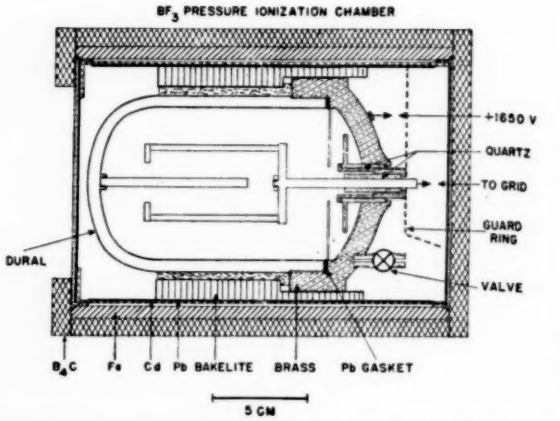

FIG. 3. Boron-trifluoride pressure ionization chamber for detection of slow neutrons. The cage-type collector with a re-entrant high potential electrode minimizes recombination of ions, and reduces ion collection time. Use of quartz insulation (skirt type on high potential) avoids deterioration of insulation in BF_3. Picein is satisfactory as sealing compound.

in the experiments. The fast neutron background, taken with 0.5 mm Cd interposed in the beam, has been subtracted so that the readings of a number of neutrons per minute refer only to the slow neutrons below the Cd resonance absorption limit.

The last two columns in Table I include calculations of p and the values of $\sigma(1+p)$ and $\sigma(1-p)$, the effective cross section of iron per atom for neutrons of spin $+\frac{1}{2}$ and $-\frac{1}{2}$ in the direction of the field (or vice-versa). The difference between the effective cross sections of the iron for the two spin orientations is actually large: 13.7 as compared to 10.3×10^{-24} cm^2 for $\sim$300°K neutrons and 14.0 as compared to 9.9×10^{-24} cm^2 for $\sim$120°K neutrons.

The total cross section (capture and scattering) for iron has been determined as $12.0\pm0.2\times10^{-24}$ cm^2 for $\sim$300°K neutrons and $12.0\pm0.7\times10^{-24}$ cm^2 $\sim$120°K neutrons;[13, 19] hence there is no change in total cross section for lower energy neutrons beyond experimental error. The capture cross section for iron is probably about 3.5×10^{-24} cm^2 from the measurements of Fink,[10] Goldhaber,[20] and Whittaker and Beyer.[21] The normal scattering cross section is thus approximately 8.5×10^{-24} cm^2, and considered from this basis

[18] Multiple separated plates with a Cd shielded channel were used in place of one thick plate in order to reduce multiple scattering, since earlier experiments had shown single thicknesses greater than one mean free path to give smaller polarization effects.

[19] Dunning, Pegram, Fink and Mitchell, Phys. Rev. **48**, 265 (1935).

[20] Goldhaber and Briggs, Proc. Roy. Soc. **A162**, 127–143 (1937).

[21] Whittaker and Beyer—in process of publication.

the difference between cross sections for the two spin values is still larger.

Dependence of magnetic scattering on neutron energy.—The change in scattering cross section should be proportional to the form factor, $\int \exp(i(\mathbf{k}_0-\mathbf{k})\mathbf{r})m(\mathbf{r})d\tau$, where $\mathbf{k}_0$ and $\mathbf{k}$ are the propagation vectors of the incident and scattered neutrons respectively and $m(\mathbf{r})$ is the magnetization density.[1, 2] Since this expression becomes larger for slower neutrons which have longer wave-length,[22] the percentage increase in transmission should also become larger.

The results in Table I and Fig. 4 show that the change in transmission for ~120°K neutrons is approximately 1.57 times that for ~300°K neutrons, while the average value of p increases by a factor of 1.27 for the lower energy neutrons. The magnetic scattering cross section for lower energy neutrons is thus in accord with the trend expected. The change in magnetic scattering cross section with lower neutron energy is thus appreciable—increasing for one spin orientation, decreasing for the other. Although the total cross section for demagnetized iron changes inappreciably, because of this differential change for the two spin values, and the exponential dependence, the change in transmission for magnetized iron shows a 57 percent increase for the low energy neutron distribution.

Experimentally, however, the neutron polarization is observed only through the differential effect of two exponential curves which decay at different rates, and hence even though the two cross sections for the two spin values differ considerably, the observed changes in transmission are a small fraction of the total number of neutrons transmitted.

Dependence of magnetic scattering on thickness of iron.—Fig. 4 shows a plot of the experimental points, superimposed on the theoretical curves, $\sim\cosh n\sigma xp$, expected from Eq. (1) in which the average of the p values given in Table I for each neutron temperature are used. The change in transmission with thickness does not disagree with the theoretical curves in Fig. 4, beyond the limits of error. However, the systematic trend of the experimental values strongly suggests that increasing thicknesses do not give quite the expected increase in transmission. This departure is what would be expected if there were tendencies for the neutrons to be depolarized within the iron and the possible reasons for such depolarization will be discussed later. Since each cm of iron transmits only about 0.36 of the incident neutrons, it is not practical to increase the thickness much beyond that used in this experiment because the intensity becomes too small in comparison to the fast neutron background.

Comparison with theory.—The magnitude of the magnetic scattering to be expected on the basis of the present theories, is uncertain, primarily because it depends on the value of the form factor for the interaction. The form factor is not accurately known and depends on ques-

[22] Mitchell and Powers, Phys. Rev. **50**, 486 (1936).

TABLE I. *Dependence of magnetic scattering of neutrons on neutron energy and thickness of iron.**

Effective Neutron Temperature	Iron Thickness in cm	Number Neutrons/Min. Transmitted**		Increase in No. Transmitted	% Increase in Transmission	p	Effective Cross Section† for Spin $+\frac{1}{2}$ and $-\frac{1}{2}$ ($\times 10^{-24}$ cm²)	
		Demagnetized	Magnetized				$\sigma(1+p)$	$\sigma(1-p)$
~300°K	0.80	719.5±1.0	725.0±1.0	5.5±1.4	0.76±0.19	0.150±0.018	13.8	10.2
~300°K	1.30	440.3±0.6	448.2±0.7	7.9±0.9	1.78±0.20	0.142±0.008	13.7	10.3
~300°K	1.95	221.08±0.24	228.41±0.25	7.33±0.35	3.32±0.16	0.130±0.003	13.6	10.4
						Average: 0.135±0.008		
~120°K	1.30	417.5±1.2	429.2±1.2	11.7±1.6	2.8±0.4	0.178±0.012	14.1	9.9
~120°K	1.95	209.3±0.6	221.0±0.6	11.7±0.8	5.6±0.4	0.158±0.005	14.0	10.0
						Average: 0.171±0.006		

* Unannealed Armco iron. In all of these experiments the precision has been calculated by use of the conventional statistical fluctuation equal to $\pm\sqrt{n}$, where n is the number of neutrons counted for any particular configuration.

** Only the percent increases in transmission are accurately comparable for the ~300°K neutrons and ~120°K neutrons, since the absolute values for the two cases have been calculated separately.

† The total neutron cross section, σ, (scattering and capture) for iron has been taken as 12.0×10^{-24} cm².

tionable assumptions as to the ratio of the neutron wave-length to the range of the atomic forces, and as to the radius of the 3D-electron shell. The greatly increased magnetic scattering for longer neutron wave-lengths shows the importance of the form factor in determining the magnitude of the observed effects in this region of neutron energies.

The observed results are within the rather wide limits estimated by Bloch. The experimental values should be somewhat less than those based on the more detailed calculations of Schwinger for zero energy (infinite wave-length) neutrons. Bethe's rough approximation of the form factor for iron, by extrapolation from the case for copper, gives values of the same order as those observed. A reasonable value for the form factor can thus be chosen to give good agreement with these experiments, and perhaps the value for the form factor may be most satisfactorily determined through such experiments. On consideration of the elementary state of the present theory and the possibility of disturbing experimental effects pointed out in a later section, the observed magnetic scattering is probably in as good agreement with the present theory as could be expected.

Test for small angle scattering. Dependence of observed magnetic scattering on collimation of the neutron beam.—In the experiments just described the intensity of the *transmitted* neutron beam *increases* when the iron is magnetized, but as will be shown in a later section the intensity of the *scattered* neutron beam *decreases*. There will thus be some compensating effect present in the experiments, but it should be small since the geometrical conditions are quite good and probability of detection of a scattered neutron therefore is small, provided that the scattering is approximately spherical. However, if considerable small-angle scattering were present, this compensation might be appreciable.

In order to test this possibility, the experiments were repeated with a much higher degree of collimation. As indicated in Fig. 1(b), four circular symmetrical cadmium channels were arranged so that neutrons scattered through an angle greater than about 6° could not be detected. Under these conditions, the observed increases in neutron transmission with the iron

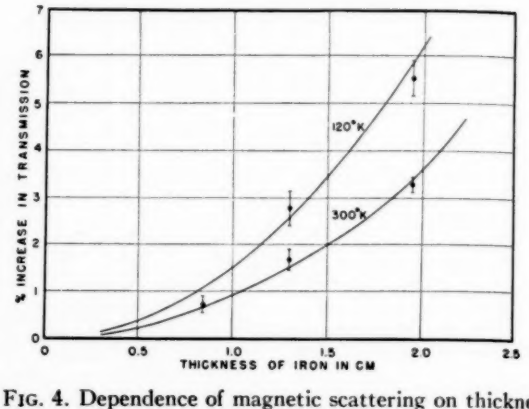

FIG. 4. Dependence of magnetic scattering on thickness of iron and neutron energy. The points represent the observed changes in neutron transmission. The curves represent the theoretical trend expected from Eq. (1), $\sim \cosh n\sigma xp$, in which the average p values from Table I for the two neutron temperatures are used.

magnetized were 3.5 percent±0.3 percent for the 1.95 cm thickness iron, and 1.7 percent±0.3 percent for the 1.30 cm thickness. These show no appreciable increase over the previous results, and it must therefore be concluded that the collimation first employed was already sufficiently good so that multiple scattering was not affecting the results markedly, and that within these limits there is no large amount of small angle scattering.

Single transmission experiments with a small magnet.—The measurements for magnetic scattering made with a small magnet constructed by Dr. J. H. Manley and kindly loaned for this experiment are of interest, since magnets of this type were used in the experiment on the sign of the neutron magnetic moment to be described later. The design of the magnet is shown in Fig. 5. Instead of solid Armco iron plate, seven strips of Swedish iron, each of 0.65 cm×1.30 cm cross section were placed side by side on the yoke with Cd strips interposed. The neutron beam, 7.5×4.5 cm in area, thus passed normally through 1.3 cm of iron while the Cd strips served both to reduce multiple scattering and to make the direction of the field in the iron parallel to the strips. In such a design, with only one thickness of iron for the neutrons to traverse, depolarization effects due to non-uniform fields outside the iron cannot affect the results. An excellent magnetic circuit was produced by careful surface grinding of all contact surfaces, and as a result a value of B−H in the iron strips of approximately 20,000 gauss

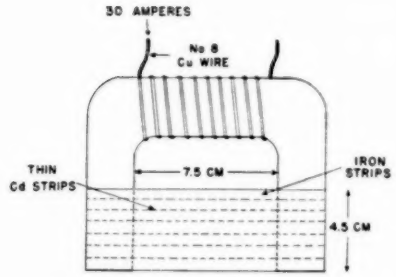

FIG. 5. Small type magnet designed by Dr. J. H. Manley. Swedish iron strips 0.65 cm×1.30 cm are placed side by side on the yoke, with Cd strips interposed. The Cd reduces multiple scattering and makes direction of field definitely parallel to strips.

was attained with relatively small power dissipation.

The observed increase in neutron transmission for the small magnet with 1.30 cm Swedish iron was 1.7 percent±0.3 percent. This is in good agreement with the value of 1.78 percent±0.2 percent previously observed, with the Armco iron of the same thickness. (See Table I.) Thus the single transmission experiments give consistent polarization effects.

Dependence of magnetic scattering on intensity of magnetization of iron.—Beyer, Carroll, Witcher and Dunning[23] have shown that the Armco iron samples do not show appreciable neutron polarization until a sharp threshold is reached which is very near complete saturation. Above this field value the observed polarization is practically constant. The measurements described here on Armco iron were all made with fields above this critical value.

Swedish iron, however, was shown to have a broader threshold. The observed polarization was appreciable with much lower magnetizing fields and approached its maximum more gradually. Thus the small magnets which were used in the experiments described here are able to produce practically the maximum polarization for the Swedish iron samples, but they were not effective with Armco iron.

The maximum polarization observed for the two types of iron, however, is seen to be practically the same. Theoretically, the observed polarization should vary approximately as the square of the intensity of magnetization. That the polarization depends on the composition and nature of the iron and does not follow such a simple function is additional evidence of the complexity of the phenomena.

This points again to the conclusion mentioned previously in connection with Fig. 4 and Table I, that neutrons may be depolarized through non-adiabatic transitions in domains within the ferromagnetic material. See next section for further discussion.

DOUBLE TRANSMISSION EXPERIMENTS

A number of experiments[5, 24] have been performed to investigate the neutron polarization phenomena through the use of two iron plates which could be magnetized parallel or antiparallel by two separate magnets and in order to secure the "polarizer-analyzer" action discussed in the introduction.

The essential arrangement is shown in Fig. 6 Two types of variations have been made: (a) Two different thicknesses of iron plates, totalling 1.30 and 1.95 cm, respectively, have been used and (b) first one and then both iron plates have been inclined at an angle of about 60° to the neutron beam in order to test the variation of polarization with the angle between neutron direction and the field direction. The thicknesses of iron used for oblique incidence were chosen so that the effective thickness was also approximately 1.30 or 1.95 cm.

The procedure used in making the observations was to take successive runs with (A) "polarizer" plate magnetized parallel to "analyzer" plate; (B) "polarizer" magnetized antiparallel to "analyzer," and (C) demagnetized.

TABLE II. *Observation of magnetic scattering of neutrons through double transmission experiments.—i.e., "polarizer-analyzer" action. Averaged results.**

EFFECTIVE THICKNESS OF IRON	MAGNETIZATION OF IRON PLATES	NUMBER OF NEUTRONS/MIN. TRANSMITTED	DIFFERENCE IN TRANSMISSION	PERCENT INCREASE IN TRANSMISSION
(a) 1.30 cm	Parallel	358.0±0.8	6.4±1.1	1.8±0.3
	Antiparallel	354.8±0.7	3.2±1.0	0.9±0.3
	Zero	351.6±0.7	0	0
(b) 1.95 cm	Parallel	181.11±0.40	6.01±0.56	3.44±0.32
	Antiparallel	178.82±0.40	3.72±0.56	2.12±0.32
	Zero	175.10±0.39	0	0

* The fast neutron background obtained by interposing Cd in the beam has been subtracted.

[23] Beyer, Carroll, Witcher and Dunning, Phys. Rev. **53**, 947 (1938).

[24] Dunning, Powers and Beyer, Phys. Rev. **51**, 51 (1937).

No significant variations outside experimental error were found between oblique incidence and normal incidence for the same effective thickness of iron, so the results have all been reduced to the same basis and averaged together. Table II shows the collected results. With both plates magnetized parallel, the experiment corresponds to those of single transmission types described previously; and the percentage increases in transmission agree very well with those in Table I.

The results for the antiparallel case, however, disagree seriously with what is to be expected. As pointed out in the introduction (Eq. (4)), if the thicknesses are equal, the transmission when antiparallel should be the same as when demagnetized. Instead, the antiparallel readings lie between the parallel and demagnetized readings.

Nonadiabatic transitions between the neutron states.—These experiments show quite conclusively that nonadiabatic transitions between the neutron states occur between the iron plates in the antiparallel case. The neutron beam is partially polarized after leaving the first plate; i.e., the number of neutrons having spin components $+\frac{1}{2}$ is different from the number having $-\frac{1}{2}$ in the direction of the field. However, with respect to a moving neutron between the plates, the magnetic field must effectively rotate, since at some point the value is zero. The frequency of this rotation under the conditions here is of the same order of magnitude as the Larmor precession frequency of the neutron, $g\mu H/h$, and transitions would be expected to occur between the neutron states.[25–27] This amounts to a reorientation of the partially polarized beams parallel to the second plate. The antiparallel case thus becomes similar to the parallel case and an increase in neutron transmission is to be expected compared to the demagnetized case. The magnitude of this increase depends on the transition probability which must be reasonably high, since of the order of 50 percent of the neutrons are reoriented. Evidence that such transitions occur has been confirmed by Frisch, von Halban and Koch.[28, 29]

[25] Güttinger, Zeits. f. Physik **73**, 169 (1931).
[26] Majorana, Nuovo Cim. **9**, 43 (1932).
[27] Rabi, Phys. Rev. **51**, 652 (1937).
[28] Frisch, von Halban and Koch, Nature **139**, 756 (1937).
[29] Frisch, von Halban and Koch, Phys. Rev. **53**, 719 (1938).

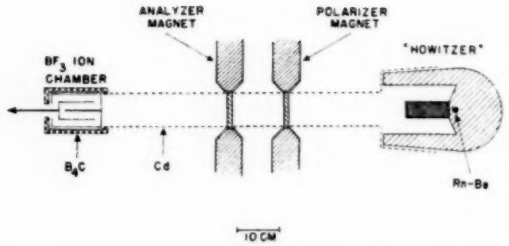

FIG. 6. Schematic arrangement of apparatus for study of neutron polarization by transmission through two successive iron plates which can be magnetized either parallel or antiparallel to each other by means of separate magnets. Measurements were made with two thicknesses of iron. Studies were also made with one and with both plates inclined at an angle of 60° with respect to the neutron beam.

A double transmission experiment was also performed by Hoffman, Livingston and Bethe[4] in which measurements were taken for the parallel and antiparallel cases, but not of the demagnetized case. They reported an increase in transmission of 1.8 percent$\pm$0.54 percent for the parallel case, which is probably consistent with our results. A comparison of the parallel and antiparallel cases given in Table II (b) shows a difference of only 1.32 percent$\pm$0.32 percent. Since their results did not include the demagnetized case the amount of reorientation cannot be established.

Nonadiabatic transitions within the iron.—The possibility of depolarization of the neutron within the iron has already been pointed out in connection with the systematic trend of the results on polarization as a function of thickness of iron, and the results of Beyer, Carroll, Witcher and Dunning[23] on the polarization as a function of magnetization intensity of the iron. Multiple scattering will, of course, account for some depolarization within the iron, but in view of the experiments described previously, testing this point, and of the excellent geometrical conditions prevailing in all experiments, is does not seem likely that multiple scattering plays a large role.

The microscopic field which the neutron "sees" as it passes through the iron atoms, the iron crystal structure, the crystal boundary regions and the atoms of the impurities present is by no means certain. However, in regions where B is high, the Larmor precession frequency is high, and transitions (i.e., depolarization) should occur

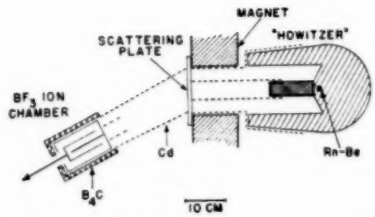

FIG. 7. Arrangement for investigating neutron polarization by scattering through a mean angle of approximately 23°. The ion chamber is shielded from the direct neutron beam by the pole pieces and by Cd.

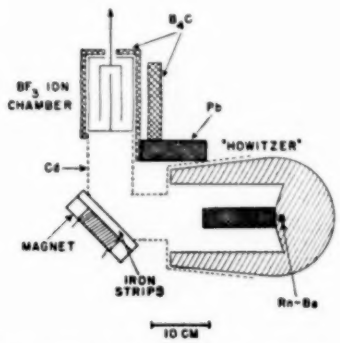

FIG. 8. Arrangement for studying amount of neutron polarization by scattering through a mean angle of approximately 90°.

within very small regions.[30] The passage of polarized neutrons through incompletely oriented "domains" (whose number becomes less as the magnetization approaches saturation as determined by temperature as well as magnetizing field), may thus give rise to nonadiabatic transitions, and hence depolarization. Disturbing effects may also occur at crystal boundary regions, and the presence of impurities may also complicate the phenomena. Especially in regions below saturation, one might well expect polarization effects to depend considerably on the type of iron used.

It has not been the purpose of these experiments to investigate this phase of the phenomena, and the Armco iron and Swedish iron samples used have been magnetized to as high values as feasible with the various magnets. Strictly speaking, however, the results given apply only to these iron samples, under these conditions of magnetization, and the results are in general very consistent.

POLARIZATION OF NEUTRONS BY SCATTERING

As shown in the previous experiments, the direct neutron beam transmitted through a plate of iron increases when the iron is magnetized. Conversely, the *scattered* neutrons should *decrease* in intensity when the iron is magnetized. Two methods utilized for measuring the changes in scattered neutron intensity are shown in Figs. 7 and 8. In Fig. 7, the ionization chamber was placed outside the direct transmitted neutron beam at an angle of approximately 23° so that neutrons scattered through small angles could be detected. In Fig. 8, a small magnet was arranged so that the back scattering at an angle of 90° could be measured. The beam was inclined at 45° to the iron. Both the "howitzer" and the ionization chamber were in the plane of the magnetized strips.

The results obtained are shown in Table III. Both experiments show definitely that the scattered neutron intensity *decreases* when the iron is magnetized. Because of the low intensity of the scattered neutron beam compared to the residual fast neutron background, the probable error is necessarily large, but in both cases it is less than one-third the observed change.

The difference between the observed magnetic scattering for the two angles is not considered significant.

THE SIGN AND MAGNITUDE OF THE MAGNETIC MOMENT OF THE NEUTRON

The investigations of the scattering of neutrons by ferromagnetic materials under various conditions are in reasonable agreement with the simple theories. However, the theories are only

TABLE III. *Scattering of neutrons from magnetized iron.*

ARRANGEMENT	READINGS	NUMBER OF NEUTRONS/MIN. RECORDED	DIFFERENCES DUE TO SCATTERING	PERCENTAGE DECREASE WITH IRON MAGNETIZED
Fig. 7 ~23° Scattering	Magnetized Demagnetized Background with Cd	123.4±0.2 124.4±0.2 99.6	−1.0±0.3 (24.8 Slow neutrons)	4.0±1.2%
Fig. 8 ~90° Scattering	Magnetized Demagnetized Background with Cd	111.61±0.18 112.41±0.18 80.3	−0.80±0.25 (32.1 Slow neutrons)	2.5±0.8%

[30] Frisch, von Halban and Koch (Nature **140**, 360 (1937)) have shown that transitions may be made to occur in very thin strips of magnetized iron where the B value is high.

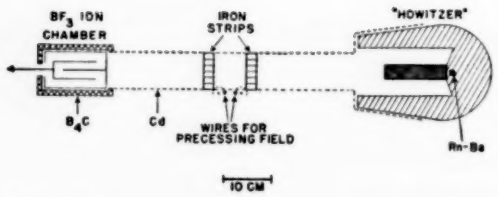

FIG. 9. Arrangement of apparatus for determination of sign and approximate magnitude of the neutron magnetic moment.

approximate, and in order to measure the magnitude of the neutron magnetic moment it is therefore important to use methods which are free from doubtful assumptions as to the exact nature of the complicated processes occurring within the ferromagnetic material. Furthermore, the sign of the neutron moment is not uniquely determined by the scattering in magnetized materials.

In order to determine the sign and magnitude of the neutron moment, it is therefore intrinsically desirable to perform experiments dependent only on the properties of the neutron in free space. Since slow neutrons have been shown to make nonadiabatic transitions in a rotating magnetic field,[6, 25, 26] this is clearly possible.

Rabi[31] has suggested a method through which these transitions may be controlled by a precessing magnetic field. A preliminary report of an experiment in which this method was used has already been published.[32] Rabi[27, 31] and Schwinger[33] have made calculations of the transition probability for a neutral atom in a precessing field which show that the probability depends upon the sign of rotation of the rotating component of the magnetic field, relative to the Larmor precession.

Thus a method is given which is applicable to the neutron for determining the sign of its magnetic moment (direction of the magnetic moment relative to the spin) as well as its magnitude. The transition probability is given by:

$$P_{-\frac{1}{2}}^{\frac{1}{2}}=\left(\frac{\hbar^2\omega^2\sin^2\theta}{\mu_n^2H_1^2+(\mu_nH_2+\hbar\omega/2)^2}\right)\times\sin^2\left(\frac{t}{2\hbar}\right)[\mu_n^2H_1^2+(\mu_nH_2+\hbar\omega/2)^2]^{\frac{1}{2}},$$

where H_1 is the rotating component of the precessing field; H_2 the constant component of the field; θ the angle between the resultant field and H_2; ω the angular velocity of the rotating component; t the time the neutron spends in the field, and μ_n the neutron magnetic moment. Since the transition probability depends on the relative signs of μ_n and ω, the sign of the neutron moment is determined by the direction of ω which produces maximum transitions. Furthermore, since this expression depends on the magnitude of the precessing field, i.e., H_1 and H_2, the magnitude of the neutron moment is in principle determined by the optimum values of H_1 and H_2 for a given configuration.

The arrangement of apparatus finally adopted for the experiment is shown in Fig. 9. The two sets of iron strips were magnetized in a direction parallel to a normal drawn outward from the paper, by means of two separate small magnets of the type shown in Fig. 5. The neutron beam was partially polarized after passing through the first set of magnetized strips. The precessing field in the region between the two magnets was formed by the resultant of the constant component H_2 produced by the stray field of the two magnets, and H_1, the rotating field (with respect to the moving neutron) caused by the two parallel wires carrying current in opposite directions. Fig. 10 shows diagrammatically the

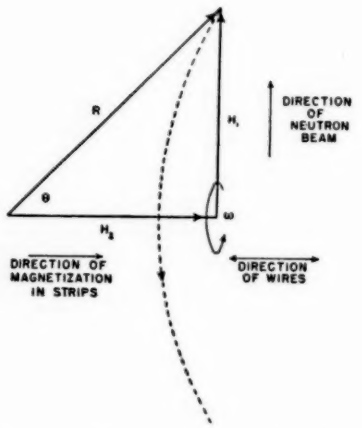

FIG. 10. Schematic diagram showing how the constant component, H_2 (the stray field) is combined with a rotating component, H_1, due to the field from the two parallel wires carrying current in opposite directions, in order to approximate a precessing field (with respect to the moving neutron), of the proper direction to induce the maximum amount of transitions.

[31] Rabi, Phys. Rev. **51**, 683 (1937).
[32] Powers, Carroll, Beyer and Dunning, Phys. Rev. **52**, 38 (1937).
[33] Schwinger, Phys. Rev. **51**, 648 (1937).

way in which the resultant precessing field is produced. The nonadiabatic transitions between the neutron states induced by this precessing field between the two sets of magnetized strips are in the end observed through testing the subsequent polarization of the neutron beam, i.e., by the change in transmitted neutron intensity through the second set of magnetized strips. The transitions produced in the partially polarized neutron beam by the controlled precessing field may thus be determined, and hence the sign and approximate magnitude of the neutron moment, without the specific interaction of the neutron with the iron coming into consideration.

Such an experiment may be in principle as accurate as desired. At the present stage of development, the sign may be determined unequivocally, but compromises must be made which greatly reduce the accuracy of measurement of the magnitude of the moment. Unfortunately, with the present neutron sources and detection methods, a wide aperture is necessary to secure sufficient intensity compared to the background, and it is not possible to secure uniform optimum conditions for complete reorientation of spins over such a large region. The approximate Maxwellian velocity distribution of the neutrons further complicates the situation. However, assuming $\mu_n \sim 2$ n.m., as might be expected from the values of the proton and deuteron magnetic moments, Mr. Julian Schwinger showed that the conditions could be made reasonably suitable over a large part of the region. By adjusting the distance between the magnets, introducing strips of iron just outside the beam, and shielding the coils, the stray field parallel to the strips was made to range from 8 to 14 gauss, and over the greater part of the region it averaged from 10 to 12 gauss. This field provided the constant component, H_2. The distance between the plates was 7 cm. For a Maxwellian velocity distribution of the neutrons, the average value of t was then approximately 3×10^{-5} sec.

TABLE IV. *Experimental data—sign and magnitude of neutron magnetic moment.*

POLARIZING FIELD (MAGNETS)	CURRENT IN ROTATING FIELD (WIRES)	NUMBER OF NEUTRONS/MIN. TRANSMITTED	% INCREASE IN TRANSMISSION
(a) Demagnetized	Zero	439.3 ±0.9	0 ±0.30
(b) Magnetized +	Zero	447.0 ±0.9	3.43 ±0.30
(c) Magnetized +	−90 Amperes	441.8 ±0.9	1.08 ±0.30
(d) Magnetized +	+90 Amperes	446.5 ±0.9	3.21 ±0.30
Background with Cd		213.3	

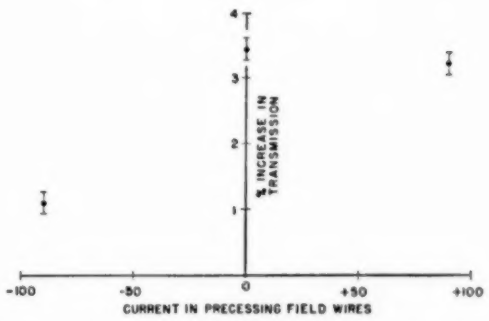

FIG. 11. Plot showing experimental points—Determination of sign and approximate magnitude of neutron magnetic moment. With the precessing field in the proper direction for a negative moment, the observed transmission is greatly reduced, but a precessing field in the opposite direction produces no observable change.

On the basis of a neutron moment of 2 n.m., under these conditions a current of 90 amperes in each wire should result in optimum values of H_1 (and H_2) in the center of the beam; i.e., a component is produced, rotating through approximately 180° with respect to the neutron, of very nearly constant magnitude ($\sim$10 gauss) and constant angular velocity. (See Fig. 10.) From the average neutron velocity, ω can be calculated.

Runs were taken successively with (a) both magnets demagnetized and zero wire field; (b) both magnets magnetized and with zero wire field—thus (a) and (b) correspond to the parallel double transmission case; (c) both magnets magnetized and wire current in the direction to give transitions for a negative neutron moment; (d) the same as (c) but with the current in the wire reversed so that transitions should not occur. Approximately 2,500,000 neutrons were counted in the course of the experiment. The averaged results for a series of 60 runs are given in Table IV.

The change in transmitted intensity from (a) to (b) in Table IV with no precessing field agrees fairly well with that in the earlier experiments of the parallel double transmission type and the single transmission type for approximately the same iron thickness.

The sign of the neutron moment.—The effect of the precessing transition field on the probability of transition, and hence of the observed neutron transmission through the two sets of magnetized strips, is clearly shown in Fig. 11.

With zero current in the wires, i.e., no precessing field, the maximum polarization is observed, with an increase in transmission over the completely demagnetized case of 3.43 ± 0.30 percent.

With the direction of current in the wires negative (see (c) in Table IV), the percentage change in transmission decreases to about one-third the value with no precessing field, showing that a considerable fraction of the neutrons made transitions, and were in effect reoriented. With the direction of the current in the wires reversed (see (d) in Table IV), the precessing field clearly has little effect on the neutrons.

Hence the results prove that the neutrons are reoriented when the angular velocity of the precessing field has the proper sign. The sign of the neutron moment is therefore definitely *negative*.

The magnitude of the neutron magnetic moment.—As pointed out, this experiment cannot be expected to yield a highly accurate value for the magnitude of neutron moment, because of the lack of uniformity in magnetic field conditions over the large beam area necessary for intensity, and because of the velocity distribution of the neutrons. However, since a large fraction of the neutrons were reoriented, the average magnetic field conditions, i.e., H_1 and H_2 must have been very near the optimum values. A rough numerical integration has been made taking into account the magnetic field values over the region of the beam, and it shows that the results are consistent with a value of -2 nuclear magnetons for the neutron moment. Considering the averaging involved, and the probable errors, the neutron moment must be within -2 ± 1 n.m., and is probably within -2 ± 0.5 n.m.

An experiment performed by Frisch, von Halban and Koch,[20] is in good agreement. With the use of a solenoid they produced a small field, H, between the "polarizer" and "analyzer," parallel to the direction of the neutron beam. The neutrons precessed about this field with an angular velocity proportional to H. Thus, with varying values of H, the depolarization of the neutron beam varied in the direction indicating the neutron moment to be negative. The conditions for complete depolarization (precessing through 90°) was reasonably consistent with the assumed magnitude of 2 n.m. The percentage changes which they observed were smaller than those observed here, although this would be expected from the configurations used.

The author wishes to express his appreciation to Professor John R. Dunning for suggesting the problem and for invaluable advice. I am much indebted to Professor I. I. Rabi and Mr. Julian Schwinger for interesting and helpful discussions, and for assistance in some of the calculations. Mr. Henry Carroll and Mr. H. G. Beyer were of great assistance in the laboratory. The Norton Company has been very generous in supplying quantities of Norton Boron Carbide for use as a shield from slow and fast neutrons.

Deep Terms in Co VI and Ni VII

L. W. PHILLIPS AND P. GERALD KRUGER
University of Illinois, Urbana, Illinois

(Received September 29, 1938)

ABOUT ninety lines in the Ni VII spectrum have been identified as radiations connecting terms from the $d^3 4p$ configuration with those arising from the d^4 ground state configuration. Classified lines are given in Table I, and forty-four of the deep terms are listed in Table II.

The corresponding transitions were identified in Co VI some time ago, and are in agreement

TABLE I. *Classified lines of* Ni VII.

Int.	Wave-Length	Wave Number	Classification $d^4 - d^3 4p$
5	205.275	487,152	$^5D_3 - (^4P)\ ^5P_3$
1	205.359	486,953	$^5D_1 - (^4P)\ ^5P_2$
8	205.582	486,425	$^5D_2 - (^4P)\ ^5P_2$
16	205.637	486,294	$^5D_4 - (^4P)\ ^5P_3$
0	205.689	486,172	$^5D_0 - (^4P)\ ^5P_1$
10	205.807	485,893	$^5D_1 - (^4P)\ ^5P_1$
12	205.885	485,707	$^5D_3 - (^4P)\ ^5P_2$
5	206.030	485,367	$^5D_2 - (^4P)\ ^5P_1$
12	208.182	480,348	$^3H_4 - (^2H)\ ^3G_3$
10	208.580	479,433	$^3H_5 - (^2H)\ ^3G_4$
4	208.679	479,205	$^3H_5 - (^2H)\ ^3G_5$
12	208.940	487,606	$^3H_6 - (^2H)\ ^3G_5$
8	211.037	473,851	$^3G_3 - (^2H)\ ^3G_3$
4	211.298	473,265	$^3G_4 - (^2H)\ ^3G_3$
12	211.433	472,963	$^3G_4 - (^2H)\ ^3G_4$
0	211.539	472,726	$^3G_4 - (^2H)\ ^3G_5$
12 Bl	211.649*	472,480	$^3G_5 - (^2H)\ ^3G_4$
14	211.759	472,236	$^3G_5 - (^2H)\ ^3G_5$
9	211.993	471,713	$^5D_2 - (^4F)\ ^3D_3$
8	212.316	470,997	$^5D_3 - (^4F)\ ^3D_3$ $^5D_1 - (^4F)\ ^3D_2$
35	212.516	470,552	$^5D_4 - (^4F)\ ^5F_5$ $^5D_3 - (^4F)\ ^5F_4$ $^5D_0 - (^4F)\ ^3D_1$
1	212.560	470,455	$^5D_2 - (^4F)\ ^3D_2$
3	212.625	470,312	$^5D_2 - (^4F)\ ^5F_3$
1	212.856	469,802	$^5D_1 - (^4F)\ ^5F_2$
30	212.904	469,696	$^5D_4 - (^4F)\ ^5F_4$
20	212.949	469,595	$^5D_3 - (^4F)\ ^5F_3$
15	213.096	469,273	$^5D_2 - (^4F)\ ^5F_2$
4	213.133	469,190	$^5D_0 - (^4F)\ ^5F_1$
5	213.258	468,916	$^5D_1 - (^4F)\ ^5F_1$
10	213.339	468,737	$^5D_4 - (^4F)\ ^5F_5$
12	213.422	468,555	$^5D_3 - (^4F)\ ^5F_2$
15	213.496	468,392	$^5D_2 - (^4F)\ ^5F_1$
25	213.515	468,349	$^5D_3 - (^4F)\ ^5D_4$
25	213.714	467,915	$^5D_2 - (^4F)\ ^5D_3$
30	213.908	467,491	$^5D_4 - (^4F)\ ^5D_4$
10	213.924	467,455	$^5D_1 - (^4F)\ ^5D_2$
15	214.042	467,198	$^5D_3 - (^4F)\ ^5D_3$
7	214.111	467,047	$^5D_0 - (^4F)\ ^5D_1$
2	214.166	466,927	$^5D_2 - (^4F)\ ^5D_2$
1	214.237	466,773	$^5D_1 - (^4F)\ ^5D_1$
6	214.440	466,330	$^5D_4 - (^4F)\ ^5D_3$
d7	214.492†	466,219	$^5D_3 - (^4F)\ ^5D_2$ $^5D_2 - (^4F)\ ^5D_1$
30	215.759	463,481	$^3H_6 - (^2G)\ ^3G_5$
20	216.064	462,828	$^3H_5 - (^2G)\ ^3G_4$
15	216.408	462,090	$^3H_4 - (^2G)\ ^3G_3$
7	216.550	461,788	$^3F_4 - (^2G)\ ^3G_5$
8	217.018	460,791	$^3F_3 - (^2G)\ ^3G_4$
12 Bl	217.138	460,536	$^3F_4 - (^2G)\ ^3G_4$
8	217.658	459,437	$^3F_3 - (^2G)\ ^3G_3$
0	217.781	459,176	$^3F_4 - (^2G)\ ^3G_3$
5	218.531	457,600	$^3G_4 - (^2G)\ ^3G_5$
5	218.766	457,109	$^3G_5 - (^2G)\ ^3G_5$
1	218.846	456,942	$^3G_3 - (^2G)\ ^3G_4$
2	219.127	456,356	$^3G_4 - (^2G)\ ^3G_4$
5	219.497	455,588	$^3G_3 - (^2G)\ ^3G_3$
1	219.782	454,997	$^3G_4 - (^2G)\ ^3G_3$
1	223.248	447,933	$^3F_3 - (^4F)\ ^3F_4$
5	223.377	447,673	$^3F_4 - (^4F)\ ^3F_4$
3	223.762	446,904	$^3F_2 - (^4F)\ ^3F_3$
3	223.819	446,789	$^3F_3 - (^4F)\ ^3F_3$
1	223.948	446,533	$^3F_4 - (^4F)\ ^3F_3$
16	224.381	445,670	$^3H_6 - (^4F)\ ^3G_5$ $^3F_3 - (^4F)\ ^3F_2$
14	224.724	444,991	$^3H_5 - (^4F)\ ^3G_4$
12	224.919	444,604	$^3H_4 - (^4F)\ ^3G_3$
1	225.182	444,085	$^3G_3 - (^4F)\ ^3F_4$
3	225.238	443,975	$^3F_4 - (^4F)\ ^3G_5$
2	225.476	443,506	$^3G_4 - (^4F)\ ^3F_4$
10	225.734	442,999	$^3G_5 - (^4F)\ ^3F_4$
2	225.760	442,948	$^3G_3 - (^4F)\ ^3F_3$ $^3F_3 - (^4F)\ ^3G_4$
3	225.889	442,696	$^3F_4 - (^4F)\ ^3G_4$
9	226.062	442,356	$^3G_4 - (^4F)\ ^3F_2$
1	226.215	442,056	$^3F_2 - (^4F)\ ^3G_3$
2	226.268	441,954	$^3F_3 - (^4F)\ ^3G_3$
7	226.347	441,800	$^3G_3 - (^4F)\ ^3F_2$
1	226.399	441,698	$^3F_4 - (^4F)\ ^3G_3$
2	226.658	441,194	$^3P_0 - (^4F)\ ^3D_1$
7	227.191	440,159	$^3P_1 - (^4F)\ ^3D_2$
2	227.377	439,799	$^3G_4 - (^4F)\ ^3G_5$
0	227.570	439,426	$^3P_1 - (^4F)\ ^3D_1$
9	227.636	439,297	$^3G_5 - (^4F)\ ^3G_5$
2	227.734	439,108	$^3G_3 - (^4F)\ ^3G_4$
1	227.831	438,922	$^3F_2 - (^4F)\ ^3D_3$
8	227.889	438,810	$^3P_2 - (^4F)\ ^3D_3$ $^3F_3 - (^4F)\ ^3D_3$
10	228.023	438,553	$^3F_4 - (^4F)\ ^3D_3$
4	228.039	438,521	$^3G_4 - (^4F)\ ^3G_4$
5	228.255	438,107	$^3G_3 - (^4F)\ ^3G_3$
0	228.299	438,022	$^3G_5 - (^4F)\ ^3G_4$
4	228.484	437,668	$^3F_2 - (^4F)\ ^3D_2$
5	228.541	437,559	$^3F_3 - (^4F)\ ^3D_2$ $^3P_2 - (^4F)\ ^3D_2$
2	228.864	436,940	$^3F_2 - (^4F)\ ^3D_1$
1	228.927	436,820	$^3P_2 - (^4F)\ ^3D_1$
4	229.569	435,599	$^3F_2 - (^4F)\ ^5F_1$

* Line width 50 cm^{-1}. † Line width 40 cm^{-1}. Bl Blend.

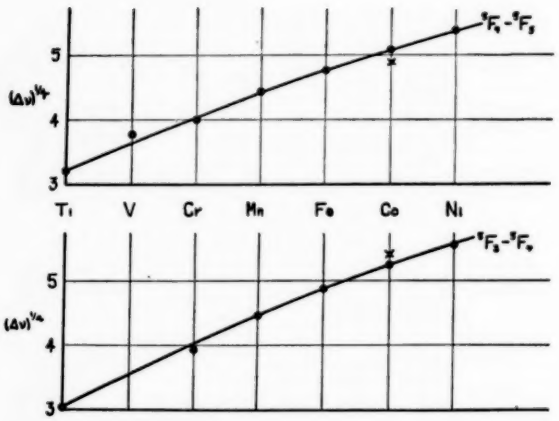

FIG. 1. ^5F separations for ions Ti I—Ni VII. Upper curve, $^5F_4-{}^5F_5$ separation; lower curve, $^5F_3-{}^5F_4$ separation. Bowen's data indicated by crosses.

TABLE III. *Alternative classification of* $^5D-{}^5F$ *in* Co VI.

		$^5F_1$		$^5F_2$		$^5F_3$		$^5F_4$		$^5F_5$
Term		358362	667	359029	794	359823	765	360588	679	361267
Value		*358366*	*670*	*359036*	*790*	*359826*	*864*	*360690*	*573*	*361263*
$^5D_0$	000	358360								
		358372								
	208	205								
		219								
$^5D_1$	208	358155								
		358153		*358828*						
	378	380								
		381		*381*						
$^5D_2$	586	357775		358442		359236				
		357772		*358447*		*359247*				
	543			542		543				
				537		*554*				
$^5D_3$	1129			357900		358693		359458		
				357910		*358693*				
	660					656		658		
$^5D_4$	1789					358037		358800		359478
								358896		*359474*

with Bowen's[1] recently published analysis except in the case of the $d^4\ {}^5D-d^3 4p\ {}^5F$ multiplet. The basic difference is in the identification of transitions originating at the $^5F_4$ level. The line 359,474 cm^{-1} which Bowen classifies as $^5D_4-{}^5F_5$ is resolved on our plates into two lines, 359,478 cm^{-1} and 359,458 cm^{-1}, with intensity ratio about 4 : 1. The weaker line of the two has been classified as $^5D_3-{}^5F_4$, and the stronger line as $^5D_4-{}^4F_5$. A line at 358,800 cm^{-1}, which may be Bowen's line 358,828 cm^{-1} (our lines are shifted an average of 6 cm^{-1} to lower wave numbers than Bowen's in this region), has been classified as $^5D_4-{}^5F_4$. The suggested alternative classification is given in Table III, with Bowen's classification in italics. Bowen's separations for the ^5D levels agree with those obtained in this laboratory to within 5 cm^{-1}, and are taken as the correct separations for the ground state. Aside from the fact that the ^5D separations obtained from this alternative classification seem to be in a little better agreement than Bowen's with the average ground state separations shown in the table, there seems to be little to choose between the two classifications if one considers only the data in Table III.

An examination of the ^5F separations, with relation to the corresponding separations in other ions of the sequence, is helpful. In Fig. 1 the fourth root of the wave number separations $^5F_3-{}^5F_4$ and $^5F_4-{}^5F_5$ are plotted against atomic

[1] Bowen, Phys. Rev. **53**, 889 (1938).

TABLE II. Ni VII *Term values.*

Configuration		J	Term Value	Configuration		J	Term Value	Configuration		J	Term Value	Configuration		J	Term Value
d^4	^5D	0	000	d^4	^3F	2	33592	$d^3(^4F)4p$	^5F	1	469191	$d^3(^4F)4p$	^3F	2	479348
		1	275			3	33705			2	470075			3	480494
		2	802			4	33961			3	471115			4	481639
		3	1520							4	472074				
		4	2379		^3G	3	37551			5	472930	$d^3(^4P)4p$	^5P	1	486170
						4	38141							2	487228
	^3P	0	29334			5	38638		^3D	1	470528			3	488673
		1	31100							2	471258				
		2	33706	$d^3(^4F)4p$	^5D	1	467048			3	472514	$d^3(^2G)4p$	^3G	3	493139
						2	467730							4	494496
	^3H	4	31052			3	468717		^3G	3	475657			5	495747
		5	31668			4	469870			4	476659				
		6	32267							5	477936	$d^3(^2H)4p$	^3G	5	510873
														4	511101
														3	511402

number for the ions Ti I to Ni VII. Separations for the ^5F level obtained from the alternative classification seem to fit this $(\Delta\nu)^{\frac{1}{2}}$ graph better than do those obtained from Bowen's classification, which are indicated by crosses. Final substantiation will have to await the identification of further combinations or intercombinations with the ^5F terms.

In conclusion, the authors wish to express their appreciation to Mr. C. E. McClellan for his assistance in making the wave-length measurement.

NOVEMBER 15, 1938 PHYSICAL REVIEW VOLUME 54

The Magnetic Anisotropy of Copper Sulphate Pentahydrate, $CuSO_4 \cdot 5H_2O$, in Relation to its Crystal Structure. Part III.

K. S. KRISHNAN AND A. MOOKHERJI
Indian Association for the Cultivation of Science, Calcutta, India

(Received September 21, 1938)

Measurements have been made of the magnetic anisotropy of $CuSO_4 \cdot 5H_2O$ at different temperatures from 26°C to −190°C. The crystal is nearly uniaxial magnetically, and its two principal susceptibilities conform roughly to the Curie law, with different Curie constants. The observed anisotropy of the crystal may be attributed to the anisotropy induced in the Cu^{++} ion under the influence of the asymmetric electric field of the neighboring negatively charged atoms. From the known positions of these atoms the field should be expected to have tetragonal symmetry. The two principal susceptibilities of the Cu^{++} ion, along the tetragonal axis of the field, and perpendicular to the axis, respectively, are calculated. The corresponding effective magneton numbers are calculated therefrom, and it is found (1) that these magneton numbers vary little with temperature, and (2) that the magneton numbers corresponding to the two principal susceptibilities of the ion are widely different.

1. INTRODUCTION

IN Parts I and II[1] of this paper we gave an account of some magnetic studies on $CuSO_4 \cdot 5H_2O$ at room temperature, and a discussion of the results in relation to the structure of the crystal. The results verify in a striking manner the views advanced by Van Vleck,[2] and Penney and Schlapp[3] regarding the origin of magnetic anisotropy in a paramagnetic crystal, namely that it is due to the asymmetry of the internal electric fields acting on the paramagnetic ions in the crystal. The crystal of $CuSO_4 \cdot 5H_2O$ is triclinic and its unit cell contains two Cu^{++} ions. Each of these ions is in the center of an octahedron formed by six negatively charged oxygen atoms.[4] The octahedron is not regular, but may be regarded as derived from a regular one by drawing out symmetrically one of its diagonals. This diagonal will thus be an axis of tetragonal symmetry for the octahedron, and therefore also for the electric field acting on the Cu^{++} ion located at the center of the octahedron. Now the tetragonal axes of the two octahedra in the unit cell make with each other an angle of 82°. We should therefore expect the internal and the external bisectors of this angle, and the normal to the two bisectors, to be the three principal magnetic axes of the crystal. The susceptibility along the first direction should be the maximum for the crystal, and that along the third the minimum; and further, since the angle between the two tetragonal axes is nearly a right angle, the intermediate susceptibility should be nearly the same as that along the first direction, i.e., should be close to the maximum. All these results deduced from the structure of the crystal are verified experimentally.

Denoting the susceptibility of the Cu^{++} ion along the tetragonal axis of the field acting on it by $K_{\parallel}$, and that perpendicular to the tetragonal axis by $K_{\perp}$, we find that at 26°C, $K_{\parallel} - K_{\perp} = 550 \times 10^{-6}$ per gram ion, and that the mean susceptibility $K = (K_{\parallel} + 2K_{\perp})/3$ at this temper-

[1] Krishnan and Mookherji, Phys. Rev. **50**, 860 (1936) and **54**, 533 (1938).
[2] Van Vleck, *The Theory of Electric and Magnetic Susceptibilities* (Oxford, 1932).
[3] Penney and Schlapp, Phys. Rev. **41**, 194 (1932).
[4] Beevers and Lipson, Proc. Roy. Soc. **A146**, 570 (1934).

ature is about 1520×10^{-6} (equal to the mean susceptibility of the crystal, corrected for its diamagnetism). The anisotropy of the Cu^{++} ion in the crystal is thus about 36 percent of its mean susceptibility, and it points to a strong asymmetry in the crystalline field acting on Cu^{++}.

The present paper deals with the temperature variation of the anisotropy and the principal susceptibilities of the crystal, and of the principal susceptibilities, $K_{\parallel}$ and $K_{\perp}$ of the Cu^{++} ion in it, from the temperature of the room to that of liquid air. The earlier theories are shown to be inadequate to explain the temperature variation of the anisotropy, and the results are considered on the basis of Van Vleck's theory.

2. The Curie-Weiss Law

The magnetic behavior of paramagnetic ions in crystals naturally differs from that of the free ions. The most striking departures are the magnetic anisotropy exhibited by the crystal, and the deviations of the temperature variations of the principal susceptibilities from the Curie law.[5] These were explained on the older theories as arising from certain internal magnetic fields, which were presumed to be of the same nature as the inner fields in ferromagnetics, and were taken to be proportional to the intensity of magnetization. On this basis the temperature variations of the three principal susceptibilities are given by the simple formulae

$$\chi_i=C/(T-\Theta_i); \qquad i=1, 2, 3; \qquad (1)$$

the Curie constant C, which is determined by the magnetic moment of the paramagnetic ion, which is assumed to be capable of turning around freely in the crystal, will naturally be the same for all the three directions, while the Θ's which are determined by the internal magnetic fields developed in the presence of the applied field, may depend on the direction of the latter in the crystal. When the Θ's are small, the mean susceptibility of the crystal, i.e., the powder susceptibility, will also conform to a formula of the same type,

$$\chi=(\chi_1+\chi_2+\chi_3)/3=C/(T-\Theta), \qquad (2)$$

where

$$\Theta=(\Theta_1+\Theta_2+\Theta_3)/3. \qquad (3)$$

Coming back to the crystal of $CuSO_4\cdot5H_2O$, its susceptibility in the powder state has been measured by de Haas and Gorter[6] over a wide range of temperatures, from 14° to 290°K, and it conforms closely to the formula

$$\chi=0.456_9/(T+0.70), \qquad (4)$$

where χ refers to one gram ion.

The temperature variation thus approximates practically to the Curie law, and the value of 0.456_9 for the Curie constant gives for the magnetic moment of Cu^{++} 1.92 Bohr magnetons, as compared with the theoretical value of 1.73 for the single spin moment. These results would suggest, on the basis of these older theories, (1) that the inner magnetic fields are very feeble; and (2) that as in many other salts of the iron group, the contribution from the orbital angular momentum of the paramagnetic ion to the observed magnetic moment is small. We should then expect the anisotropy of the crystal to be small, and the temperature variations of the three principal susceptibilities to conform to formula (1), in which the Θ's should be small, and the Curie constant C should have the same value, namely about 0.457, for all the three principal directions.

We have already seen that the anisotropy of the crystal is by no means small. We shall show presently that the principal susceptibilities also do not conform to Eq. (1).

3. Experimental

The general method adopted in the present measurements is the same as that described by us and Mr. Bose in a recent paper.[7] The main part of the apparatus is the cryostat for maintaining the temperature of the crystal constant at any desired value. The crystal is suspended freely inside a thin-walled copper tube, closed at the bottom, and immersed deeply in a liquid

[5] If the higher multiplet levels of the paramagnetic ion, being low, are also occupied, and the magnetic moments corresponding to these levels differ from that of the ground state, e.g. Eu^{+++}, Sm^{+++}, the temperature variation of the susceptibilities of even the free ions may deviate from the Curie law, but in a manner that may be readily predicted.

[6] de Haas and Gorter, Leiden Comm. 210 d (1930).

[7] In course of publication in Phil. Trans. Roy. Soc. London.

bath of petroleum ether of boiling point 30°–50°C. The temperature of the bath was controlled automatically by a constant volume air-thermometer, of thin-walled copper, immersed in the bath. When the temperature of the bath rises above the desired value, the air in the thermometer expands and closes the electric circuit of an air-pump which slowly sucks liquid air into a small copper vessel immersed in the bath and thus cools it. When the temperature of the bath falls below the desired value, the air in the thermometer contracts, the electric current through the air-pump circuit is cut off automatically, and that through a small heating coil, also immersed in the cryostatic bath, is made, and the temperature of the bath rises. In practice the two circuits, through the air-pump and the heating coil respectively, alternate in quick succession, and the temperature remains steady to within 0.1°C.

Below about −140°C the petroleum ether becomes very viscous, and temperatures lower than this cannot be maintained with the above arrangement. The only temperatures lower than this at which measurements are made are those of liquid oxygen or air, used as bath liquid instead of the petroleum ether, and allowed to evaporate at atmospheric pressure. The electrical connections for temperature control are cut off in this arrangement.

All the temperature measurements are made with a calibrated copper-constantan thermocouple.

The magnetic measurements are made in the same manner as in Part II. The suspension for the crystal, however, now consists of two parts. The upper part is a calibrated quartz fiber, which remains at room temperature always, and its torsional constant is therefore independent of the temperature of the cryostat; and the lower part is a much stouter fiber which may be regarded as practically rigid.

4. Results

Measurements of magnetic anisotropy are made for five different suspensions of the crystal, which are numbered in the same manner as in Parts I and II; suspensions (2), (7) and (8) which correspond to low anisotropies, are omitted in the present measurements. The results are given in Tables I to V.

Suppose the torsion-head has been adjusted such that the torsion on the quartz fiber may be zero when the crystal has taken up its natural orientation in the magnetic field, namely with the direction of the maximum susceptibility for the crystal in the horizontal plane along the field. Let us call this position of the torsion-head its zero-position. Let α_0 be the angle through which the torsion-head has to be rotated from the above zero position so as to bring the crystal just to its unstable orientation in the field. Let us denote by λ the quantity $\Delta\chi \cdot mH^2/(2Mc)$, where m is the mass of the crystal, M is its molecular weight, H is the magnetic field, c is the constant of torsion of the suspension fiber, and $\Delta\chi$ is the difference between the maximum

TABLE I. *Suspension (1): 'c' axis vertical. ($\bar{1}00$) sets at 27°+ε, and ($\bar{1}\bar{1}0$) at 53°+ε, to the field; ε increases from 0 at room temperature to 1.5° at 82°K. $\Delta\chi = 183\times10^{-6}$ at 299°K.*

Temp. °K	304.9	270.8	251.8	231.5	210.7	194.5	170.2	148.2	137.8	90.1	81.5
ρ	0.98	1.10	1.16	1.26	1.38	1.51	1.68	1.95	2.02	3.01	3.26

TABLE II. *Suspension (3): ($\bar{1}00$) and ($\bar{1}11$) vertical. ($\bar{1}00$) sets at 45½°, and ($\bar{1}11$) at 14°, to the field; except at the two lowest temperatures, where the setting angle differs from the above by about 1°. $\Delta\chi = 263\times10^{-6}$ at 299°K.*

Temp. °K	295.8	270.6	248.7	231.0	211.6	194.5	189.4	174.3	148.1	90.1	82.0
ρ	1.01	1.08	1.14	1.22	1.33	1.46	1.48	1.59	1.86	2.87	3.00

TABLE III. *Suspension (4): ($\bar{1}\bar{1}0$) and ($\bar{1}11$) vertical. ($\bar{1}\bar{1}0$) sets at 62½°, and ($\bar{1}11$) at 9½°, to the field, at all the temperatures. $\Delta\chi = 264\times10^{-6}$ at 299°K.*

Temp. °K	271.1	251.9	231.8	211.0	194.5	171.1	143.1	90.1	83.0
ρ	1.08	1.14	1.23	1.33	1.45	1.63	1.95	2.90	3.08

TABLE IV. *Suspension (5): (100) horizontal: 'c' axis sets at 59°+ε, and the intersection of ($\bar{1}00$) and ($\bar{1}11$) at 8°−ε, to the field; ε increases from 0 at room temperature to ½° at 90°. $\Delta\chi = 146\times10^{-6}$ at 299°K.*

Temp. °K	304.9	271.4	251.0	230.2	210.1	194.5	176.0	158.9	148.4	90.1
ρ	0.99	1.08	1.13	1.23	1.33	1.42	1.52	1.67	1.77	2.70

TABLE V. *Suspension (6): (110) horizontal. 'c' axis sets at 44°+ε, and the intersection of ($\bar{1}\bar{1}0$) and ($\bar{1}11$) at 12½°−ε, to the field; ε increases from 0 at room temperature to 2° at 90°K. $\Delta\chi = 213\times10^{-6}$ at 299°K.*

Temp. °K	271.4	250.2	231.1	211.0	194.5	190.5	170.1	149.8	90.1
ρ	1.09	1.14	1.21	1.33	1.41	1.44	1.60	1.77	2.71

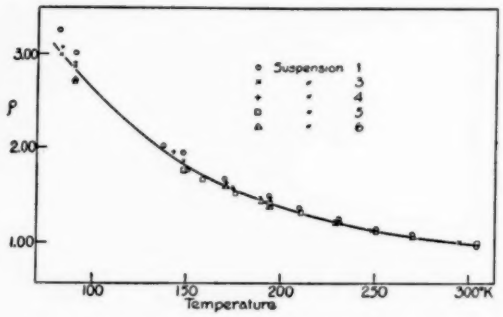

FIG. 1.

and the minimum susceptibilities of the crystal in the horizontal plane, per gram molecule. The quantity λ is connected with the observed critical angle α_0 by the relation (see Part II)

$$\lambda=(\alpha_0-\pi/4-\sigma)/\cos 2\sigma \qquad (5)$$

where

$$\sin 2\sigma=1/(2\lambda). \qquad (6)$$

From observations on α_0 at different temperatures with the suspension and the field the same, we can calculate with the help of relations (5) and (6) the corresponding values of λ.

The quantity ρ in the tables denotes the ratio of the value of λ at any given temperature to that at 26°C. Obviously, this will also be the ratio of the anisotropies $\Delta\chi$ at the two temperatures.

The values of ρ for the different suspensions are plotted against temperature in Fig. 1.

5. Some General Features of the Temperature Variation of the Anisotropy of the Crystal

An examination of the data entered in the above tables, shows firstly that the setting directions are practically independent of temperature; the largest variation as we pass from room temperature to that of liquid air is only 2°; and secondly that the value of ρ at any given temperature is more or less the same for all the five suspensions. This is exhibited clearly in Fig. 1, where the experimental points for all the suspensions are seen to lie close to the mean curve; the values for suspension (1) lie slightly above the curve, and those for the suspensions (5) and (6) slightly below it.

We may conclude from these results that the principal magnetic axes of the crystal are practically the same at all the temperatures. We have seen that at room temperature the crystal is nearly uniaxial magnetically, and the axis makes with the a, b and c axes of the crystal angles of 154°, 64° and 51°, respectively. Denoting the susceptibilities along the axis and perpendicular to it by $\chi_{\parallel}$ and $\chi_{\perp}$, respectively, we found in Part II that at room temperature, namely 299°K, $\chi_{\perp}-\chi_{\parallel}=275\times10^{-6}$. The present measurements show that at the other temperatures also, the crystal will remain approximately uniaxial, and the direction of the axis will remain the same; and the anisotropy $\chi_{\perp}-\chi_{\parallel}$ may be taken to be roughly equal to $\rho\times275\times10^{-6}$, where ρ is the value obtained from the mean curve plotted in Fig. 1. The values of $\chi_{\perp}-\chi_{\parallel}$ given in Table VI were obtained in this manner.

Combining these data with the values for the mean susceptibility, $\chi=(\chi_{\parallel}+2\chi_{\perp})/3$, obtained by de Haas and Gorter, we can calculate the principal susceptibilities of the crystal, $\chi_{\parallel}$ and $\chi_{\perp}$, separately, at different temperatures. These

TABLE VI. *Principal susceptibilities of copper sulphate pentahydrate crystal.*

Temp. °K	ρ	$(\chi_{\perp}-\chi_{\parallel})\times10^6=275\rho$	$\chi=(\chi_{\parallel}+2\chi_{\perp})/3\times10^6$	$\chi_{\parallel}\times10^6$	$\chi_{\perp}\times10^6$	$\chi_{\parallel}(T-2.0)$	$\chi/(T+1.8)$
299	(1.00)	275	1525	1342	1617	0.399	0.486
280	1.06	291	1628	1434	1725	0.399	0.486
260	1.12	308	1753	1548	1856	0.399	0.486
240	1.19	327	1899	1681	2008	0.400	0.485
220	1.28	352	2070	1835	2187	0.400	0.485
200	1.40	385	2277	2020	2405	0.400	0.485
180	1.54	424	2529	2246	2670	0.400	0.485
160	1.72	473	2844	2529	3002	0.400	0.486
140	1.95	536	3248	2891	3427	0.399	0.486
90.1	2.84	781	5032	4511	5292	0.398	0.486
						mean = 0.399	0.486

calculated values are also entered in Table VI. All the χ's have been corrected for the diamagnetism of the crystal. The anisotropy of the diamagnetism of the crystal, as judged from the observed anisotropy of diamagnetic sulphates,[8] should be negligible.

As will be seen from the figures given in the last two columns of the table, the two principal susceptibilities of the crystal conform closely to the formulae

$$\chi_{\parallel}=0.399/(T-2.0) \qquad (7)$$

and

$$\chi_{\perp}=0.486/(T+1.8). \qquad (8)$$

Though both of them are of the Weiss type, the Curie constants for the two directions are widely different, a result which, as we mentioned before, is not expected on the Weiss theory.

Since the Θ's are small, the mean susceptibility also naturally obeys a formula of the same type. It is easily verified that Eqs. (7) and (8) lead to expression (4) for the mean susceptibility, as they should.

6. The Principal Susceptibilities of the Cupric Ion in the Crystal

Viewing these results on the basis of Van Vleck's theory, we can calculate the anisotropy, $K_{\parallel}-K_{\perp}$, of the Cu^{++} ion in the crystal, due to the asymmetry of the crystalline electric field acting on it. Since the field has tetragonal symmetry, and the tetragonal axes of the fields acting on the two Cu^{++} ions in the unit cell are nearly perpendicular to each other, we have the simple relation (see Part II)

$$K_{\parallel}-K_{\perp}=2(\chi_{\perp}-\chi_{\parallel}), \qquad (9)$$

from which $K_{\parallel}-K_{\perp}$ is known at different temperatures. Since further $K_{\parallel}+2K_{\perp}=\chi_{\parallel}+2\chi_{\perp}$ (the χ's, as we mentioned before, denote the principal susceptibilities of the crystal, which have been corrected for its diamagnetism), we can calculate from the data given in Table VI, the values of $K_{\parallel}$ and $K_{\perp}$ separately, at different temperatures. The results are given in Table VII.

[8] Krishnan and Banerjee, Phil. Trans. Roy. Soc. **A235**, 343 (1936).

Table VII. *The effective Bohr magneton values of the magnetic moment of the* Cu^{++} *ion in the copper sulphate pentahydrate crystal.*

Temp. °K	$K_{\parallel}\times10^{6}$	$K_{\parallel}(T+4\cdot5)$	$n_{\parallel}$	$n_{\perp}$
299	1892	0.574	2.13	1.80
280	2016	0.574	2.13	1.80
260	2164	0.572	2.13	1.80
240	2335	0.571	2.12	1.80
220	2539	0.570	2.12	1.80
200	2790	0.571	2.12	1.80
180	3094	0.571	2.12	1.81
160	3475	0.572	2.12	1.81
140	3963	0.573	2.11	1.81
90.1	6073	0.574	2.10	1.81
		mean = 0.572		

Since evidently $K_{\perp}=\chi_{\parallel}$, and the values for $\chi_{\parallel}$ have already been given, the values for $K_{\perp}$ have not been entered in the table.

Let us denote the effective Bohr magneton values of the magnetic moment of the Cu^{++} ion when the applied magnetic field is along the tetragonal axis of its crystalline field, and when it is perpendicular to it, by $n_{\parallel}$ and $n_{\perp}$, respectively;

$$n_{\parallel}^{2}/K_{\parallel}=n_{\perp}^{2}/K_{\perp}=3kT/(N\beta^{2}), \qquad (10)$$

where $\beta=eh/4\pi mc$ is the Bohr magneton, N is the Avogadro number and k is the Boltzmann constant. The values of $n_{\parallel}$ and $n_{\perp}$, calculated from $K_{\parallel}$ and $K_{\perp}$ in relation (10), are also given in Table VII.

The most striking feature of the anisotropy of the Cu^{++} ion under the crystal fields is that whereas the effective magneton numbers for both the principal directions of the field vary little with temperature, showing that both the principal susceptibilities of the Cu^{++} ion obey practically the Curie law of inverse dependence on T, the magneton numbers for the two principal directions are widely different. To be more precise, the two principal susceptibilities of the ion conform to the formulae

$$K_{\parallel}=0.572/(T+4.5) \qquad (11)$$

and

$$K_{\perp}=0.399/(T-2.0), \qquad (12)$$

with small Curie temperatures, and widely different Curie constants.

Lattice Vibrations in Polar Crystals

R. H. LYDDANE, *The Johns Hopkins University, Baltimore, Maryland*

AND

K. F. HERZFELD, *The Catholic University of America, Washington, D. C.*

(Received June 8, 1938)

This paper investigates the free vibrations of a polar crystal of the sodium chloride type. The main purpose is the calculation of the Coulomb force, which has been done by an extension of the Madelung method. For numerical evaluation, a short range repulsion is assumed, and the van der Waals forces are neglected. The results are: For long waves one finds in the acoustical branch three waves whose frequencies are inversely proportional to the wave-length, in agreement with Born. The optical branch has two transverse waves (Reststrahlen) with a Coulomb force of $4\pi/3$ times the polarization, as Born has calculated, and one longitudinal one with a Coulomb force of $-8\pi/3$ times the polarization. For short waves the vibrations are in general not exactly transverse or longitudinal, but even in the optical branch there remain separate modes of vibration with different frequencies for a given wave-length. In addition, the neutral simple cubic lattice is considered. It is shown that the free vibrations are characterized by $D=0$. The influence of the shape of the crystal is discussed.

I. INTRODUCTION

THE problem of vibrations in crystals is important for many of their properties; for example, the specific heat and the optical behavior. Accordingly, it has been treated by many authors. A group of papers investigates the distribution of the frequencies under the simplifying assumption that each particle is bound only to its neighbors. This treatment was originated by Born and v. Kármán,[1] a simplified procedure introduced by Debye,[2] and much new information gained in recent papers by Blackman.[3] On the other hand, electric forces play a considerable role in many cases, and their range is so great that the above assumption is not a good approximation. The problem of calculating the electric force which is exerted on one particle by all the others during oscillation was attacked by Born[4] for long transverse waves in polar cubic crystals. His result was in agreement with the formula for the so-called Lorentz-Lorenz force, which expresses the interaction of the polarized molecules in the quasi-statical case. Born used his value for all possible modes of vibration in these crystals. Since 1912 Ewald[5] has been working on a method to calculate the propagation of electromagnetic waves in crystals. His interest lies mainly in the dispersion of light and propagation of x-rays, but his method is applicable also to the present problem. He himself has made calculations only on transverse waves. Thompson,[6] however, has developed the general formula for the propagation of arbitrary vibrations. Broch,[7] has recently started an investigation of the proper vibrations of a one-dimensional polar lattice.

This paper is intended to answer the following questions: First of all, no actual calculation of the electric force has been made for waves comparable with the lattice distance. According to the preceding theories, such waves are of prime importance to the specific heat. Secondly, Born's results seem to conflict with the direct calculation made by Herzfeld for another purpose. (See Section V.) Thirdly, the preceding methods leave some questions of principle in doubt. While it seems physically clear that the properties of the crystal (at least, at temperatures somewhat removed from the absolute zero) should be independent of the form, the electro-

[1] M. Born and Th. v. Kármán, Physik. Zeits. **13**, 297 (1912).
[2] P. Debye, Ann. d. Physik **39**, 789 (1912).
[3] M. Blackman, Zeits. f. Physik **86**, 421 (1933); Proc. Roy. Soc. **A148**, 384 (1935); Proc. Roy. Soc. **A159**, 416 (1937).
[4] M. Born, Ann. d. Physik **61**, 87 (1920).
[5] P. P. Ewald, Ann. d. Physik **49**, 1, 117 (1916).
[6] M. Born and J. H. C. Thompson, Proc. Roy. Soc. **A147**, 594 (1934); J. H. C. Thompson, Proc. Roy. Soc. **A149**, 487 (1935).
[7] E. Broch, Proc. Camb. Phil. Soc. **33**, 485 (1937).

static forces converge so badly that it does not seem obvious that the physical result is reconcilable with the assumption of electrostatic forces. It is true that Born[8] has given reasons for this independence of the form, but a more detailed investigation seemed advisable.

II. The Forces and Frequencies in a General Crystal

To calculate the frequencies of a vibrating crystal, one assumes that the crystal is in a definite state of vibration, and calculates the force on one constituent particle due to all the others, under the assumption that the distortion from the equilibrium position is small. This restoring force will be linear in the displacements of the constituent particles (the assumption of small displacements implying that the vibrations will be harmonic), so that one has the usual secular equation for harmonic motion with many degrees of freedom to solve for the frequencies pertaining to the previously fixed state of vibration.

The first question then, is the determination of the state of vibration of the crystal; that is, what function of its position in the crystal is the displacement of a particle. This will be, as in the case of an elastic continuum, largely influenced by the boundary conditions, which in turn depend upon the shape of the crystal, among other things. One knows, however, from the work of Weyl, that the influence of the boundary conditions on the higher frequencies is small if the crystal is large, provided the forces have a short range. This question will not be further investigated here; what is more interesting is the question whether, in a polar lattice, the very slow decrease of the Coulomb force with increasing separation will cause particles at great distances to contribute noticeably to the force on a given particle of the crystal, and thus cause the shape of the crystal to influence the frequency spectrum. In accordance with the above, the boundary conditions to be imposed here are to be those which make the calculations as simple as possible. They will be those characterizing the "periodic lattice" introduced by Born.[8] The assumption here is that one has a crystal block, whose sides are parallel to those of the unit cell, of dimensions $G_1 \times G_2 \times G_3$ cells, which one builds up to an infinite lattice by adding other blocks of the same shape and size. The boundary conditions to be imposed are that the displacements of two particles at corresponding points in any two blocks are the same. It will be shown later that the influence of the other blocks on the forces, and hence the frequencies, is really not great.

One should assume standing waves in the lattice (compatible with the boundary conditions), but since the force at a lattice point is linear in the displacements of the particles causing it, provided that the latter are small, one can, instead, write the standing wave as a linear combination of progressive waves, work with a progressive wave, and take a linear combination of the forces at the end. In the interest of simplicity of calculation, this will be done.

Let us consider first a general lattice, with a unit cell specified by the three vectors $\mathbf{a}_1$, $\mathbf{a}_2$, $\mathbf{a}_3$. The cells are distinguished by the index l which is an abbreviation for the triple of integers l_1, l_2, l_3; the particles in a cell are distinguished by the index k. The equilibrium position of the kth particle in the lth cell is given by $\mathbf{r}(k;l) = l_1\mathbf{a}_1 + l_2\mathbf{a}_2 + l_3\mathbf{a}_3 + \mathbf{r}(k;0)$; $\mathbf{r}(k;0)$ is the equilibrium position of the kth particle in the origin cell. The displacement of the l, kth particle at any time is assumed to be

$$\mathbf{u}(k;l) = \mathbf{U}(k) \exp\{-i\omega t + i(\mathbf{s}\cdot\mathbf{r}(k;l))\}, \quad (1)$$

where $\mathbf{U}(k)$ is a vector giving the characteristic amplitude of the particle of type k. The direction of the vector $\mathbf{s}$ is the direction of propagation of the wave, and its magnitude is 2π divided by the wave-length.

The assumption of a periodic lattice made above now yields the condition that

$$\mathbf{s} = \pi(n_1/G_1)\mathbf{b}_1 + (n_2/G_2)\mathbf{b}_2 + (n_3/G_3)\mathbf{b}_3.$$

The $\mathbf{b}$'s are the lattice vectors inverse to the $\mathbf{a}$'s and n_1, n_2, and n_3 are integers, $-G_i < n_i \leqslant G_i$.

If $\mathbf{K}(k;l)$ is the force on the l, kth particle, the equations of motion are

$$m_k \partial^2\mathbf{u}(k;l)/\partial t^2 = \mathbf{K}(k;l). \quad (2)$$

[8] For this, as indeed for almost all the notation used in this paper, see the article by M. Born and M. Göppert-Mayer, *Handbuch der Physik* XXIV/2, p. 623.

If the potential energy of the interaction between two particles of types k and k', whose difference in position is $\mathbf{r}$, is given by $\phi_{kk'}(|\mathbf{r}|)$, then

$$K_x(k;l) = -\mathbf{S}'_{l'} \sum_{k'} [(\partial/\partial x)\phi_{kk'}(|\mathbf{r}|)]_{\mathbf{r}'}$$

$$\mathbf{r}' = \mathbf{r}(kk';l-l') + \mathbf{u}(k;l) - \mathbf{u}(k';l').$$

The symbol $\mathbf{S}$ indicates the summation over the three indices abbreviated by l'; the prime attached indicates that the l, kth particle is to be omitted. $\mathbf{r}(kk';l-l')$ is defined as $\mathbf{r}(k;l) - \mathbf{r}(k';l')$.

Since the displacements are small, this can be developed in a Taylor series, in which only terms to the first degree in the displacement are preserved:

$$K_x(k;l) = -\mathbf{S}'_{l'} \sum_{k'} [(\partial/\partial x)\varphi_{kk'}(|\mathbf{r}|)]_{\mathbf{r}=\mathbf{r}(kk';\,l-l')}$$

$$-\sum_y \mathbf{S}'_{l'} \sum_{k'} [(\partial^2/\partial x \partial y)\varphi_{kk'}(|\mathbf{r}|)]_{\mathbf{r}=\mathbf{r}(kk';\,l-l')}$$

$$\times (u_y(k;l) - u_y(k';l')).$$

Here the first term represents the force on a particle in the equilibrium lattice, which must vanish. Writing

$$\varphi_{xy}(kk';l-l') = [(\partial^2/\partial x \partial y)\varphi_{kk'}(|\mathbf{r}|)]_{\mathbf{r}=\mathbf{r}(kk';\,l-l')}$$

and substituting for $\mathbf{u}(k;l)$ its value from Eq. (1), we obtain

$$K_x(k;l) = \exp\{-i\omega t + i(\mathbf{s}\cdot\mathbf{r}(k;l))\}$$

$$\times \{\sum_y \mathbf{S}'_{l'} \sum_{k'} U_y(k')\varphi_{xy}(kk';l-l')$$

$$\times \exp[-i(\mathbf{s}\cdot\mathbf{r}(k';l'))]$$

$$-\sum_y U_y(k) \mathbf{S}'_{l'} \sum_{k'} \varphi_{xy}(kk';l-l')\}.$$

The first term here represents the force on the l, kth particle in its equilibrium position due to the displacements of the other particles; the second the force on the displaced l, kth particle due to the undisplaced lattice of the other particles. The possibility of breaking the force into these two terms rests, of course, on the assumption of small displacements. The second term, in a cubic holohedry, is zero, as will be shown later.

Since in a polar lattice the interaction between two particles (ions) is the sum of their Coulomb interaction and other terms, (van der Waals and repulsive) and since only the Coulomb part presents any difficulty in evaluation, one breaks the force $\mathbf{K}(k;l)$ into the sum of two terms

$$[e_k(\mathbf{F}(k)+\mathbf{G}(k)) + \mathbf{R}(k)]\exp\{-i\omega t + i(\mathbf{s}\cdot\mathbf{r}(k;l))\}$$

where $\mathbf{F}(k)+\mathbf{G}(k)$ represents (except for the phase factor) the electric field of the contribution of the Coulomb interaction to the force, and $\mathbf{R}(k)$ the part of the force due to all other interactions. $\mathbf{F}(k)$ is that term in the field due to the displacements of other particles; $\mathbf{G}(k)$ that due to the displacement of the particle l, k. If the Coulomb interaction is denoted by $\psi_{kk'}(|\mathbf{r}|) = (e_k e_{k'})/|\mathbf{r}|$ and the coefficients $(kk';xy)$ and $[kk';xy]$ defined by

$$(kk';\,xy) = \mathbf{S}'_{l'} \psi_{xy}(kk';l-l') \times \exp[-i(\mathbf{s}\cdot\mathbf{r}(kk';l-l'))], \quad (4)$$

$$[kk';xy] = \mathbf{S}'_{l'} \psi_{xy}(kk';l-l'),$$

then the Coulomb field, from Eq. (3), is

$$F_x(k) = (1/e_k)\sum_y \sum_{k'} (kk';xy)\,U_y(k'),$$

$$G_x(k) = -(1/e_k)\sum_y \sum_{k'} [kk':xy]\,U_y(k).$$

One observes that $[kk';xy]$ is the value that $(kk';xy)$ assumes when $\mathbf{s}=\mathbf{0}$, i.e., for infinitely long waves. $(\mathbf{s}\cdot\mathbf{r}(kk';l-l'))$ is simply the phase difference between the l, kth and l', kth particles.

If $(kk';xy)_a$ and $[kk';xy]_a$ are defined as the corresponding quantities for the repulsive interaction, so that

$$R_x(k) = \sum_y \sum_{k'} \{(kk';xy)_a U_y(k') - [kk';xy]_a U_y(k)\},$$

and substitutions in Eq. (2) are made for $\mathbf{u}(k;l)$ and $\mathbf{K}(k;l)$, the equations of motion assume the form:

$$-m_k\omega^2 U_x(k) = \sum_y \sum_{k'} \{[(kk';xy)+(kk';xy)_a]U_y(k') - [[kk';xy]+[kk';xy]_a]U_y(k)\}. \quad (5)$$

These form a set of $3k$ linear homogeneous equations in $3k$ unknowns; the condition that the determinant of the coefficients vanish gives the usual secular equation for the frequencies.

The problem now is to calculate the coefficients $(kk';xy)$ for a general value of $\mathbf{s}$. First, $\psi_{xy}(kk';l-l')$ may be written as

$$[(\partial^2/\partial x\partial y)\psi_{kk'}(|\mathbf{r}-\mathbf{r}(k';l')|)]_{\mathbf{r}=\mathbf{r}(k;\,l)},$$

so that

$$\begin{aligned}(kk';xy)=&\sum_{l'}{}'[(\partial^2/\partial x\partial y)\psi_{kk'}(|\mathbf{r}-\mathbf{r}(k';l')|)]_{\mathbf{r}=\mathbf{r}(k;\,l)}\\&\times\exp[-i(\mathbf{s}\cdot\mathbf{r}(kk';l-l'))]\\=&[\sum_{l'}{}'(\partial^2/\partial x\partial y)\exp[-i(\mathbf{s}\cdot\mathbf{r}(kk';l-l'))]\\&\times\psi_{kk'}(|\mathbf{r}-\mathbf{r}(k';l')|)]_{\mathbf{r}=\mathbf{r}(k;\,l)},\end{aligned}$$

or if the convergence of the series is sufficiently good,

$$\begin{aligned}(kk';xy)=&[(\partial^2/\partial x\partial y)\sum_{l'}{}'\exp[-i(\mathbf{s}\cdot\mathbf{r}(kk';l-l'))]\\&\times\psi_{kk'}(|\mathbf{r}-\mathbf{r}(k';l')|)]_{\mathbf{r}=\mathbf{r}(k;\,l)}.\end{aligned}$$

While this may seem a slightly dubious procedure in the case of the poorly convergent Coulomb interaction, we will proceed with it, and show that it is justified by the results.

Putting in $(e_ke_{k'})/|\mathbf{r}|$ for $\psi_{kk'}(|\mathbf{r}|)$, one may write

$$F_x(k)\exp[-i\omega t+i(\mathbf{s}\cdot\mathbf{r}(k;l))]$$

as

$$\begin{aligned}-\exp(-i\omega t)\sum_y\sum_{k'}e_{k'}U_y(k')&[(\partial^2/\partial x\partial y)\sum_{l'}{}'\\&\times\exp[i(\mathbf{s}\cdot\mathbf{r}(k';l'))](|\mathbf{r}-\mathbf{r}(k';l')|)^{-1}]_{\mathbf{r}=\mathbf{r}(k;\,l)}\end{aligned}$$

or in a somewhat different form,

$$\begin{aligned}[-\partial/\partial x\sum_y\partial/\partial y\sum_{l'}{}'\sum_{k'}e_{k'}U_y(k')&\\\times\exp\{-i\omega t+i(\mathbf{s}\cdot\mathbf{r}(k';l'))\}&\\\times(|\mathbf{r}-\mathbf{r}(k';l')|)^{-1}]_{\mathbf{r}=\mathbf{r}(k;\,l)}.&\end{aligned}$$

The interpretation of this expression is the following. The sum over l' and k' gives the electric potential at an arbitrary point $\mathbf{r}$ due to a set of charges $e_{k'}U_y(k')\exp[-i\omega t+i(\mathbf{s}\cdot\mathbf{r}(k';l'))]$ at the lattice points. Differentiation with respect to y gives the potential of a set of dipoles at the lattice points; the moments of the dipoles are in the y direction, and the magnitude of the moment of the l', k'th dipole is

$$e_{k'}U_y(k')\exp[-i\omega t+i(\mathbf{s}\cdot\mathbf{r}(k';l'))].$$

The summation over y adds in the potentials of corresponding sets of dipoles in the x and z directions, the differentiation with respect to x gives the x component of the field, and the evaluation gives the field at the l, kth lattice point. This expression then, as is physically obvious, also could be obtained by replacing each displaced charge in the lattice by an undisplaced charge plus a dipole plus a quadrupole plus and so on. Neglecting the higher poles, and observing that the force due to the undisplaced charges is zero, we obtain the above result for the field, since the dipole put in the l', k'th position must have a vector moment equal to the product of the charge and the displacement, or

$$e_{k'}\mathbf{U}(k')\exp[-i\omega t+i(\mathbf{s}\cdot\mathbf{r}(k';l'))].$$

The coefficient $(kk';xy)$ therefore, except for a factor represents the field in the x direction due to a polarization in the y direction of the simple lattice k', whose magnitude varies periodically in space.

The procedure to be followed to calculate the Coulomb force may, then, be summarized as follows: one sets at each point l' of the simple lattice k' a charge $\exp[-i(\mathbf{s}\cdot\mathbf{r}(kk';l-l'))]$, finds the potential due to this "auxiliary lattice" of charges at an arbitrary point, differentiates twice, with respect to x and to y, and evaluates at the point l, k. The result multiplied by $e_ke_{k'}$ is the value of $(kk';xy)$, which is to be substituted in Eq. (5). It must be noted that $(kk';xy)$ is symmetric with respect to interchange of x and y, from its definition. Furthermore, the following relation holds:

$$(kk';xx)+(kk';yy)+(kk';zz)=0.$$

This, of course, is simply the Laplace equation, as appears from the definition of the coefficients, because one is calculating the exciting field; that is, the field at the position of a dipole after the removal of that dipole; and after the removal of the dipole there is no charge at the lattice point. Born writes instead on the right side

$-(4\pi e)/\Delta$ because he considers a uniform compensating charge extending over the crystal. If the crystal is polarized and the charges are displaced, this uniform compensating charge also has to be displaced, and gives under certain conditions a surface charge, which just compensates the effect of the right side and is responsible for the difference of force between transverse and longitudinal waves of great wave-length.

We are using the static potential for the electric field, neglecting any retardation. It is obvious that this is permissible if the wave-length of the particle wave is short compared with the wave-length of the light wave with the same frequency, that is, if $\omega/c \ll |\mathbf{s}|$. This is, for a polar lattice, always fulfilled for the acoustical branch and the short waves of the optical branch, but one might doubt its validity for the long waves of the optical branch. However, the direct calculation of Ewald[5] gives for the long transverse waves of the optical branch (Reststrahlen) the same result as the static calculation,[9] and therefore we feel justified in applying it also to the long longitudinal ones.

It is appropriate to consider here the effect of the other blocks which have been added to the crystal to make an infinite lattice. If the wave-length is finite in all three coordinate directions, the first nonvanishing moment of a block is one of the fourth order, which is proportional to the wave-length times the size of the block, cubed. The field at a distance is therefore that of a fifth-order pole, and the ratio of the effect of all the other blocks to the effect of the infinite crystal will be of the order of magnitude of the wave-length divided by the size of the block, cubed. Now, in a macroscopic crystal the number of vibrations with a wave-length comparable to the size of the crystal is extremely small, and it is precisely these vibrations which are strongly influenced by the boundary conditions, even for short-range interactions. Hence, the effect of the other blocks is, for all practical purposes, negligible.

[9] J. H. C. Thompson, reference 6, discusses the problem of retardation in general according to the Ewald method and finds for long waves one term in which it has to be taken into account. But this term represents that wave which in the infinite crystal compensates the primary light wave.

III. Polar Cubic Crystals

The present calculation for polar lattices will be concerned exclusively with the lattice of the sodium chloride type. In order to discuss the solutions of the secular equation, we must make some assumption about the form of the short range interaction. For simplicity we assume that this interaction acts only between nearest neighbors and that the potential energy of interaction is of the form $f(r)$. Letting $(\partial^2 f/\partial r^2)_{r=a} = 4\pi e^2 c_1/a^3$ and $(\partial f/r\partial r)_{r=a} = 4\pi e^2 c_2/a^3$ where a is the distance between nearest neighbors, one can immediately write down the coefficients of the repulsive force. They are all zero with the exception of $(12; xx)_a$ and $[12; xx]_a$ in which x assumes the values x, y, and z:

$$(12; xx)_a = (4\pi e^2/a^3)[c_1 \cos as_x + c_2(\cos as_y + \cos as_z)], \quad (6)$$

$$[12; xx]_a = (4\pi e^2/a^3)(c_1 + c_2).$$

The lattice vectors $\mathbf{a}_1$, $\mathbf{a}_2$, and $\mathbf{a}_3$ are orthogonal for the NaCl lattice, and may be taken in the directions of the three coordinate axes. Then for this lattice $\mathbf{s} = (\pi/a)(n_1/G_1, n_2/G_2, n_3/G_3)$. It will be convenient to define a vector $\boldsymbol{\tau}$ by $\mathbf{s} = (2\pi/a)\boldsymbol{\tau}$. It will be much simpler not to divide the lattice up into cells, but to consider it as comprised of two simple lattices, that of the positive ions, and that of the negative. Then k assumes only two values, of which 1 will be taken to refer to the positive ions, and 2 to the negative ions. Since every positive ion is surrounded by positive ions in precisely the same way that every negative ion is surrounded by negative ions, $(11; xy) = (22; xy)$. Similarly $(12; xy)$ must be $= (21; xy)$.

Let us consider the range of possible values of $\boldsymbol{\tau}$. Since, as stated in Section II, $|n_i| \leqslant G_i$, and $\tau_i = n_i/2G_i$, $|\tau_i| \leqslant \frac{1}{2}$. The discussion, however, can be limited to positive values of all three components of $\boldsymbol{\tau}$ since changing the sign of one of them changes no physical feature of the wave. Furthermore, if τ_1, τ_2, τ_3 are replaced by $\frac{1}{2} - \tau_1$, $\frac{1}{2} - \tau_2$, $\frac{1}{2} - \tau_3$, respectively, one has the same wave as before, since this is equivalent to replacing $\mathbf{U}(2)$ by its negative. One will obtain the same frequencies, and the same relation between the amplitudes except for this change in sign. Finally, any permutation of τ_1, τ_2, τ_3 gives again

a wave with the same frequencies and amplitude ratios.[10] This does not appear from the form of the coefficients for the Coulomb force given below, but calculation of their values shows it to be true, as it must be. Thus one can restrict oneself to values of τ given by $0<\tau_1<\frac{1}{2}$, $0<\tau_2<\frac{1}{4}$, $0<\tau_3<\frac{1}{4}$.

One of the simple lattices, the lattice of positive ions, for example, in this crystal forms a face-centered cubic array. The "auxiliary lattice" will be for simplicity considered to be simple cubic. The points are identified only by the values of l' and the charge at the point l' is $\exp[-2\pi i(\tau\cdot 1-1')]f(l_1'+l_2'+l_3')$ where $f(n)=0$ if n is odd, and 1 if n is even (obviously $f(n+2)=f(n)$), and 1′ is a vector defined as (l_1', l_2', l_3'). A point of this lattice where the charge is zero is a point of the lattice of negative ions; one where the charge is different from zero is a point of the lattice of positive ions. Then to find $(11; xy)$ or $(21; xy)$ by the procedure stated above, the calculation is exactly the same up to the final evaluation at the point l. This is to be made at a point for which the charge of the auxiliary lattice is not zero ($l_1+l_2+l_3$ is even) to get $(11; xy)$; at a point for which the charge is zero ($l_1+l_2+l_3$ odd) to get $(21; xy)$.

The potential of the auxiliary lattice will be found here by an extension of the Madelung method.[11] The simple cubic lattice is broken up into lines and planes of points in the usual manner of this method. The lines are taken parallel to the x axis and the planes normal to the z axis. The lattice sums are divided into three parts: (0) the sum over the line containing the point l; (1) the sum over the other lines in the same plane; and (2) the sum over the other planes. 0, 1, and 2 will be used as indices to distinguish the parts of the coefficients coming from each of these three partial sums, so that

$$(kk'; xy)=(kk'; xy)_0+(kk'; xy)_1+(kk'; xy)_2.$$

The separate evaluation of the three parts of each coefficient follows.

0. The evaluation of $(kk'; xy)_0$ may be carried out most easily by directly differentiating term by term the sum giving the potential due to the points in the line containing the point l. If the general point in the lattice be denoted by l', the points in this sum are those for which $l_1'=l_1+\mu$, $l_2'=l_2$, and $l_3'=l_3$, where μ is a non-zero integer. Hence $\mathbf{r}(l-l')=(\mu a, 0,0)$. As a sample, $(11; xx)_0$ will be calculated explicitly; only the results for the others will be given. The charge at a point,

$$f(l_1'+l_2'+l_3')\exp[-2\pi i(\tau\cdot 1-1')]$$
$$=f(l_1+\mu+l_2+l_3)\exp(2\pi i\tau_x\mu).$$

Since for $(11; xx)_0$, $l_1+l_2+l_3$ is to be taken as even, this becomes $f(\mu)\exp(2\pi i\tau_x\mu)$. Furthermore

$$[\partial^2/\partial x^2(|\mathbf{r}-\mathbf{r}(l')|)^{-1}]_{\mathbf{r}=\mathbf{r}(l)}$$
$$=[3(x(l-l'))^2-(r(l-l'))^2]/(r(l-l'))^5=2/|\mu a|^3.$$

Combining these, we obtain

$$(11; xx)_0=e^2\sum_{\mu=-\infty}^{+\infty}{}' f(\mu)\exp(2\pi i\tau_x\mu)(2/|\mu a|^3)$$
$$=(4e^2/a^3)\sum_{\mu=1}^{\infty}(f(\mu)\cos 2\pi\tau_x\mu)/\mu^3$$
$$=(4e^2/a^3)\sum_{\nu=1}^{\infty}(\cos 2\pi\tau_x(2\nu))/(2\nu)^3$$

from the definition of f. Similarly $(11; yy)_0=(11; zz)_0=-(\frac{1}{2})(11; xx)_0$,

$$(12; xx)_0=-2(12; yy)_0=-2(12; zz)_0$$
$$=-(4e^2/a^3)\sum_{\nu=1}^{\infty}(\cos 2\pi\tau_x(2\nu+1))/(2\nu+1)^3.$$

All the other coefficients with the subscript zero vanish.

1. One calculates first the potential at an arbitrary point due to the line of charges designated by $1'=(l_1', l_2+\mu, l_3)$, (μ fixed, $\neq 0$) proceeds with the differentiation and evaluation at l, and then sums over all the lines (that is, over μ). If $p=l_1'-l_1$, then $\mathbf{r}(l-l')=(pa, \mu a, 0)$. Again $(11; xx)_1$ will be evaluated for example. If there be given, in a Cartesian coordinate system (ξ, η, ζ) a set of charges e_p at the points $(\xi_p, 0, 0)$ and if the charges be periodic along

[10] This assumes that the G_i's are so large that there is a value of $n_1/2G_1$ very close to every value of $n_2/2G_2$ and so forth. The G_i's are $\sim 10^8$ for a macroscopic crystal.

[11] E. Madelung, Physik. Zeits. **19**, 524 (1918).

the axis with a period a', then the potential at any point is given by

$$\varphi(\xi,\rho)=(2/a')\sum_{n=-\infty}^{+\infty}{}'\sum_p e_p K_0(2\pi|n|\rho/a')$$
$$\times\exp[2\pi i n(\xi-\xi_p)/a']-(2/a')\ln\rho\sum_p e_p,$$

where $\rho^2=\xi^2+\eta^2$ and K_0 is the Hankel function of zero order. The summation over n is to omit $n=0$, and that over p is over one complete period of the charge distribution. In the present case $\xi_p=pa$,

$$e_p=f(l_1+p+l_2+\mu+l_3)\exp[2\pi i(\tau_x p+\tau_y\mu)]$$
$$=f(p+\mu)\exp[2\pi i(\tau_x p+\tau_y\mu)],$$

since again $l_1+l_2+l_3$ is even. Thus since $\tau_x=n_1/2G_1$, the period $a'=2G_1a$, and in the summation p runs from 0 to $2G_1-1$. Substituting, we obtain

$$\varphi(\xi,\rho)=(1/G_1a)\exp(2\pi i\tau_y\mu)$$
$$\times\sum_n{}'K_0(\pi|n|\rho/G_1a)\exp(\pi i n\xi/G_1a)\sum_{p=0}^{2G_1-1}f(\rho+u)$$
$$\times\exp[-\pi i(n-n_1)p/G_1]-(1/G_1a)\ln\rho\sum_p e_p.$$

The last term is retained here because of the possibility that τ_x may be $=0$, in which case $\Sigma e_p=G_1\exp(2\pi i\tau_y\mu)$. Let us consider separately the summation over p. This is equal to

$$\{f(\mu)+\exp[-(\pi i/G_1)(n-n_1)]f(\mu+1)\}$$
$$\times\sum_{p=0}^{G_1-1}\exp[-(2\pi i/G_1)(n-n_1)p].$$

This last sum is a geometrical series whose sum is zero unless

$$n=n_1+\kappa G_1=G_1(\kappa+2\tau_x),$$

κ any integer or zero, and is equal to G_1 in the latter case. If $n_1=0$ or G_1, zero or -1 is not a possible value for κ. Hence

$$\varphi(\xi,\rho)=(1/a)\exp(2\pi i\tau_y\mu)\sum_{\kappa=-\infty}^{+\infty}K_0(\pi\rho|\kappa+2\tau_x|/a)$$
$$\times\exp[\pi i\xi(\kappa+2\tau_x)/a]\{f(\mu)+\exp(\pi i\kappa)f(\mu+1)\}$$
$$-(1/G_1a)\ln\rho\sum_p e_p.$$

By differentiation, we have

$$(\partial^2/\partial\xi^2)\varphi(\xi,\rho)=-(\pi^2/a^3)\exp(2\pi i\tau_y\mu)$$
$$\times\sum_\kappa(\kappa+2\tau_x)^2K_0(\pi|\mu||\kappa+2\tau_x|)$$
$$\times\exp[\pi i\xi(\kappa+2\tau_x)/a]\{f(\mu)+(-1)^\kappa f(\mu+1)\}.$$

The evaluation of this is to be made at the point $(\xi,\eta,\zeta)=(0,\mu a,0)$ so that

$$(11;xx)_1=-(\pi^2e^2/a^3)\sum_{\mu=-\infty}^{+\infty}{}'\exp(2\pi i\tau_y\mu)$$
$$\times\sum_\kappa(\kappa+2\tau_x)^2K_0(\pi|\mu||\kappa+2\tau_x|)$$
$$\times\{f(\mu)+(-1)^\kappa f(\mu+1)\}$$
$$=-(2\pi^2e^2/a^3)\sum_{\mu=1}^{\infty}\cos 2\pi\tau_y\mu\sum_\kappa(-1)^{\kappa\mu}$$
$$\times(\kappa+2\tau_x)^2K_0(\pi\mu|\kappa+2\tau_x|).$$

Proceeding in exactly the same way, one finds

$$(11;yy)_1=(2\pi^2e^2/a^3)\sum_{\mu=1}^{\infty}\cos 2\pi\tau_y\mu$$
$$\times\{\sum_\kappa(-1)^{\kappa\mu}(\kappa+2\tau_x)^2K_0''(\pi\mu|\kappa+2\tau_x|)$$
$$+[(-1)^{2\tau_x\mu}/\pi^2\mu^2G_1]\sum_p\exp(4\pi i\tau_x p)\},$$

$$(11;zz)_1=-(2\pi^2e^2/a^3)\sum_{\mu=1}^{\infty}\cos 2\pi\tau_y\mu\{\sum_\kappa(-1)^{\kappa\mu}$$
$$\times(|\kappa+2\tau_x|/\pi\mu)K_1(\pi\mu|\kappa+2\tau_x|)$$
$$+[(-1)^{2\tau_x\mu}/\pi^2\mu^2G_1]\sum_p\exp(4\pi i\tau_x p)\},$$

$$(11;xy)_1=-(2\pi^2e^2/a^3)\sum_{\mu=1}^{\infty}\sin 2\pi\tau_y\mu\sum_\kappa(-1)^{\kappa\mu}$$
$$\times(\kappa+2\tau_x)|\kappa+2\tau_x|K_1(\pi\mu|\kappa+2\tau_x|),$$
$$(11;xz)_1=(11;yz)_1=0.$$

The coefficients $(12;xy)_1$ are of the same form as the coefficients $(11;xy)_1$, but each of the former contains an additional factor of $(-1)^{\kappa-1}$ within the summation sign ($(-1)^{2\tau_x-1}$ for the $1/\mu^2$ term).

2. Here one proceeds in a fashion analogous to that under (1). One calculates first the potential of that one of the planes designated by $l'=(l_1', l_2', l_3+\mu)$, differentiates, evaluates, and sums over μ. If $p=l_1'-l_1$ and $q=l_2'-l_2$, then $\mathfrak{r}(l-l')=(pa, qa, \mu a)$. The same coordinate system (ξ, η, ζ) is chosen, and the potential of the (ξ, η)-plane bearing a periodic distribution of charges is written down:

$$\psi(\xi,\eta,\zeta)=(2\pi/a'b')\{\sum_{n,\,m=-\infty}^{+\infty}\sum_{p,\,q}e_{pq}\times(\exp(-k_{nm}|\zeta|)/k_{nm})\exp[2\pi in(\xi-\xi_p)/a']\times\exp[2\pi im(\eta-\eta_q)/b']-|\zeta|\sum_{p,\,q}e_{pq}\}.$$

Here e_{pq} is the charge at $(\xi_p, \eta_q, 0)$ and

$$k_{nm}^2=4\pi^2((n^2/a'^2)+(m^2/b'^2)).$$

The term with $n=m=0$ is to be omitted in the summation, and p and q run over one complete period. For the present calculation, $\xi_p=pa$, $\eta_q=qa$, and

$$e_{pq}=f(l_1+p+l_2+q+l_3+\mu)\times\exp[2\pi i(\tau_x p+\tau_y q+\tau_z\mu)]=f(p+q+\mu)\times\exp[2\pi i(\tau_x p+\tau_y q+\tau_z\mu)].$$

Since $\tau_x=n_1/2G_1$ and $\tau_y=n_2/2G_2$, $a'=2G_1a$, $b'=2G_2a$, and p runs from 0 to $2G_1-1$, q from 0 to $2G_2-1$. Substituting, and carrying out the summation over p and q as in the case of the line, one obtains

$$\psi(\xi,\eta,\zeta)=(\pi/2a)\exp(2\pi i\tau_z\mu)\sum_{s,\,t=-\infty}^{+\infty}\times(\exp(-g_{st}|\zeta|/a)/g_{st})\exp[\pi i\xi(s+2\tau_x)/a]\times\exp[\pi i\eta(t+2\tau_y)/a][1+(-1)^{s+t}]\times\{f(\mu)+(-1)^t f(\mu+1)\}-(\pi/2G_1G_2a^2)|\zeta|\sum_{p,\,q}e_{pq},$$

where $g_{st}^2=\pi^2[(s+2\tau_x)^2+(t+2\tau_y)^2]$. Here again, if $\tau_x=\tau_y=0$ or $\frac{1}{2}$, $s=t=-2\tau_x$ is to be omitted. Differentiating, and observing that the quantity in curled brackets is equal to $(-1)^{\mu t}$, we find

$$(\partial^2/\partial\xi^2)\psi(\xi,\eta,\zeta)=-(\pi^3/2a^3)\exp(2\pi i\tau_z\mu)\times\sum_{s,\,t}(-1)^{\mu t}[1+(-1)^{s+t}](\exp(-g_{st}|\zeta|/a)/g_{st})\times(s+2\tau_x)^2\exp[\pi i\xi(s+2\tau_x)/a]\times\exp[\pi i\eta(t+2\tau_y)/a].$$

The evaluation is to be made at the point $(\xi, \eta, \zeta)=(0, 0, \mu a)$, so that finally

$$(11;xx)_2=-(\pi^3e^2/a^3)\sum_{\mu=1}^{\infty}\cos 2\pi\tau_z u\sum_{s,\,t}(-1)^{\mu t}\times[1+(-1)^{s+t}](\exp(-g_{st}\mu)/g_{st})(s+2\tau_x)^2.$$

The remaining coefficients are:

$$(11;yy)_2=-(\pi^3e^2/a^3)\sum_{\mu}\cos 2\pi\tau_z\mu\sum_{s,\,t}(-1)^{\mu t}\times[1+(-1)^{s+t}](\exp(-g_{st}\mu)/g_{st})(t+2\tau_y)^2,$$

$$(11;zz)_2=(\pi e^2/a^3)\sum_{\mu}\cos 2\pi\tau_z\mu\sum_{s,\,t}(-1)^{\mu t}\times[1+(-1)^{s+t}]\exp(-g_{st}\mu)g_{st},$$

$$(11;xy)_2=-(\pi^3e^2/a^3)\sum_{\mu}\cos 2\pi\tau_z\mu\sum_{s,\,t}(-1)^{\mu t}\times[1+(-1)^{s+t}](\exp(-g_{st}\mu)/g_{st})\times(s+2\tau_x)(t+2\tau_y),$$

$$(11;xz)_2=-(\pi^2e^2/a^3)\sum_{\mu}\sin 2\pi\tau_z\mu\sum_{s,\,t}(-1)^{\mu t}\times[1+(-1)^{s+t}]\exp(-g_{st}\mu)(s+2\tau_x),$$

$$(11;yz)_2=-(\pi^2e^2/a^3)\sum_{\mu}\sin 2\pi\tau_z\mu\sum_{s,\,t}(-1)^{\mu t}\times[1+(-1)^{s+t}]\exp(-g_{st}\mu)(t+2\tau_y).$$

Again, the coefficients $(12;xy)_2$ can be obtained from the coefficients $(11;xy)_2$ by multiplying each by a factor $(-1)^{t-1}$ inside the summation sign.

IV. The Influence of Polarizibility

The effect of the fact that the ions are not really rigid charges, but are polarizible, is important for all waves in the crystal. One may write in general the result of the calculation of the Coulomb force as

$$F_i(1)=(4\pi e_1/a^3)(\gamma_{i\alpha}(1)U_\alpha(1)+\gamma_{i\alpha}(2)U_\alpha(2)),$$

$$F_i(2)=(4\pi e_2/a^3)(\gamma_{i\alpha}(2)U_\alpha(1)+\gamma_{i\alpha}(1)U_\alpha(2)),$$

where the components of the vectors are now numbered from 1 to 3 instead of being labeled with x, y, and z, and where the appearance of a Greek letter suffix indicates summation over that suffix. The effect of the polarizibility is that one must replace the dipole moment due to the displacement of the ion. $e_iU_i(j)$, by $e_jU_i(j)$

$+p_i(j)$, where $p_i(j)=\alpha_j F_i(j)$, and α_j is the polarizibility of the ion of type j. Hence

$$(\delta_{i\alpha}-(4\pi\alpha_1/a^3)\gamma_{i\alpha}(1))F_\alpha(1)$$
$$+(4\pi\alpha_i/a^3)\gamma_{i\alpha}(2)F_\alpha(2)$$
$$=(4\pi e/a^3)(\gamma_{i\alpha}(1)U_\alpha(1)+\gamma_{i\alpha}(2)U_\alpha(2)),$$
$$(4\pi\alpha_1/a^3)\gamma_{i\alpha}(2)F_\alpha(1)$$
$$+(\delta_{i\alpha}-(4\pi\alpha_2/a^3)\gamma_{i\alpha}(1))F_\alpha(2)$$
$$=-(4\pi e/a^3)(\gamma_{i\alpha}(2)U_\alpha(1)+\gamma_{i\alpha}(1)U_\alpha(2)),$$

where $(\delta_{i\alpha})$ is the unit matrix.

Since for NaCl $(4\pi\alpha_1/a^3)=0.111$ and $(4\pi\alpha_2/a^3)=2.00$,[12] one can simplify by neglecting terms containing α_1. One has then, letting $k=(4\pi\alpha_2/a^3)$

$$F_i(1)+k\gamma_{i\alpha}(2)F_\alpha(2)$$
$$=(4\pi e/a^3)(\gamma_{i\alpha}(1)U_\alpha(1)+\gamma_{i\alpha}(2)U_\alpha(2),$$
$$(\delta_{i\alpha}-k\gamma_{i\alpha}(1))F_\alpha(2)$$
$$=-(4\pi e/a^3)(\gamma_{i\alpha}(2)U_\alpha(1)+\gamma_{i\alpha}(1)U_\alpha(2).$$

These equations are to be solved for $F_i(1)$ and $F_i(2)$; the result is the corrected Coulomb field which is to be substituted in the equations of motion.

V. The Coulomb Field for Waves Long Compared to the Crystal

In the particularly interesting case of long waves, the components of $\boldsymbol{\tau}$ may be regarded as small quantities, and the coefficients may be expanded in terms of them about $\boldsymbol{\tau}=\mathbf{0}$. The results give for the field (up to and including terms linear in the components of $\boldsymbol{\tau}$)

$$F_1(1)=-(4\pi e/a^3)[-(\tfrac{1}{6})(U_1(1)-U_1(2))$$
$$+(\tau_1/2\tau^2)(\boldsymbol{\tau}\cdot\mathbf{U}(1)-\mathbf{U}(2)],$$
$$F_2(1)=-(4\pi e/a^3)[-(\tfrac{1}{6})(U_2(1)-U_2(2))$$
$$+(\tau_2/2\tau^2)(\boldsymbol{\tau}\cdot\mathbf{U}(1)-\mathbf{U}(2)],$$
$$F_3(1)=-(4\pi e/a^3)[(\tfrac{1}{3})(U_3(1)-U_3(2))$$
$$-((\tau_1^2+\tau_2^2)/2\tau^2)(U_3(1)-U_3(2))$$
$$+(\tau_3/2\tau^2)\{\tau_1(U_1(1)-U_1(2))$$
$$+\tau_2(U_2(1)-U_2(2))\}]$$

and $\mathbf{F}(2)=\mathbf{F}(1)$.

[12] The values of α_1 and α_2 are taken from K. Fajans and G. Joos, Zeits. f. Physik **23**, 1 (1924).

Special consideration given to the case $\boldsymbol{\tau}=\mathbf{0}$ (infinitely long waves) shows that then all terms in τ_1, τ_2 and τ_3 in these equations are to be dropped. One sees from these equations what the value of $\mathbf{G}(k)$ must be. By its definition $\mathbf{G}(k)$ may be obtained from $\mathbf{F}(k)$ by replacing $\mathbf{U}(k')$ by $\mathbf{U}(k)$ in the expression for $\mathbf{F}(k)$ and then letting $\boldsymbol{\tau}$ approach zero. For the present case, then, $\mathbf{G}(1)=\mathbf{G}(2)=\mathbf{0}$.

In the event that the wave-length is infinite, one may put the average electric moment per unit volume $(e/2a^3)(\mathbf{U}(1)-\mathbf{U}(2))$, equal to the (uniform) polarization $\mathbf{P}$. If the polarization is in the x direction, $\mathbf{F}=(4\pi/3)\mathbf{P}$; if it is in the z direction, $\mathbf{F}=-(8\pi/3)\mathbf{P}$. These two cases are apparently physically identical; how then is one to account for the difference in the result?

The reason for the difference, mathematically at least, is apparent. One has summed a conditionally convergent series in two different orders, and should not be surprised at obtaining two different results. It is pertinent to inquire as to what the physical meaning of this difference is. For the sake of the discussion of this meaning, a third method of carrying out the summation will be considered. If one calculates the field at a point due to a cubic lattice of constant dipoles by grouping together all those at a given distance from the point, and then adding the results of the groups, the field turns out to be zero.

It is apparent that the physical analog of the conditional convergence of the series is the fact that the shape of the crystal exerts a distinguishing influence upon the field at a point in it, so that the value of the field in a strictly infinite crystal is quite undefined. For in the case of the method of summation last mentioned, one adds the contributions from the points within a spherical shell and then adds shell upon shell, so that the final result is the summation over a very large sphere. In the Madelung method, one adds together the contributions of planes, so that here the final result is the summation over a slab which is infinite in two directions and large in the third. The polarization is, for this method, either normal to or along the favored direction. One has, then, for a sphere the field $\mathbf{F}=\mathbf{0}$; for a slab with the polarization normal $\mathbf{F}=-(8\pi/3)\mathbf{P}$; for a slab with the

polarization parallel $\mathbf{F}=(4\pi/3)\mathbf{P}$. Let us compare these results with those of continuum theory.

In the continuum theory one calculates (for homogeneous polarization) the exciting field as due to three contributions: the influence of the true external charges, which gives the electric displacement $\mathbf{D}$; the influence of the induced charges on the surface of a spherical cavity surrounding the point at which the field is to be calculated, which gives the Lorentz-Lorenz force $(4\pi/3)\mathbf{P}$; and the influence of the surface charges on the outer surface of the dielectric. For a sphere, the latter gives $-(4\pi/3)\mathbf{P}$. Therefore the exciting field in the center of a sphere is $\mathbf{D}+(4\pi/3)\mathbf{P}-(4\pi/3)\mathbf{P}=\mathbf{D}$. In our calculations with no external charges $\mathbf{D}=\mathbf{0}$. If the dielectric is a slab with the field normal, the charges on the faces of the slab give $-4\pi\mathbf{P}$, reducing $\mathbf{D}$ to $\mathbf{E}=\mathbf{D}-4\pi\mathbf{P}$. The exciting field is $\mathbf{D}+(4\pi/3)\mathbf{P}-4\pi\mathbf{P}=\mathbf{D}-(8\pi/3)\mathbf{P}$. In our case $(\mathbf{D}=\mathbf{0})$ we have in fact found $-(8\pi/3)\mathbf{P}$. If the dielectric is a slab with the field parallel, the external surface charges are induced at the ends of the slab, which are so remote, in comparison to their size that they do not contribute appreciably. Therefore $\mathbf{D}+(4\pi/3)\mathbf{P}$ is the exciting field. For this case we calculate by direct summation $(4\pi/3)\mathbf{P}$.[13]

VI. Waves Long Compared to the Lattice Distance but Short Compared to the Size of the Crystal

The importance of the preceding discussion for our purpose lies in the fact that conditions with regard to the convergence difficulty are completely different if the wave-length is long but not infinite. For here the equations for $\mathbf{F}(k)$ become:

$$\mathbf{F}(1)=\mathbf{F}(2)=-(4\pi e/a^3)[-(\tfrac{1}{6})(\mathbf{U}(1)-\mathbf{U}(2))+(\boldsymbol{\tau}/2\tau^2)(\boldsymbol{\tau}\cdot\mathbf{U}(1)-\mathbf{U}(2))],$$

which expressions are completely symmetrical in x, y, and z, and are independent of the manner in which the planes in the crystal have been chosen. (The same result, as would be expected, is observed for such of the shorter waves as have been calculated). One concludes, therefore, that the field in an infinite crystal in a real state of vibration with a finite wave-length does have meaning, and that the phase difference in space between the polarizations at the various lattice points has removed the conditionality of the convergence, as Born[8] has pointed out. Since this is true, the exchange of the order of summation and differentiation made at the beginning of the calculation is justified by the results.

Upon including the correction for polarizability, one has for the Coulomb force

$$e_1\mathbf{F}(1)=-e_2\mathbf{F}(2)=(4\pi e^2/a^3)\times(1+k/3)^{-1}(1-k/6)^{-1}[(\tfrac{1}{6})(1+k/3)\times(\mathbf{U}(1)-\mathbf{U}(2))-(\boldsymbol{\tau}/2\tau^2)(\boldsymbol{\tau}\cdot\mathbf{U}(1)-\mathbf{U}(2))].$$

The repulsive force is

$$\mathbf{R}(1)=-\mathbf{R}(2)=-(4\pi e^2/a^3)(c_1+2c_2)(\mathbf{U}(1)-\mathbf{U}(2)).$$

The secular equation to be satisfied is that resulting from the set of equations

$$-m_k\omega^2\mathbf{U}(k)=e_k\mathbf{F}(k)+\mathbf{R}(k).$$

The result is that if μ is the reduced mass, then

$$\omega^6[\mu\omega^2-(4\pi e^2/a^3)(c_1+2c_2-(\tfrac{1}{6})(1-k/6)^{-1})]^2\times[\mu\omega^2-(4\pi e^2/a^3)(c_1+2c_2+(\tfrac{1}{3})(1+k/3)^{-1}]=0,$$

which gives the following results:

(a) There are three possible vibrations (with a given wave vector $\boldsymbol{\tau}$) whose frequency is zero. These are characterized by $\mathbf{U}(1)=\mathbf{U}(2)$, so that the displacements of neighboring particles are but very little different. In other words, these are the three frequencies belonging to the acoustical branch. They are zero only because we have neglected the contribution to the forces of terms proportional to squares of the components of $\boldsymbol{\tau}$. Inclusion of these would give $\omega^2\sim\tau^2$, or $\omega\sim\tau$, as it should be in the acoustical branch. Without this inclusion we can say no more about the characteristics of these vibrations beyond the statement that the amplitudes of the two kinds of particles are equal, and that hence the electric field vanishes in this approximation.

(b) There are two vibrations for which

$$\omega^2=(4\pi e^2/\mu a^3)(c_1+2c_2-(\tfrac{1}{6})(1-k/6)^{-1}).$$

[13] This calculation for infinite waves is identical with that carried out by K. F. Herzfeld, J. Opt. Soc. Am. **17**, 26 (1928).

These are characterized by $m_1\mathbf{U}(1)+m_2\mathbf{U}(2)=\mathbf{0}$ and $(\boldsymbol{\tau}\cdot\mathbf{U}(1)-\mathbf{U}(2))=0$. The former condition implies that the two kinds of particles are vibrating exactly out of phase and with an amplitude ratio inversely proportional to that of the masses; the latter condition that the direction of vibration of a particle is normal to the direction of motion of the wave; that is, that these waves are transverse. The fact that this frequency appears twice in the secular equation corresponds to the existence of two possible independent modes of vibration normal to the wave vector. The electric field for these vibrations is given by

$$\mathbf{F}(1)=\mathbf{F}(2)=(4\pi e/a^3)(\tfrac{1}{6})[1-(k/6)]^{-1}\times(\mathbf{U}(1)-\mathbf{U}(2))=(4\pi/3)\mathbf{P},$$

in which we have introduced again the polarization vector $\mathbf{P}$.[14]

(c) The remaining vibration has

$$\omega^2=(4\pi e^2/\mu a^3)\{c_1+c_2+(\tfrac{1}{3})[1+(k/3)]^{-1}\}.$$

The amplitudes are characterized by $m_1\mathbf{U}(1)+m_2\mathbf{U}(2)=\mathbf{0}$ and $[\boldsymbol{\tau}\cdot\mathbf{U}(1)-\mathbf{U}(2)]=\mathbf{0}$. This, then, is a vibration like the preceding two, with the exception that it is longitudinal. The electric field here is $\mathbf{F}(1)=\mathbf{F}(2)=-(8\pi/3)\mathbf{P}$.

The results both for the acoustical branch and for the transverse waves in the optical branch agree with what has been known,[8] but the result for the longitudinal waves is a new one.

One must be careful to recognize that the reappearance here of $(4\pi/3)\mathbf{P}$ and $-(8\pi/3)\mathbf{P}$ for the electric field is not for the same formal reason as in Section V. There it was a question of the dependence of the convergence of the sum over the lattice on the shape of the crystal, whereas there is no such difficulty here. Here it is a question of the difference between longitudinal and transverse waves; that is, whether the displacement is in the direction in which it varies in space, or perpendicular to it. The result is independent of the shape of the crystal and of the manner in which it is broken up into planes to calculate the electric field.

It is not surprising, however, that in the transition from very long to infinitely long waves, the transverse waves give the same result as uniform polarization along an infinite slab, the longitudinal waves the same as uniform polarization normal to the slab. Consider for a moment forced vibrations, for example a plane light wave falling on the slab. Then plane waves (transverse) with the polarization along the slab are possible. If, on the other hand, a light wave should fall on the (narrow) sides of the slab, there would be diffraction effects, so that no plane wave, polarized normal to the slab and progressing along it, is possible (the thickness of the slab is now considered small compared to the wave-length). The converse is true for longitudinal waves. Such waves, progressing along a slab, would be subject to edge effects, which we call diffraction for the transverse waves.

It must be pointed out that the polarizability correction to the Coulomb force and the repulsive force (provided it acts only on nearest neighbors) do not change the solutions of the secular equation as far as the types of waves (that is, the conditions on the amplitudes) are concerned, but only alter the numerical values of the frequencies. This is true for all the waves that we consider here, and for reasons to be given in section VIII, we will give only the uncorrected values of the Coulomb force for the other waves to be discussed.

VII. Short Waves

Case I

$\boldsymbol{\tau}=(\frac{1}{4},\frac{1}{4},\frac{1}{4})$. This represents the vibration in which one of the simple lattices (composed of all the particles of one kind) remains at rest; the other vibrating so that all particles in a given plane normal to the line $x=y=z$ (the direction of propagation of the wave, which is the diagonal of the cube) are in phase, and successive planes are exactly out of phase. (One remembers that the phase difference between the particles 1 and 1′ is $\exp[2\pi i(\boldsymbol{\tau}\cdot 1-1')]$. The Coulomb force, uncorrected, is

$$e_1F_i(1)=-(4\pi e^2/a^3)(0.1438)(U_j(1)+U_k(1)),$$

$$e_2F_i(2)=-(4\pi e^2/a^3)(0.1438)(U_j(2)+U_k(2))$$

$$(i\neq j\neq k).$$

[14] This result is in agreement with that of Heckmann, Zeits. f. Krist. **61**, 250 (1925).

The repulsive force is

$$\mathbf{R}(1) = -(4\pi e^2/a^3)(c_1+2c_2)\mathbf{U}(1),$$
$$\mathbf{R}(2) = -(4\pi e^2/a^3)(c_1+2c_2)\mathbf{U}(2).$$

The solution of the secular determinant shows that there are two sets of three vibrations each, one set for the vibration of the Na lattice and one for that of the Cl lattice. Of each of these two sets, two vibrations are transverse, with the same frequency, and one is longitudinal. The transverse frequencies are given by

$$\omega^2 = (4\pi e^2/m_i a^3)(c_1+2c_2-0.1438);$$

the longitudinal by

$$\omega^2 = (4\pi e^2/m_i a^3)(c_1+2c_2+0.2876).$$

As τ changes from (0, 0, 0) to $(\frac{1}{4}, \frac{1}{4}, \frac{1}{4})$, the frequencies in the acoustical branch rise greatly, and those in the optical branch drop slightly, until when τ arrives at $(\frac{1}{4}, \frac{1}{4}, \frac{1}{4})$ both branches have frequencies of the same order of magnitude; in fact, they are in the ratio of the square roots of the masses.[15] This is one of the points of similarity which these vibrations have to the shortest waves of the acoustical and optical branches in the Born-v. Kármán linear lattice. In this case only one type of particle takes part in a vibration, and the two branches are closest together, since the optical branch frequencies are a minimum and the acoustical are a maximum. The frequencies of the two branches are in the inverse ratio of the square roots of the masses. In the three-dimensional lattice, however, there is at least one other direction in which the two branches are as close together for the shortest waves as this one, and another direction in which the longitudinal wave in the optical branch has a lower frequency.

Case II

$\tau = (\frac{1}{2}, 0, 0)$. Here the direction of propagation is along the x axis, and particles in any plane normal to the x axis are in phase, since successive lattice planes are exactly out of phase. The Coulomb force is calculated to be:

$$e_1F_1(1) = (4\pi e^2/a^3)(-0.1724U_1(1)+0.5984U_1(2)),$$
$$e_1F_2(1) = (4\pi e^2/a^3)(0.0862U_2(1)-0.2992U_2(2)),$$
$$e_1F_3(1) = (4\pi e^2/a^3)(0.0862U_3(1)-0.2992U_3(2)),$$

the repulsive force:

$$R_1(1) = -(4\pi e^2/a^3)[(c_1+2c_2)U_1(1) + (c_1-2c_2)U_1(2)],$$
$$R_2(1) = -(4\pi e^2/a^3)[(c_1+2c_2)U_2(1)-c_1U_2(2)],$$
$$R_3(1) = -(4\pi e^2/a^3)[(c_1+2c_2)U_3(1)-c_1U_3(2)].$$

The value of $e_2\mathbf{F}(2)$ can be obtained from that of $e_1\mathbf{F}(1)$, and that of $\mathbf{R}(2)$ from that of $\mathbf{R}(1)$, by interchanging $\mathbf{U}(1)$ and $\mathbf{U}(2)$ in the above expressions.

It appears by inspection that the waves can be divided again into longitudinal and transverse, the former are a vibration in the x direction, and the latter a vibration in the y or z direction. The secular determinant breaks into three; each is of the form

$$\begin{vmatrix} A-(m_1a^3/4\pi e^2)\omega^2 & B \\ B & A-(m_2a^3/4\pi e^2)\omega^2 \end{vmatrix} = 0,$$

the solution of which is

$$\omega^2 = (4\pi e^2/a^3)\{(A/2\mu) \pm [(A/2\mu)^2-(A^2-B^2)/m_1m_2]^{\frac{1}{2}}\}.$$

For the two longitudinal waves, $A = 0.1724+c_1+2c_2$, $B = 0.5984-c_1+2c_2$. For the four transverse waves, $A = -0.0862+c_1+2c_2$, $B = -0.2992+c_1$. For the acoustical branch (lower frequency of a pair), the displacements of the two types of particles are in the same direction; for the optical branch, in the opposite direction.

Case III

$\tau = (\frac{1}{2}, \frac{1}{4}, 0)$. This is the shortest wave possible in the crystal, provided that of the equivalent pair of wave vectors (τ_1, τ_2, τ_3) and $(|\frac{1}{2}-\tau_1|, |\frac{1}{2}-\tau_2|, |\frac{1}{2}-\tau_3|)$ one always chooses the one of longer wave-length. The direction of propagation is in the (x, y) plane, at an angle of about 60° with the x axis. The Coulomb force here is:

$$e_1F_1(1) = (4\pi e^2/a^3)(-0.03135U_1(1) + 0.4371U_1(2)),$$
$$e_1F_2(1) = (4\pi e^2/a^3)0.06270U_2(1),$$
$$e_1F_3(1) = (4\pi e^2/a^3)(-0.03135U_3(1) - 0.04371U_3(2)),$$

and the repulsive force:

$$R_1(1) = -(4\pi e^2/a^3)[(c_1+2c_2)U_1(1) + (c_1-c_2)U_1(2)],$$
$$R_2(1) = -(4\pi e^2/a^3)(c_1+2c_2)U_2(1),$$
$$R_3(1) = -(4\pi e^2/a^3)[(c_1+2c_2)U_3(1) - (c_1-c_2)U_3(2)].$$

[15] This statement is true for the transverse and longitudinal vibrations separately.

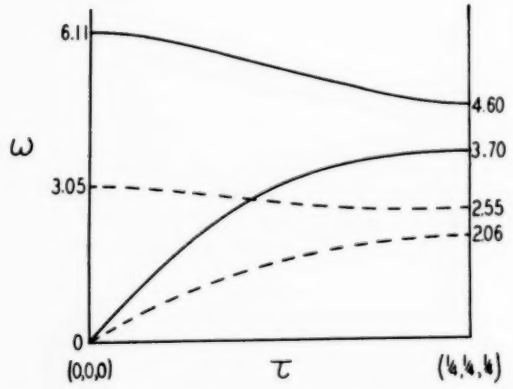

FIG. 1. This graph represents the frequencies in a sodium chloride crystal (in units of 10^{13} sec.$^{-1}$) as functions of the magnitude of τ, as τ changes from (0, 0, 0) to $(\frac{1}{4}, \frac{1}{4}, \frac{1}{4})$; that is, for waves of all possible lengths traveling along the cube diagonal. The terminal points of each curve have been calculated, and the curves in between are merely sketched, taking advantage of the knowledge that, for example, the highest curve must be horizontal at both ends. The curves for longitudinal waves are drawn solid, for transverse broken (each of the transverse curves represents two frequencies). In each case the upper curve represents the optical branch, the lower the acoustical branch.

The normal vibrations are along the x, the y, or the z direction again, but they cannot be divided into longitudinal and transverse. The secular determinant breaks into three, of the same type as for $\tau=(\frac{1}{2}, 0, 0)$. The same frequencies are given by the vibrations along the x or the z direction, for which A is equal to $0.03135+c_1+2c_2$ and B is equal to $\pm(0.4371-c_1+c_2)$. The vibration along the x direction is neither longitudinal nor transverse; that along the z direction is transverse. The two frequencies of the vibration along the y direction, which is neither longitudinal nor transverse, are given by

$$\omega^2=(4\pi e^2/m_i a^3)(-0.06270+c_1+2c_2).$$

But here the distinction between longitudinal and transverse waves means but little, since for the x and z vibrations not only the frequencies, but the displacements themselves are indistinguishable, as solution of the secular equation for the amplitudes shows.

VIII. Numerical Values of the Frequencies

To obtain numerical values of these frequencies, one must make an estimate of the size of the repulsive forces. For this purpose, we assume that the function $f(r)$ which gives the repulsive interaction between nearest neighbors is of the form $be^{-r/\rho}$ and evaluate the constants b and ρ by the method of Born and Mayer.[16] If we remember that the van der Waals interaction is to be neglected, this gives for the two constants appearing in the frequencies $c_1=0.4220$ and $c_2=-0.0427$. The numerical results for the frequencies follow. (The frequencies are stated in multiplies of 10^{13} sec.$^{-1}$.)

Long waves, optical branch:

Transverse: 3.051; Longitudinal: 6.113 (The transverse frequency calculated from the Reststrahlen frequency is $\omega=3.06$. Such good agreement is to be regarded as fortuitous.)

$(\frac{1}{4}, \frac{1}{4}, \frac{1}{4})$:

Transverse, Na lattice vibrating: 2.553; Transverse, Cl lattice vibrating: 2.057; Longitudinal, Na lattice vibrating: 4.595; Longitudinal, Cl lattice vibrating: 3.701.

$(\frac{1}{2}, 0, 0)$:

Transverse: 3.263, 1.862; Longitudinal: 4.255, 3.205.

$(\frac{1}{2}, \frac{1}{4}, 0)$:

Vibration along x or z direction: 3.545, 2.820; Vibration along y direction: 3.044, 2.452.

If one calculates these frequencies with the polarizibility correction to the Coulomb force included, the results are bad. The transverse frequency for the long waves drops to about two-thirds of its present value; the transverse frequencies for $(\frac{1}{2}, 0, 0)$ and the frequencies for the vibrations in the x or z directions for $(\frac{1}{2}, \frac{1}{4}, 0)$ become imaginary. As Heckmann has pointed out (reference 14) for the long waves, such a

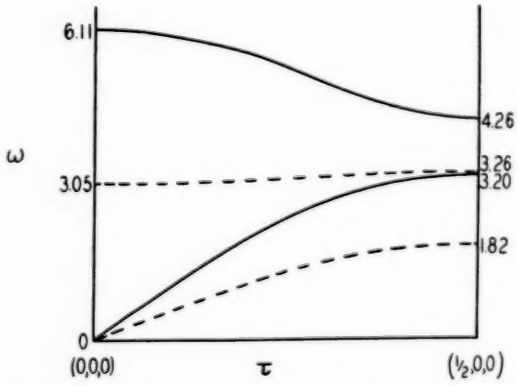

FIG. 2. This represents the frequencies of all possible waves traveling along the edge of the cube. Again the waves are divisible into longitudinal and transverse and again the curves are sketched.

[16] M. Born and J. E. Mayer, Zeits. f. Physik **75**, 1 (1932).

result is probably due to the fact that the ions in the immediate vicinity of a given ion cannot be considered to be point charges, the deviation of their behavior from that of point charges affecting strongly the polarizing electric field. In other words, the repulsive forces would appear to influence the polarization of the ion.[17]

IX. The Neutral System

There is another possible application of the preceding calculation. Suppose that one has a simple cubic lattice, lattice distance a, composed of identical particles kept in place by some elastic, isotropic binding. Let the lattice be a block of dimensions $G_1 \times G_2 \times G_3$ particles, and let it be built up to an infinite periodic lattice as before. Let the displacement of the lth particle be denoted by $\mathbf{x}(l) = (x_1(l), x_2(l), x_3(l))$, and let there be a dipole moment $e\mathbf{x}(l)$ associated with the displacement $\mathbf{x}(l)$. An arbitrary displacement of the particles of the lattice may be analyzed into a Fourier series:

$$\mathbf{x}(l) = \sum_{\tau} \mathbf{g}(\tau) \exp\left[2\pi i(\boldsymbol{\tau}\cdot l)\right],$$

where $\boldsymbol{\tau} = (l_1'/G_1,\ l_2'/G_2,\ l_3'/G_3)$ and the sum over τ indicates the triple sum over all integers $|l_1'| \leqslant G_1,\ |l_2'| \leqslant G_2,\ |l_3'| \leqslant G_3$. $\mathbf{g}(\tau)$ is a function of the time t. One can calculate the force on one particle due to the dipole moments of all the other particles for one of these Fourier components by the calculation above for the Coulomb force, provided that one makes the two kinds of particles identical; that is, sets $\mathbf{U}(1) = \mathbf{U}(2) = \mathbf{g}(\tau)$ and $e_1 = e_2 = e$.

The equations of motion, if $\mathbf{F}(\tau) \exp\left[2\pi i(\boldsymbol{\tau}\cdot 1)\right]$ is the force of the interaction, are $m(\partial^2/\partial t^2)\mathbf{g}(\tau) = -k\mathbf{g}(\tau) + \mathbf{F}(\tau)$, in which k is the constant of the elastic restoring force. Now, from the results of the preceding calculation, $\mathbf{F}(\tau)$ will contain $g_1(\tau)$, $g_2(\tau)$, $g_3(\tau)$ and none of the other Fourier components of the displacements. Hence for each value of $\boldsymbol{\tau}$ there will be three normal vibrations of the system, the coordinates for which will be

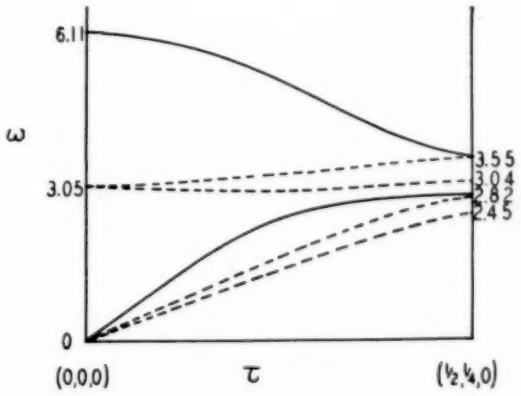

Fig. 3. Here are represented the frequencies as $\boldsymbol{\tau}$ changes from (0, 0, 0) to $(\frac{1}{2}, \frac{1}{4}, 0)$. To aid in drawing the curves the point in the center, $(\frac{1}{4}, \frac{1}{8}, 0)$, has also been calculated. The two broken curves ending on the right at 3.55 and 1.61 represent transverse waves; the others are in general neither, but are drawn broken or solid in accordance with their behavior at large wave-length.

linear combinations of the three coefficients $g_1(\tau)g_2(\tau)$ and $g_3(\tau)$. One can then write $\partial^2\mathbf{g}(\tau)/\partial t^2 = -\omega^2\mathbf{g}(\tau)$, and has the secular equation to solve resulting from $(-m\omega^2 + k)\mathbf{g}(\tau) - \mathbf{F}(\tau) = 0$. The results for this calculation follow.

(1) Long waves ($\boldsymbol{\tau} \ll 1$)

$$\mathbf{F}(\tau) = (4\pi e^2/a^3)\left[(\tfrac{1}{3})\mathbf{g}(\tau) - (\boldsymbol{\tau}/\tau^2)(\boldsymbol{\tau}\cdot\mathbf{g}(\tau))\right].$$

There are two transverse vibrations with $m\omega^2 - k = -(4\pi e^2/a^3)(\frac{1}{3})$ and one longitudinal with $m\omega^2 - k = (4\pi e^2/a^3)(\frac{2}{3})$. Transverse and longitudinal mean here, of course, that $\boldsymbol{\tau}$ and $\mathbf{g}(\tau)$ are normal and collinear, respectively.

(2) $\boldsymbol{\tau} = (\frac{1}{2}, 0, 0)$

$$F_1(\tau) = (4\pi e^2/a^3)(-0.770)g_1(\tau),$$
$$F_2(\tau) = (4\pi e^2/a^3)0.385 g_2(\tau),$$
$$F_3(\tau) = (4\pi e^2/a^3)0.385 g_3(\tau).$$

These are the vibrations for which all particles in a plane normal to the x axis vibrate in phase, and successive lattice planes are exactly out of phase. There are two transverse waves with $m\omega^2 - k = -0.385(4\pi e^2/a^3)$ and one longitudinal with $m\omega^2 - k = 0.770(4\pi e^2/a^3)$. The results for this wave are very similar to those for the long waves (0.385 instead of 0.333) since one has the same polarization, except that every alternate plane has the sign of its polarization reversed. Since the effect, for long waves, of planes other than the one containing the lattice point is small, the result is understandable.

[17] These results make it probable that a better calculation of the specific heats in the Debye approximations might be accomplished by taking separately N longitudinal and $2N$ transverse vibrations in part fulfillment of the suggestion of Born and Göppert-Mayer (reference 8, p. 651).

(3) $\tau=(\frac{1}{2}, \frac{1}{2}, 0)$

$$F_1(\tau)=(4\pi e^2/a^3)(-0.213)g_1(\tau),$$
$$F_2(\tau)=(4\pi e^2/a^3)(-0.213)g_2(\tau),$$
$$F_3(\tau)=(4\pi e^2/a^3)0.426g_3(\tau).$$

This wave progresses along the diagonal of the face of the cube, since alternate lattice planes have opposite phase. Here the normal vibrations again can be divided into longitudinal and transverse. There is one transverse vibration in the z direction with $m\omega^2-k=-0.426(4\pi e^2/a^3)$ and one in the direction $(\frac{1}{2}, -\frac{1}{2}, 0)$ with $m\omega^2-k=0.213(4\pi e^2/a^3)$. The longitudinal wave has $m\omega^2-k=0.213(4\pi e^2/a^3)$. This wave presents the feature hitherto not met with of having different frequencies for the two transverse waves.

(4) $\tau=(\frac{1}{2}, \frac{1}{2}, \frac{1}{4})$

$$F_1(\tau)=(4\pi e^2/a^3)(-0.104)g_1(\tau),$$
$$F_2(\tau)=(4\pi e^2/a^3)(-0.104)g_2(\tau),$$
$$F_3(\tau)=(4\pi e^2/a^3)(0.208)g_3(\tau).$$

The normal vibrations for this wave can be taken along the x, y, and z directions, and cannot be separated into longitudinal and transverse. The frequency for vibrations in the x and y directions is $m\omega^2-k=0.104(4\pi e^2/a^3)$; for vibrations in the z direction, $m\omega^2-k=-0.208\times(4\pi e^2/a^3)$.

(5) $\tau=(\frac{1}{2}, \frac{1}{2}, \frac{1}{2})$

This is the wave in which nearest neighbors are always exactly out of phase; it is the shortest wave possible in the lattice. The force due to the interaction vanishes, so that all three frequencies are given by $m\omega^2-k=0$. All three vibrations are here geometrically identical.

X. The Field Vectors

The quantity calculated in the preceding sections is the actual microscopic electric force at the place of a particle, the so-called exciting field. Macroscopically one has to distinguish between the electric field **E** and the electric displacement **D** which are connected by $\mathbf{D}=\mathbf{E}+4\pi\mathbf{P}$. **P** is, of course, the total dipole moment per unit volume. The formal definition of **E** and **D** requires the measurement of the force on a macroscopic probe, situated in an appropriately arranged slit. It is obvious from this definition that **E** and **D** in this macroscopic sense have meaning only if the wave-length of our vibrations is large in all directions compared with the lattice distance, because otherwise averaging over many lattice distances means also averaging over several wave-lengths and gives, therefore, zero for **D**, **E** and **P**.

We have to restrict ourselves, therefore, to the above case, in which it is possible to distinguish sharply between transverse and longitudinal waves. As is well known, one defines **D** as the force exerted on a probe in a slit at right angles to the field, while **E** is measured in a channel parallel to the field. One sees easily that in the latter case one also can substitute a slit which has one long dimension in the direction of the field. While all the dimensions of the slits ought to contain many lattice distances, we are going to build the slits up of narrow slits with a short dimension, small compared with a. We designate the field vectors so defined by primes. We first start with longitudinal waves.

Consider a narrow slit between lattice planes: Due to the factors $\exp(2\pi i s\xi/a)$, $\exp(2\pi i t\eta/a)$, the average value of the field and therefore $\mathbf{D}'=\mathbf{0}$. Consider next a slit in the lattice plane, with the dipoles of that plane removed. The same argument holds. Therefore **D** is zero as it must be so that the condition of transversality for **D** is fulfilled.

Consider next the average field in a horizontal slit *with* the dipoles. The field in the slits between lattice planes is zero as above. Next take a narrow slit, cutting the dipoles of a lattice plane. The average value of the field is equal to the charge per unit surface times -4π. (Consider a flat shell, one surface in the slit, the other between lattice planes, and apply Gauss' theorem.) This slit extends over a distance equal to the dipole displacement, so that the average value is $-4\pi\mathbf{P}$. That is **E**,[18] and $\mathbf{D}=-4\pi\mathbf{P}+4\pi\mathbf{P}=\mathbf{0}$.

That this is **E** according to the usual definition (measuring the force in a channel parallel to the field) can be seen because the dipoles that have to be removed to make the channel do not contribute appreciably. One sees, however, that the same argument holds also for transverse waves, as the result is independent of the order of sum-

[18] See H. A. Lorentz, *Theory of Electrons* (Leipzig, 1909), p. 134, last formula.

mation. Therefore the free vibrations considered here are described by

$$\mathbf{D}=\mathbf{0}, \quad \mathbf{E}=-4\pi\mathbf{P},$$

which is in agreement with the interpretation of $\mathbf{D}$ as the field due to external sources.

According to electromagnetic theory, the refractive index n is related to the dielectric constant ϵ by $n^2=\epsilon$. The refractive index itself is determined by the frequency of the long transverse waves of the optical branch. On the other hand, the dielectric polarization of a slab between two condenser plates corresponds to the *longitudinal* deformation. Nevertheless, everything comes out correctly. Consider again the neutral simple cubic lattice. Then the optical transverse frequency is given by

$$m\omega^2-k=-(4\pi e^2)/3a^3.$$

On the other hand, the external force polarizing the slab in $\mathbf{D}$; everything else has been included in our summation. Therefore

$$(k+(8\pi e^2)/3a^3)\mathbf{z}=e\mathbf{D}. \tag{7}$$

$\mathbf{z}$ is the amplitude of the displacement; $k+(8\pi e^2)/3a^3$ is $m\omega^2_{\text{long}}$. But as

$$\epsilon-1=(4\pi\mathbf{P})/\mathbf{E}=(4\pi e\mathbf{z})/a^3\mathbf{E},$$

one calculates, by subtracting $(4\pi e^2/a^3)\mathbf{z}$ on both sides of (7),

$$(k-(4\pi e^2)/3a^3)\mathbf{z}=e\mathbf{E},$$

and gets the required connection.

We express our thanks to Dr. Maria Göppert-Mayer for many helpful discussions.

LETTERS TO THE EDITOR

Prompt publication of brief reports of important discoveries in physics may be secured by addressing them to this department. Closing dates for this department are, for the first issue of the month, the eighteenth of the preceding month, for the second issue, the third of the month. Because of the late closing dates for the section no proof can be shown to authors. The Board of Editors does not hold itself responsible for the opinions expressed by the correspondents.

Communications should not in general exceed 600 words in length.

Nuclear Isomerism in Rhodium

Pontecorvo[1] has recently pointed out that Rh^{104} emits numerous electrons of energy 35–60 kev. He ascribes these electrons to the internal conversion of the gamma-radiation emitted when the Rh^{104} nucleus goes from an excited state (4.2-minute period) to the ground state. From the ground state there is beta-emission which gives Pd^{104} and is ascribed to the 44-second period. The emission of the gamma-ray from the excited state is an alternative process to the direct emission of a beta-ray from the excited state. In this latter connection the beta-ray spectra associated with the two periods are of interest.

A study of these beta-ray spectra had already been undertaken in this laboratory with a cloud chamber in a magnetic field. It has been found that the beta-ray spectra associated with these two periods are identical in shape and end point within the limits of error of the measurements. Samples of Rh in the form of thin sheets (184 mg per square cm) were bombarded by neutrons (from Li bombarded by 1.2 Mev deuterons) after passing through paraffin. The 4.2 minute and 44 second isomers were separated by varying the time of activation and time of observation. The contamination of the undesired isomer was reduced to 3.7 percent for the spectrum of the 44-second period and to 0.8 percent for the spectrum of the 4.2-minute period. The visually extrapolated upper limit obtained was 2.25 Mev for both spectra and the shape of the two curves was very nearly identical. Konopinski-Uhlenbeck diagrams were plotted to obtain a better value for the difference of the upper limits. The end points obtained were 2.74 Mev for the 44-second period and 2.76 Mev for the 4.2-minute period. The estimated error in each of the end points is 0.06 Mev. The 44-second Konopinski-Uhlenbeck upper limit has been reported by Gaerttner, Turin, and Crane[2] as 2.8 Mev.

The similarity of the two beta-ray spectra in both shape and end point is in agreement with Pontecorvo's results. In addition, since the direct emission of beta-particles from the excited state would probably give the spectrum associated with the 4.2-minute period a shape unlike that from the 44-second period, these results indicate that the presence of the direct beta-transitions to any considerable extent is unlikely.

E. C. CRITTENDEN, JR.
R. F. BACHER

Cornell University,
Ithaca, New York.
October 27, 1938.

[1] B. Pontecorvo, Phys. Rev. **54**, 542 (1938).
[2] Gaerttner, Turin, and Crane, Phys. Rev. **49**, 793 (1936).

On the Formation of Deuterons by Proton Combination

The probability of the reaction $H+H=D+e^+$ at stellar temperatures was studied in a paper which appeared recently in the *Physical Review*.[1] In that discussion the Gamow-Teller modification[2] of the Fermi beta-theory was adopted in order that the change in spin between a ^1S state of two protons (most favorable to their close approach) and the resulting ^3S state of the deuteron could take place. It has been suggested to the authors that the symmetry considerations which allow this transition be amplified.

The initial proton state is antisymmetric to an interchange of space and spin coordinates and the final deuteron state is symmetric in this respect. If this were a complete description of the exchange symmetry properties the transition desired would be forbidden. The point which was not made explicit in the original discussion is that to use configuration space in considering beta-processes one must include another coordinate, namely the isotopic spin, which represents the neutron and the proton as two states of one particle. The ^1S function of two protons is symmetric to interchange of this coordinate, whereas the deuteron function is antisymmetric. In the complete coordinate system, therefore, the positron emission assumed accompanies a transition from one antisymmetrical state to another and may be permitted.

H. A. BETHE

Cornell University,
Ithaca, New York.

C. L. CRITCHFIELD

George Washington University,
Washington, D. C.,
November 2, 1938.

[1] Bethe and Critchfield, Phys. Rev. **54**, 248 (1938).
[2] Gamow and Teller, Phys. Rev. **49**, 895 (1936).

Sign Preference in Cloud Condensation on Gaseous Ions

In a recent paper Loeb, Kip and Einarsson[1] gave data and formulated a theory as to the nature of the sign preference in the condensation of various vapors on ions in a C. T. R. Wilson cloud chamber. There it was indicated that condensation about ions in vapors of nonpolar liquids should show *no sign preference*. Publication of that paper was withheld for a year because after the initial experiments on supposedly C. P. vapors of C_6H_6 later measurements on C_6H_6 and CCl_4 had shown definite sign preference. Careful purification of C_6H_6 by Edmund Chambers and Einarsson had eventually shown that pure dry C_6H_6 showed no sign preference but that with 10 percent of

TABLE I.

SUBSTANCE	CONTAMINATED WITH	EXPANSION RATIO	SIGN PREFERENCE
C_6H_6	Pure, B.P. 80.0°C.	1.8	No sign preference
C_6H_6	With 0.007% H_2O by weight	1.7	Negative
C_6H_6	With 0.057% H_2O by weight (Saturated)	1.5	Negative
CCl_4	Pure, B.P. 76.4°C	1.4	No sign preference

C_6H_6 saturated with water added to 90 percent pure C_6H_6 a definite sign preference was shown for the negative ion. The work on C_6H_6 has been repeated and measurements have been carried out to determine the minimum percentage of H_2O which could be detected. Measurements were made on carefully purified CCl_4. As further experiments in this direction had to be abandoned for the present because of the departure of one of us (J.W.B.), the results to date are here presented. The commercial C. P. grade C_6H_6 was carefully purified by standard chemical procedures and finally boiled in a reflex condenser over metallic Na for three hours. The fraction boiling at 80°C was used and all glassware used was heated to 100° to remove moisture from the gases. The commercial grade of C. P. CCl_4 was purified according to standard practice and was redistilled, the fraction boiling within 0.5°C of the accepted boiling point was used (see Table I). In the case of C_6H_6 with 0.007 percent H_2O the negative cloud was very weak; only a few drops were observed. Indications are that the condensation on the negative ions in this case was clearly due to water vapor present in small traces. The fields used to draw out ions in both cases were of the order of two volts per cm.

J. W. BECKMAN*
LEONARD B. LOEB

Physics Department,
University of California,
Berkeley, California,
October 31, 1938.

* Chemist under W.P.A.
[1] Loeb, Kip and Einarsson, J. Chem. Phys. **6**, 264 (1938).

A New Form of the Electromagnetic Energy Equation When Free Charged Particles are Present

To deal with the energy relations in electron beam tubes a new form of the electromagnetic energy equation is required which expresses conservation of energy in a region in which both free charged particles and electromagnetic fields are present. At the outset we shall make the restriction that the electrons or other charged particles are so far distant from each other that classical rather than quantum theory applies, a condition which is fulfilled within many orders of magnitude in any vacuum device.

This restriction makes it possible to ignore the electromagnetic origin of mass, for the electric field and magnetic fields can each be divided into two parts, that arising from charges at a distance which is microscopically uniform, and that excess which is appreciable only in the immediate neighborhood of the individual charged particles. The excess electric field appears as the mass and the excess magnetic field as the kinetic energy of the particles. Accordingly, in the electromagnetic equations which will be used E refers to the electric field due to particles at a distance, or what amounts to the same thing, to the field of a smoothed-out charge distribution, and the same holds for H, the magnetic field.

The equation,

$$\frac{1}{2}\frac{\partial}{\partial t}\int_\tau (E^2+H^2)d\tau + c\int_\sigma \mathbf{E}\times\mathbf{H}\cdot d\boldsymbol{\sigma} + \Sigma\int \rho_i \mathbf{v}_i\cdot\mathbf{E}d\tau = 0, \quad (1)$$

then applies in a region evacuated except for the presence of groups of charge distribution ρ_1, ρ_2, etc. Each has the respective space distribution of velocity $\mathbf{v}_1$, $\mathbf{v}_2$, etc., and each is characterized also by the same particle mass, m_1, m_2, etc. This is a slight generalization of Eq. (155–2) of Page's *Introduction to Theoretical Physics*, second edition.

Let us confine our attention to a single charge distribution in the third term of Eq. (1). The dot product of $\mathbf{v}$ with the differential equation of motion

$$d\mathbf{v}/dt = (e/m)(\mathbf{E}+\mathbf{v}\times\mathbf{H}/c) \quad (2)$$

gives

$$\mathbf{v}\cdot\mathbf{E} = (m/2e)d(v^2)/dt. \quad (3)$$

This permits the elimination of E. As integrand we then have $\rho d(v^2)/dt$ which we convert to partial derivatives:

$$\rho d(v^2)/dt = \rho\partial(v^2)/\partial t + \rho\mathbf{v}\cdot\nabla(v^2). \quad (4)$$

If we bear in mind that ρ and v^2 are scalars and $\mathbf{v}$ a vector the last term can be rearranged by means of the relation

$$\nabla\cdot(u\mathbf{v}) = u\nabla\cdot\mathbf{v}+\mathbf{v}\cdot\nabla u$$

to give

$$\nabla\cdot(v^2\rho\mathbf{v}) - v^2\nabla\cdot(\rho\mathbf{v}).$$

We now note that

$$\nabla\cdot(\rho\mathbf{v}) = -\partial\rho/\partial t$$

and that

$$\rho d(v^2)/\partial t + v^2\partial\rho/\partial t = (\partial/\partial t)(\rho v^2)$$

so that Eq. (4) becomes

$$\rho\partial(v^2)/\partial t = \nabla\cdot(v^2\rho\mathbf{v}) + (\partial/\partial t)(\rho v^2).$$

By converting the volume integral of the second term above to a surface integral, and using ψ for the current density $\rho\mathbf{v}$, we find Eq. (1) takes the form

$$\frac{1}{2}\frac{\partial}{\partial t}\int_\tau (E^2+H^2)d\tau + c\int \mathbf{E}\times\mathbf{H}\cdot d\boldsymbol{\sigma} + \Sigma(m_i/2e)\frac{\partial}{\partial t}\int \rho_i v_i^2 d\tau + \Sigma(m_i/2e)\int_\sigma v_i^2\psi_i\cdot d\boldsymbol{\sigma} = 0, \quad (5)$$

in which the rate of change of kinetic plus electromagnetic energy in the region is related to the energy flows of both types across the boundary.

Incidentally, we see that although the third term of Eq. (1) is the rate at which the electromagnetic field does work on the charges within τ this is not the rate of increase of kinetic energy in the region because of the outflow of kinetic energy across σ.

L. TONKS

Research Laboratory,
General Electric Company,
Schenectady, New York,
October 18, 1938.

Photoconductivity in Willemite

The experiments of Gudden and Pohl on the photoconductivity of luminescent zinc sulfide show that there is a correlation between luminescence and photoconductivity in some crystals. Early this past summer, it was noted by Mr. F. B. Quinlan and the author that willemite is photoconducting when exposed to radiation of wave-length 2537A. Rough measurements were subsequently made on the spectral dependence of this effect. Two samples were employed—a natural crystalline mass from Franklin, New Jersey, and an artificial fused mass containing about 1 percent of Mn.

A concave grating was used as a monochromator, and a mercury vapor uviarc was used as a source. The ultraviolet intensities were measured by means of a thin windowed sodium photo-cell which was kindly calibrated by Dr. B. T. Barnes of Nela Park. The small photocurrents of the crystal, which were in the neighborhood of 10^{-12} amp., and of the photo-cell were amplified by an FP-54 electrometer tube. The galvanometer used in conjunction with the amplifier had a long period, so that the measured currents may have been partly "secondary." Saturation of the photocurrent was not observed up to voltages of 800 volts.

Figure 1 shows the spectral response curve for the two specimens. Curve A is for the natural willemite and is the average of two runs. The experimental error was largest in the short wave-length portion of the curve and may be as high as ten percent. Curve B is for the artificial specimen and may have a larger error in the same region.

The illustrated peak for the artificial specimen lies very close to the peak for excitation of luminescence by ultraviolet light. The apparent rise of photoelectric efficiency at lower wave-lengths does not correspond to any known variation in luminescence efficiency.

It is yet too early to say that this correlation between luminescence and photoconductivity in willemite places this substance in the same class as the zinc sulfide phosphors in other respects.

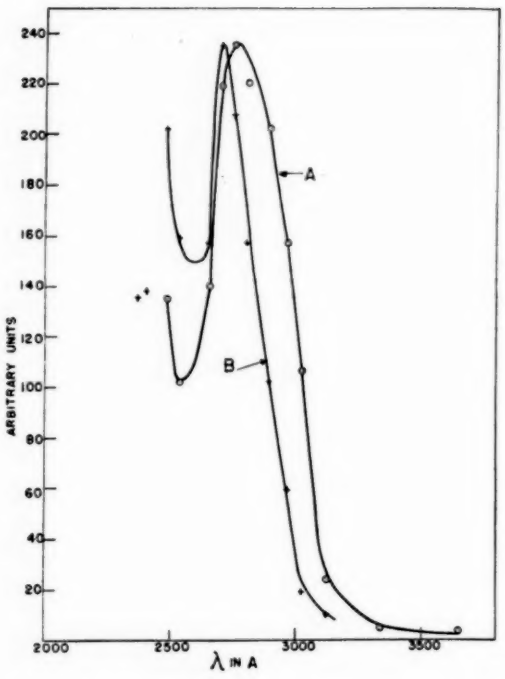

FIG. 1. Photoelectric response in willemite. Points were taken at the principal ultraviolet lines of the mercury spectrum.

This work was done at the Research Laboratory of the General Electric Company in Schenectady, New York. It is a pleasure to express my thanks to the Laboratory for the privilege of working there. I am grateful to Dr. F. Seitz for suggesting this problem, and to Mr. F. B. Quinlan for invaluable assistance.

ROBERT HOFSTADTER

Palmer Physical Laboratory,
Princeton University,
Princeton, New Jersey,
October 26, 1938.

Proceedings of the New England Section of the American Physical Society

Minutes of the South Hadley, Massachusetts Meeting, October 15, 1938

THE twelfth regular meeting of the New England Section was held at Mount Holyoke College on October 15, 1938. The morning session was devoted to contributed papers, business meeting, and the invited papers by A. T. Jones and Elizabeth R. Laird. At the business meeting the following officers were elected for the ensuing year:

G. F. Hull, *Chairman*
K. S. Van Dyke, *Vice Chairman*
J. C. Boyce, *Secretary-Treasurer*
K. T. Bainbridge and W. W. Watson,
Members of Program Committee.

A rising vote of thanks was extended to the Department of Physics at Mount Holyoke for their generous hospitality.

The afternoon session consisted of two invited papers, "Investigations in Artificial Radioactivity" by J. J. Livingood, and "Electron Optics" by R. P. Johnson.

One hundred persons attended the meeting. The Mount Holyoke Physics Laboratories were open for inspection throughout the day.

The winter meeting will be held at Harvard University on January 21, 1939.

Abstracts of the contributed papers and titles of the invited papers are given below.

J. C. Boyce, *Secretary-Treasurer,*
New England Section

Abstracts

1. **Collector Electrode Currents in Discharges of Different Current Density.** Rogers D. Rusk, *Mount Holyoke College.*—Measurements have been made in discharge tubes of small diameter (a few mm) with a half-insulated collecting wire and also with the same wire without insulation. These show that the collector does not receive proportionate increases in current at space potential for increases in the current density of the discharge. When used as a half-collector the measurements gave the magnitude of the drift current through the tube at the lower current densities (0.04 amp./cm²). But for current densities a hundred times larger, the half-collector indicated only a fraction of the actual drift current through the tube, and full collector likewise failed to indicate the total (random plus drift) current. A similar failure of a collector to indicate true drift current magnitudes has been pointed out recently by Heatley.[1]

[1] Phys. Rev. **52**, 238 (1937).

2. **High Pressure Arc as Spectroscopic Source.** W. W. Watson, *Yale University.*—Because of the fact that as the gas pressure is raised (to several atmospheres) the excitation in an arc is increasingly thermal (Farkas, Olsson), the population of many discrete excited states of molecules may be much enhanced. At reduced gas pressure the electron impact excitation cannot populate these levels because of the probable large change in internuclear distance involved and to predissociation into the ever-present repulsion states. Pertinent details of a new "high pressure" spectrum of PbH ($^2\Sigma \rightarrow {}^2\Sigma$, $\nu_e = 18530.3$, $\omega_e' = 455.6$, $B_0' = 2.660$, $\omega_e'' = 1565.2$, $B_e'' = 4.972$) may be cited as an example. The spectroscopic possibilities and limitations of the high pressure arc are discussed.

3. **The Ultraviolet Absorption Spectra of Simple Hydrocarbons.** Emma P. Carr and Hildegard Stücklen, *Mount Holyoke College.*—Examination of the ultraviolet absorption spectra of twenty-six unsaturated hydrocarbons, including olefins, diolefins and cyclic hydrocarbons in the region 2300 to 1600A, using a fluorite vacuum spectrograph, has shown that (1) the light absorbed by a given hydrocarbon molecule is determined by the number of hydrogen atoms directly bound to the carbon atoms of the double bond and is independent of the size or arrangement of the alkyl group and (2) there is a progressive shift of absorption toward longer wave-lengths as the number of these hydrogen atoms is decreased; (3) the spectra of all cyclic hydrocarbons examined show vibrational fine structure and (4) the spectra of diolefins containing (a) isolated (b) adjacent double bonds are very similar, which is in accord with the chemical reactivity of these hydrocarbons. With compounds containing conjugated double bonds the spectra show a shift of absorption toward the visible of 6000 cm^{-1} and a much stronger intensity, a result which also parallels the greatly increased reactivity of hydrocarbons of this type. The results in general can be used for identification of the structure of a pure hydrocarbon and give new evidence as to the energy relationships of the carbon-carbon double bond.

4. **A Test for the Adequacy of Theory in the Light of Experiment.** Richard A. Beth, *Worcester Polytechnic Institute.*—Precision measurements involving physical constants may usually be written in the form

$$e^{\alpha_1} m^{\alpha_2} h^{\alpha_3} c^{\alpha_4} F^{\alpha_5} p^{\alpha_6} q^{\alpha_7} \cdots = X \pm \Delta,$$

where the experimental value X does not involve, in the

first order at least, any assumed values of the physical constants on the left. Each such determination may be reduced to a linear "observation equation" by taking logarithms of both sides. Its weight is proportional to $(X/\Delta)^2$. By the least squares adjustment of observations[1] any over-determined number of such equations may be solved for the best values of the unknowns; *and* the *absolute values of the probable errors* may be calculated from the weighted observation equations alone, without knowledge of the proportionality factor between the weights and $(X/\Delta)^2$. The test for the adequacy of the whole complex of theory and experimental evaluation used lies in the comparison of the calculated errors with the deviations and the original Δ's. If a change of theory or interpretation of experiment is suggested, its adequacy in accounting for previous discrepancies may be tested by a new calculation. If a given observation equation is under particular suspicion, it may simply be omitted in a new calculation to see whether the suspicion is justified, but this alone does not suggest what more adequate theory should be substituted. As an illustration, a provisional evaluation of eight types of experiments involving only e, m, and h was made, the experimental determination of R_∞ being excluded. The results are:

$$e = (4.8028 \pm 0.0012) \times 10^{-10} \text{ e.s.u.};$$
$$m = (9.1118 \pm 0.0031) \times 10^{-28} \text{ g};$$
$$h = (6.6077 \pm 0.0027) \times 10^{-27} \text{ erg sec.}$$

These lead to a value of $2\pi^2 me^4/ch^3$ which is larger by one part in 122 ± 12 than the direct experimental value of R_∞.

[1] See Wright and Hayford, *Adjustment of Observations*, pp. 93–148.

5. **Radioactive Air Inhalation as a Health Hazard.** ROBLEY D. EVANS AND CLARK GOODMAN, *Massachusetts Institute of Technology.*—The inhalation of radioactive gases has long been known to be hazardous. Quantitative data on the delayed effects of alpha-radiation are now being collected from case histories of earlier workers in radium refineries. There is a suggestion that radon inhalation may lead to lung cancer, even 10 to 15 years after termination of the radioactive exposure. Quantitative confirmation of these after effects of ionizing particle-bombardment of tissue is being sought through experimentation on animals. It is urged that until more is known about these delayed effects of heavy-particle radiation, all persons exposed to neutron radiation provide a large factor of safety in the dosages received. It also seems essential to reduce the radon and thoron content of the air in industrial establishments using radioactive substances.

6. **Determination of the Radon and Thoron Content of Air.** CLARK GOODMAN AND ROBLEY D. EVANS, *Massachusetts Institute of Technology.*—The double-ionization chamber apparatus[1] easily allows determination of radon concentrations down to 10^{-13} curie per liter of air. Samples obtained in evacuated glass bulbs (500 cc) do not undergo extensive decay during shipment to the laboratory because of the conveniently long half-period of radon, 3.82 days. Thoron has a half-period of only 54.8 sec. and is most easily determined from its only long-lived decay product ThB ($T = 10.6$ hours). A portable sampling device, operating on 110 a.c., has been developed which circulates the air to be measured over a small collecting disk maintained at a negative potential of about 2000 volts. These disks are shipped by air mail to the laboratory where alpha- or beta-measurements are made. Extrapolation of the observed activity back to the end of the collection period provides a direct measure of the thoron content of the air. The instrument is calibrated in a chamber containing a known thoron concentration. Ordinary laboratory air contains less than 10^{-13} curie of radon or thoron per liter. The radon content in contemporary radium-dial painting plants varies from 4×10^{-12} to 25×10^{-12} curie per liter of air. The thoron content in thorium-mantle factories ranges from 250×10^{-12} to 4400×10^{-12} curie per liter.

[1] R. D. Evans, Rev. Sci. Inst. **6**, 99–112 (1935).

7. **Transparency of Sea-Water in the Pacific Ocean.** R. T. YOUNG, JR., *Worcester Polytechnic Institute.*—Measurements of the relative transparency of sea-water have been made at twenty-five stations on the Pacific Ocean off the coast of Southern California. In all cases measurements were made to a depth of 60 meters. The data were obtained with a transparency meter of the type developed by Hans Pettersson of Götesborg. The light sensitive element was a Weston Photronic cell. A Schott VG-9 green filter was used at all stations. Curves of relative transparencies are shown for various stations. In general, the curves fall into two groups: (1) those showing a minimum transparency at a depth of 30 or 40 meters and (2) those showing a continually increasing transparency from the surface down. Laboratory measurements were made on the transparency of suspended sediments and the variation of transparency with concentration of particles determined. With the instrument used in this work a change of 10 percent in the meter readings corresponds to a change of 0.15 mg per liter particle concentration of average size 5μ.

8. **Sources of Error in High Frequency Measurements of the Dielectric Properties of Glass.** ROSEMARY HUDSON, *Wellesley College.*—A study has been made of sources of error in measurements of power factor at high frequencies by the resistance variation method in order to determine whether the rise in power factor of certain glasses at frequencies above 10^5 or 10^6 found by various observers is a spurious effect. Since the power factor is represented by $R\omega C$, where R is the equivalent series resistance of the condenser, possible sources of error which might cause an apparent rise in power factor at high frequencies included the resistances of the leads and electrodes of the condensers and the stray reactances of the leads. If stray reactances exist in the leads to a condenser, the effect on apparent capacity of stray capacity is a constant for all frequencies, but the effect of stray inductance is to increase the effective capacity as the frequency increases. It was found that small differences in length or position of the leads to the precision and test condensers produced a difference in inductance which was not negligible at high frequencies

and that when these differences were carefully eliminated the observed capacity was constant over the range of high frequencies used. Under these conditions the measured power factor still increased with frequency at frequencies above 10^5. Experiments are now in progress to determine whether this rise can be accounted for by inequalities in resistances.

9. **Electronic Conduction in Insulating Crystals Under Very High Field Strength.** A. VON HIPPEL, *Massachusetts Institute of Technology.*—Current-voltage characteristics and photoelectric response have been measured in single crystals up to the breakdown point. Ten million volts per centimeter have been reached in mica, and phenomena have been observed acoustically, making a crystalline type of light-counter feasible. The dark-currents and photocurrents observed give information about the mechanism of electric conduction under very high field strength.

10. **The Paramagnetic Susceptibility of Copper-Nickel and Zinc-Nickel Alloys.** MARY A. WHEELER, *Yale University.*—Alloys of nickel were prepared with 0 to 60 percent copper and with 0 to 30 percent zinc. As nickel has 0.6 of a positive hole per atom in the *3d* band this band should not be completely filled in alloys with less than 60 percent copper or 30 percent zinc and such alloys should be ferromagnetic at sufficiently low temperatures. The Curie points were measured if they lay above room temperature and the abruptness of the transition noted as an indication of homogeneity. A Weiss-Foëx magnetic balance was used to measure the paramagnetic susceptibility of these alloys as a function of the temperature from room temperature (or from the Curie temperature) to 950°K, in a field of 11,000 oersteds. The graph of the reciprocal of the susceptibility against the temperature is a straight line only for those alloys of high nickel content. For the other alloys the graph is a curve concave towards the temperature axis at the higher temperatures.

11. **Quadrupole Contributions to London's Dispersion Forces.** HENRY MARGENAU, *Yale University.*—It is often of interest to know the magnitude of the contribution of higher electric moments to van der Waals forces. Their exact calculation is involved. It appears, however, that a useful approximation can be attained with the use of a simple harmonic oscillator model in which the number of electrons is replaced by empirical f values. Simple perturbation theory leads to a formula involving only measurable quantities (polarizability, absorption frequency, oscillator strength). The formula is applicable when the dispersion curve of the substance can be represented with the use of a single resonant frequency. Numerical values of the terms in question are calculated for a number of molecules. Except in the case of the alkalis, where the convergence of the sequence in inverse powers of R fails at distances around 6A, the R^{-10} term is generally negligible, while the R^{-8} term contributes appreciably in the region of the van der Waals minimum.

12. **The Exact Solution of Lorentz' Pair of Triangles.** W. B. CARTMEL, *Montreal.*—If we apply rigorous mathematics (such as the method of the complete quadrilateral),[1] to the solution of Lorentz' triangles, we find a homographic relation between the two triangles, leading to the covariant equations

$$\begin{aligned} t_x &= l/c\{1-v/c\cos(\theta+\pi/4)+\tfrac{1}{2}v^2/c^2[1+\cos^2(\theta+\pi/4)]\}, \\ t_y &= l/c\{1-v/c\sin(\theta+\pi/4)+\tfrac{1}{2}v^2/c^2[1+\cos^2(\theta+\pi/4)]\}. \end{aligned} \quad (1)$$

This covariance was first discovered by Minkowski,[2] and has been admitted by Einstein,[3] in his Eq. (24). If we write

$$x_1'=x, \quad x_2'=iy, \quad x_3'=z, \quad x_4'=(x^2+y^2)^{\frac{1}{2}}, \quad (2)$$

we arrive at the Lorentz transformation without having to do violence to the time, which is a pure scalar. Eqs. (2) are almost identical with Sylvester's biaxial homology (see Darboux, chap. V), since they give us a new pair of axes $(x+iy)$ and $(x-iy)$, which are the principal axes of our function. These directions may also be found from

$$\begin{aligned} Sq-Vq &= w-ix-jy-kz, \\ Sq^2-Vq^2 &= w^2+x^2+y^2+z^2. \end{aligned}$$

Einstein objects to Minkowski's solution because of the rotation through an angle of $\pi/4$, but whether we apply the methods of the pure mathematician or quaternions, the solution is always found by first finding the principal axes from a rotation. Einstein's Eq. (24) is equivalent to the matrix of the strain function in an irrotational medium, from which we may derive two crossed ellipses by a rotation of our axes. From these crossed ellipses it is easy to derive the fringe shift formula

$$\Delta F=\tfrac{1}{2}l/\lambda\cdot v^2/c^2\cdot\sin\Omega\sin 2(\theta-\tfrac{1}{2}\Omega)\Big|_{\theta=\frac{1}{2}\Omega}^{\theta=\pi/4}$$

$$\Delta F=\tfrac{1}{2}l/\lambda\cdot v^2/c^2\cdot\cos\Omega\cos 2(\theta-\tfrac{1}{2}\Omega)\Big|_{\theta=\pi/4}^{\theta=\pi/4+\frac{1}{2}\Omega}$$

in which Ω is the angle of obliquity of the interferometer. The fringe shift curve has a period of $\pi/2$, hence Kennedy's null result with an oblique interferometer, is explained by the fact that he took readings 90° apart.

[1] G. Darboux, *Principes de Geometrie Analytique* (Gauthier-Villars, Paris, 1917), p. 54.
[2] H. Minkowski, Goettinger Nachrichten, 53 (1908).
[3] A. Einstein, Princeton Lectures, Vieweg, Braunschweig (1922).

13. **Recent Investigations of Organ Pipes.** A. T. JONES, *Smith College.*

14. **Plan and Equipment of Mount Holyoke Physics Laboratory.** ELIZABETH R. LAIRD, *Mount Holyoke College.*

15. **Investigations in Artificial Radioactivity.** J. J. LIVINGOOD, *Harvard University.*

16. **Electron Optics.** R. P. JOHNSON, *General Electric Co.*

Author Index to Abstracts of South Hadley Meeting

Beth, Richard A.—No. 4

Carr, E. P. and H. Stücklen—No. 3

Cartmel, W. B.—No. 12

Evans, R. D.—see Goodman, C.

—— **and C. Goodman**—No. 5

Goodman, C.—see Evans, R. D.

—— **and R. D. Evans**—No. 6

Hudson, Rosemary—No. 8

Johnson, R. P.—No. 16

Jones, A. T.—No. 13

Laird, Elizabeth R.—No. 14

Livingood, J. J.—No. 15

Margenau, Henry—No. 11

Rusk, Rogers D.—No. 1

Stücklen, H.—see Carr, E. P.

von Hippel, A.—No. 9

Watson, W. W.—No. 2

Wheeler, Mary A.—No. 10

Young, R. T. Jr.—No. 7